on a surface of constant γ.

3.1.5.4 Equation Solution Using Real Quantities

The complete global matrix equation for the acoustic-flow problem with plane wave inputs and outputs and rigid walled ducts is obtained by adding the connecting duct boundary damping matrix $[A]$ to Equation 3.23 to give

$$\left([S] - \omega^2[P] + 2\mathrm{i}M\omega[C] + \mathrm{i}\omega[A]\right)\left\{\phi'_g\right\} = \{Q\} \tag{3.50}$$

The computer language used for this work did not support the use of complex arithmetic, so that the complex equations had to be reformed in terms of real quantities. By splitting the acoustic velocity potential vector $\left\{\phi'_g\right\}$ and the source vector $\{Q\}$ into real and imaginary parts, Equation 3.50 can be separated into real and imaginary terms to give the following equations

$$\begin{aligned} \left([S] - \omega^2[P]\right)\left\{\phi'_g\right\}^{\mathrm{r}} - \left(2M\omega[C] + \omega[A]\right)\left\{\phi'_g\right\}^{\mathrm{i}} &= \{Q^{\mathrm{r}}\} \\ \left(2M\omega[C] + \omega[A]\right)\left\{\phi'_g\right\}^{\mathrm{r}} + \left([S] - \omega^2[P]\right)\left\{\phi'_g\right\}^{\mathrm{i}} &= \{Q^{\mathrm{i}}\} \end{aligned} \tag{3.51}$$

which can be combined to give the matrix equation

$$\begin{bmatrix} \left([S] - \omega^2[P]\right) & \left(-2M\omega[C] - \omega[A]\right) \\ \left(2M\omega[C] + \omega[A]\right) & \left([S] - \omega^2[P]\right) \end{bmatrix} \begin{Bmatrix} \left\{\phi'_g\right\}^{\mathrm{r}} \\ \left\{\phi'_g\right\}^{\mathrm{i}} \end{Bmatrix} = \begin{Bmatrix} \{Q^{\mathrm{r}}\} \\ \{Q^{\mathrm{i}}\} \end{Bmatrix} \tag{3.52}$$

The matrices in this global equation are formed by assembling the element volume and surface matrices using the conventional FEM assembly procedure. In the ISOHERM32 and ISOHERM12 element models separate connectivity matrices must be used to assign the global geometric nodes and the velocity potential nodes to the elements within the model. This has the advantage that on a plane wave boundary termination, several geometric nodes can be assigned to a single velocity potential node since the acoustic and flow velocity potentials are constant over the uniform flow, plane wave interface. Further reductions in the DOF can also be made by

applying constraint equations to force the acoustic and flow velocities at nodes on the rigid boundaries to be parallel to the boundaries.

3.1.6 Solution with Higher Order Mode Boundary Conditions

In order to extend the solution to frequencies above the cut-on frequency for higher order modes it is necessary to consider higher order mode propagation within the connecting straight ducts. The present work considers only rigid walled connecting ducts and uniform flow within these ducts. The exact solution within the straight ducts will be developed first.

3.1.6.1 Higher Order Modes in a Straight Duct with Uniform Flow

This section looks at the propagation of higher order modes within a straight duct with a uniform cross-section of arbitrary shape and uniform flow. The geometry of the model is show in Figure 3.2 with the $x-$axis along the longitudinal axis of the duct. The governing equation for this problem was developed in Section 3.1.3 and is given by Equation 3.13 which was derived from the convected wave equation assuming a harmonic time dependence. A separation of variables solution of form

$$\phi' = X(x)\Phi(y,z) \tag{3.53}$$

can be used. This leads to two equations, the first is given by

$$\frac{\partial^2\Phi}{\partial y^2} + \frac{\partial^2\Phi}{\partial z^2} + \omega_c^2\Phi = 0 \tag{3.54}$$

which is the two-dimensional Helmholtz equation for the duct cross-section. The FEM solution of this equation was considered in Section 2.3.1. The mode shape and eigenvalue for the m^{th} mode are defined respectively as $\Phi_m(y,z)$ and ω_{c_m} with the eigenvalues ordered from smallest to largest with increasing m. The second equation can be used to find X and is given by

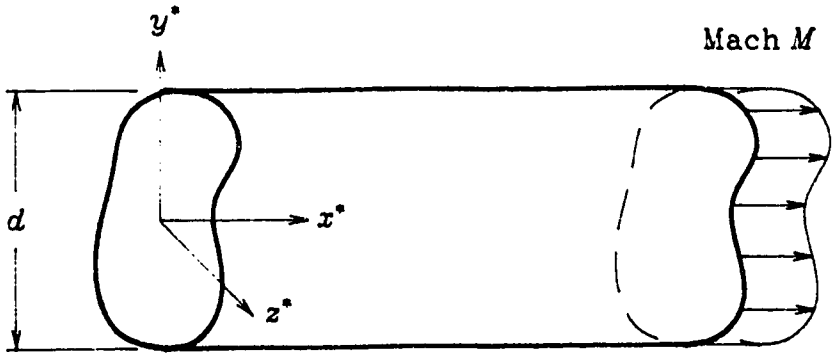

Figure 3.2 Straight Duct with a Uniform Cross-section

$$(1-M^2)\frac{d^2X}{dx^2} - 2iM\omega\frac{dX}{dx} + (\omega^2 - \omega_{c_m}^2)\,X = 0. \tag{3.55}$$

Letting $X = e^{-i\omega_m x}$ and substituting into Equation 3.55 then yields a quadratic equation which can be solved for the values of ω_m given by

$$\omega_m = \frac{-\omega M \mp \sqrt{\omega^2 - (1-M^2)\,\omega_{c_m}^2}}{1-M^2}. \tag{3.56}$$

The general solution can then be given as

$$\phi' = \sum_{m=0}^{\infty} \Phi_m(y,z)\left(A_{1m}e^{-i\omega_m^+ x} + A_{2m}e^{+i\omega_m^- x}\right) \tag{3.57}$$

where

$$\omega_m^{\pm} = \frac{\mp\omega\,(M \mp \alpha_m)}{1-M^2} \quad \text{and} \quad \alpha_m = \sqrt{1-(1-M^2)\frac{\omega_{c_m}^2}{\omega^2}}. \tag{3.58}$$

For the lowest mode ($m = 0$) the frequency parameter $\omega_{c_0} = 0$ and Φ_0 is constant over the cross-section. The terms of Equation 3.57 with $m = 0$ then reduce to the solution for plane wave propagation given by Equation 3.30. For the higher order modes ($m > 0$), if α_m is real then the terms of Equation 3.57 correspond to progressive waves which propagate unattenuated. This occurs when the frequency is above the cut-on frequency given by

$$\omega = \omega_{c_m}\sqrt{1-M^2} \tag{3.59}$$

which decreases as the flow velocity increases and is independent of the direction of flow. If there is no flow ($M = 0$), then the cut-on frequency for the m^{th} mode is ω_{c_m}. Below the cut-on frequency $\omega_m^{\pm}$ are complex (entirely imaginary if there is no flow) and the modes are then referred to as evanescent waves which decay with distance along the duct. The terms of Equation 3.57 with ω_m^+ in the exponent decay exponentially in the negative x direction and terms with ω_m^- in the exponent decay exponentially in the positive x direction. The rate of decay increases as the driving frequency ω becomes smaller.

3.1.6.2 Higher Order Mode Anechoic Termination

The right hand side of the governing acoustic equation for the FEM acoustic-flow model (Equation 3.20) is a surface integral containing the normal derivative of the acoustic velocity potential $d\phi'/dn$. To evaluate this integral, $d\phi'/dn$ must be determined at the interfaces of the connecting straight ducts to the FEM model. Consider the j^{th} duct connecting to the model shown in Figure 3.1. As was done in looking at plane wave boundary conditions, the acoustic velocity potential within the straight duct, based on the connecting duct non-dimensional coordinates and frequency, must be converted to a formulation based on the quantities used in the FEM model. Above the cut-on frequency (α_m real) the outward propagating or transmitted wave is associated with the terms of Equation 3.57 with ω_m^+ in the exponent so that for the anechoically terminated j^{th} straight duct

$$\phi' = \sum_{m=0}^{\infty} \Phi_m(y_s, z_s) B_m^{\text{trans}} e^{-i\omega_m^+ x} \tag{3.60}$$

where

$$\omega_m^+ = -\frac{\omega(M_j - \alpha_m)}{1 - M_j^2} \quad \text{and} \quad \alpha_m = \sqrt{1 - \left(1 - M_j^2\right)\frac{\omega_{c_m}^2 d^2}{\omega^2 d_j^2}}. \tag{3.61}$$

Below the cut-on frequency (α_m imaginary), so that the evanescent mode decays moving outward from the FEM model, the terms of Equation 3.57 with ω_m^- in the exponent must be used. This is equivalent to using Equation 3.60 with

$$\begin{aligned} \omega_{m_r}^+ &= -\frac{\omega M_j}{1-M_j^2} \\ \omega_{m_i}^+ &= -\frac{\omega}{1-M_j^2}\sqrt{\left(1-M_j^2\right)\frac{\omega_{c_m}^2 d^2}{\omega^2 d_j^2}-1} \end{aligned} \tag{3.62}$$

where $\omega_{m_r}^+$ and $\omega_{m_i}^+$ are the real and imaginary parts of ω_m^+. The normal derivative of ϕ' is then

$$\frac{d\phi'}{dn} = \frac{d\phi'}{dx} = \sum_{m=0}^{\infty} \Phi_m(y_s, z_s)\left(-\mathrm{i}B_m^{\text{trans}}\omega_m^+\right) e^{-\mathrm{i}\omega_m^+ x}. \tag{3.63}$$

At the FEM model interface to the straight duct ($x = 0$) the acoustic velocity potential reduces to

$$\phi' = \sum_{m=0}^{\infty} \Phi_m(y_s, z_s) B_m^{\text{trans}} \tag{3.64}$$

and the normal derivative

$$\frac{d\phi'}{dn} = \frac{d\phi'}{dx} = \sum_{m=0}^{\infty} \Phi_m(y_s, z_s)\left(-\mathrm{i}B_m^{\text{trans}}\omega_m^+\right) \tag{3.65}$$

The last two equations will be used in Section 3.1.6.4 in the development of the FEM model of a duct junction with higher order mode boundary conditions.

3.1.6.3 Higher Order Mode Incident Wave Termination

Again consider the j^{th} duct connecting to the FEM model shown in Figure 3.1. For the specified incident wave termination, the terms of Equation 3.57 with ω_m^- in the exponent form the incident wave and the terms with ω_m^+ in the exponent form the reflected wave. The acoustic velocity potential in the straight duct is then

$$\phi' = \sum_{m=0}^{\infty} \Phi_m(y_s, z_s)\left(B_m^{\text{refl}} e^{-\mathrm{i}\omega_m^+ x} + B_m^{\text{inc}} e^{+\mathrm{i}\omega_m^- x}\right) \tag{3.66}$$

where ω_m^+ is real and given by Equation 3.61 above the cut-on frequency. Below the cut-on frequency, ω_m^+ is complex and given by Equation 3.62. Similarly ω_m^- is real above the cut-on frequency and given by

$$\omega_m^- = \frac{\omega\left(M_j + \alpha_m\right)}{1 - M_j^2}. \tag{3.67}$$

Below the cut-on frequency the real and imaginary parts of ω_m^- are

$$\begin{aligned} \omega_{m_r}^- &= \frac{\omega M_j}{1 - M_j^2} \\ \omega_{m_i}^- &= \frac{\omega}{1 - M_j^2}\sqrt{\left(1 - M_j^2\right)\frac{\omega_{c_m}^2 d^2}{\omega^2 d_j^2} - 1}. \end{aligned} \tag{3.68}$$

The solutions below the cut-on frequency have been selected so that the incident evanescent modes decay moving toward the FEM model and the reflected modes decay moving away from the model. The normal derivative of the acoustic velocity potential is then

$$\frac{d\phi'}{dn} = \frac{d\phi'}{dx} = \sum_{m=0}^{\infty} \Phi_m(y_s, z_s)\left(-\mathrm{i}\omega_m^+ B_m^{\mathrm{refl}} e^{-\mathrm{i}\omega_m^+ x} + \mathrm{i}\omega_m^- B_m^{\mathrm{inc}} e^{+\mathrm{i}\omega_m^- x}\right). \tag{3.69}$$

Evaluating the equation for ϕ' and $\frac{d\phi'}{dn}$ at the connecting duct interface to the model ($x = 0$) gives

$$\phi' = \sum_{m=0}^{\infty} \Phi_m(y_s, z_s)\left(B_m^{\mathrm{refl}} + B_m^{\mathrm{inc}}\right) \tag{3.70}$$

and

$$\frac{d\phi'}{dn} = \frac{d\phi'}{dx} = \sum_{m=0}^{\infty} \Phi_m(y_s, z_s)\left(-\mathrm{i}\omega_m^+ B_m^{\mathrm{refl}} + \mathrm{i}\omega_m^- B_m^{\mathrm{inc}}\right) \tag{3.71}$$

These last two equations are used to develop the FEM models of a duct junction in the following section.

3.1.6.4 Junction with Incident Wave and Anechoic Terminations

Consider the FEM model of a duct junction shown in Figure 2.11. In this model it is assumed that there is a known incident wave in a straight connecting duct

at Station 1 and anechoic straight duct terminations at Station 2 and Station 3. This model will be used to illustrate the equation development. The resulting equations have also been programmed with only one outlet to solve duct bend problems. The equations developed could easily be extended to model junctions with four or more connecting ducts. Station 1 does not necessarily have to be the flow inlet. The directions of flow can be selected arbitrarily, provided the resulting flow boundary conditions satisfy mass continuity.

The modal matrix $[\Phi]_1$ of FEM model mode shapes will be used for the incident wave termination at Station 1 and defined as

$$[\Phi]_1 = [\{q_0\}\{q_1\}\{q_2\}\cdots\{q_n\}]_1. \tag{3.72}$$

The vectors $\{q_0\}$,$\{q_1\}$, $\{q_2\}\ldots\{q_n\}$ are the eigenvectors of nodal quantities for the terminating duct cross-section acoustic modes determined from the FEM solution of the eigenvalue problem. This problem is governed by the two-dimensional Helmholtz equation given by Equation 3.53 and was considered for two and three-dimensional problems in Section 2.3. The vector for the acoustic velocity potential and derivative nodal quantities at this termination is then given by

$$\{\phi'_g\}_1 = [\Phi]_1(\{a\} + \{b\}) \tag{3.73}$$

where $\{a\}$ is a vector defining the assumed known incident wave modal mixture and $\{b\}$ is the vector defining the unknown reflected wave modal mixture at the termination.

This discretized formulation is then used in Equation 3.70 and Equation 3.71 which leads to an equation for the acoustic velocity potential at any point on the terminating cross-section given by

$$\phi' = \langle N\rangle\{\phi'_g\}_1 = \langle N\rangle[\Phi]_1(\{a\} + \{b\}) \tag{3.74}$$

and the normal derivative of ϕ' by

$$\frac{d\phi'}{dn} = \mathrm{i}\langle N\rangle[\Phi]_1\left(\{\omega^- a\} - \{\omega^+ b\}\right) \tag{3.75}$$

where

$$\{\omega^+ a\} = \begin{Bmatrix} \omega_0^+ a_0 \\ \omega_1^+ a_1 \\ \omega_2^+ a_2 \\ \vdots \\ \omega_n^+ a_n \end{Bmatrix} \text{ and } \{\omega^- b\} = \begin{Bmatrix} \omega_0^- b_0 \\ \omega_1^- b_1 \\ \omega_2^- b_2 \\ \vdots \\ \omega_n^- b_n \end{Bmatrix}. \tag{3.76}$$

The wave number parameters ω_0^-, ω_1^-, $\omega_2^- \ldots \omega_n^-$ can be obtained using Equation 3.66 and Equation 3.67 and ω_0^+, ω_1^+, $\omega_2^+ \ldots \omega_n^+$ can be obtained using Equation 3.61, and Equation 3.62.

The source terms in the global matrix equation, given by Equation 3.20, associated with this termination are then

$$\{Q_1\} = \int_{S_1}\{N\}\frac{d\phi'}{dn}ds = \mathrm{i}\int_{S_1}\{N\}\langle N\rangle ds\,[\Phi]_1(\{\omega^- a\} - \{\omega^+ b\}). \tag{3.77}$$

Let

$$[\Phi\omega^+] = \left[\omega_1^+\{q_1\} \quad \omega_2^+\{q_2\} \quad \cdots \quad \omega_n^+\{q_n\}\right] \tag{3.78}$$

and

$$[\Phi\omega^-] = \left[\omega_1^-\{q_1\} \quad \omega_2^-\{q_2\} \quad \cdots \quad \omega_n^-\{q_n\}\right] \tag{3.79}$$

then

$$\{Q_1\} = \mathrm{i}[A_1]\left([\Phi\omega^-]_1\{a\} - [\Phi\omega^+]_1\{b\}\right) \tag{3.80}$$

where $[A_1] = \int_{S_1}\{N\}\langle N\rangle ds$. Similarly at the anechoic termination at Station 2, $\{\phi_g'\}_2 = [\Phi]_2\{c\}$ where $\{c\}$ is the vector defining the unknown transmitted modal mixture and Equation 3.65 gives $\{Q_2\} = -\mathrm{i}[A_2][\Phi\omega^+]_2\{c\}$. Also at the anechoic termination at Station 3, $\{\phi_g'\}_3 = [\Phi]_3\{d\}$ and $\{Q_3\} = -\mathrm{i}[A_3][\Phi\omega^+]_3\{d\}$ where $\{d\}$ defines the unknown transmitted modal mixture at this boundary. The matrices

$[A_1]$, $[A_2]$, $[A_3]$ are obtained by integrating on an element basis over each surface and assembling the element matrices into the associated global surface matrix. The element matrix is given by

$$[A_e] = [J_g]^T \int_{-1}^{1} \int_{-1}^{1} \{F\}\langle F\rangle J_s \, d\xi \, d\gamma \, [J_g] \tag{3.81}$$

when integrated in the element domain over a surface of constant ζ using the three-dimensional ISOHERM32 element, and by

$$[A_e] = [J_g]^T \int_{-1}^{1} \{F\}\langle F\rangle J_\xi \, d\xi \, [J_g] \tag{3.82}$$

when integrated along the edge of the two-dimensional ISOHERM12 element along a line of constant γ.

Note that $\{a\}$, $\{b\}$, $\{c\}$, $\{d\}$, $[M\omega^+]$ and $[M\omega^-]$ can be complex. The global matrix equation for the finite element model given by Equation 3.23 for hard walled ducts can be split into real and imaginary parts to give

$$\left([B^r] + \mathrm{i}[B^i]\right)\left(\{\phi'_g\}^r + \mathrm{i}\{\phi'_g\}^i\right) = \{Q^r\} + \mathrm{i}\{Q^i\} \tag{3.83}$$

where $[B^r] = [S] - \omega^2[P]$ and $[B^i] = 2M\omega[C]$. In terms of all real quantities this can be expanded to obtain the equation

$$\begin{bmatrix} [B^r] & [-B^i] \\ [B^i] & [B^r] \end{bmatrix} \begin{Bmatrix} \{\phi'_g\}^r \\ \{\phi'_g\}^i \end{Bmatrix} = \begin{Bmatrix} \{Q^r\} \\ \{Q^i\} \end{Bmatrix}. \tag{3.84}$$

The vector $\{\phi'_g\}$ can be separated into internal node quantities $\{\phi_{int}\}$ and connecting boundary quantities $\{\phi_{bnd}\}$. Similarly $\{Q\}$ can be separated into internal and boundary quantities resulting in the equation

$$[BB] \begin{Bmatrix} \{\phi^r_{int}\} \\ \{\phi^r_{bnd}\} \\ \{\phi^i_{int}\} \\ \{\phi^i_{bnd}\} \end{Bmatrix} = \begin{Bmatrix} \{0\} \\ \{Q^r_{bnd}\} \\ \{0\} \\ \{Q^i_{bnd}\} \end{Bmatrix} \tag{3.85}$$

where the matrix $[BB]$ is defined as

$$[BB] = \begin{bmatrix} [B^r] & [-B^i] \\ [B^i] & [B^r] \end{bmatrix} \tag{3.86}$$

The order of the equations can be changed and partitioned between internal and boundary quantities to give

$$\begin{bmatrix} [D_{11}] & [D_{12}] \\ [D_{21}] & [D_{22}] \end{bmatrix} \begin{Bmatrix} \begin{Bmatrix} \phi^r_{int} \\ \phi^i_{int} \end{Bmatrix} \\ \begin{Bmatrix} \phi^r_{bnd} \\ \phi^i_{bnd} \end{Bmatrix} \end{Bmatrix} = \begin{Bmatrix} \begin{Bmatrix} 0 \\ 0 \end{Bmatrix} \\ \begin{Bmatrix} Q^r_{bnd} \\ Q^i_{bnd} \end{Bmatrix} \end{Bmatrix}. \tag{3.87}$$

This is equivalent to the following equations:

$$\begin{aligned} [D_{11}] \begin{Bmatrix} \phi^r_{int} \\ \phi^i_{int} \end{Bmatrix} + [D_{12}] \begin{Bmatrix} \phi^r_{bnd} \\ \phi^i_{bnd} \end{Bmatrix} &= \begin{Bmatrix} 0 \\ 0 \end{Bmatrix} \\ [D_{21}] \begin{Bmatrix} \phi^r_{int} \\ \phi^i_{int} \end{Bmatrix} + [D_{22}] \begin{Bmatrix} \phi^r_{bnd} \\ \phi^i_{bnd} \end{Bmatrix} &= \begin{Bmatrix} Q^r_{bnd} \\ Q^i_{bnd} \end{Bmatrix}. \end{aligned} \tag{3.88}$$

The first equation can be solved for the internal unknowns to yield

$$\begin{Bmatrix} \phi^r_{int} \\ \phi^i_{int} \end{Bmatrix} = -[D_{11}]^{-1}[D_{12}] \begin{Bmatrix} \phi^r_{bnd} \\ \phi^i_{bnd} \end{Bmatrix}, \tag{3.89}$$

which can be used in the second equation to eliminate the internal unknowns giving

$$[E] \begin{Bmatrix} \phi^r_{bnd} \\ \phi^i_{bnd} \end{Bmatrix} = \begin{Bmatrix} Q^r_{bnd} \\ Q^i_{bnd} \end{Bmatrix} \tag{3.90}$$

where

$$[E] = [D_{22}] - [D_{21}][D_{11}]^{-1}[D_{12}]. \tag{3.91}$$

The boundary vectors can be expanded to give

$$[E] \begin{Bmatrix} \{\phi'_g\}^r_1 \\ \{\phi'_g\}^r_2 \\ \{\phi'_g\}^r_3 \\ \{\phi'_g\}^i_1 \\ \{\phi'_g\}^i_2 \\ \{\phi'_g\}^i_3 \end{Bmatrix} = \begin{Bmatrix} \{Q^r_1\} \\ \{Q^r_2\} \\ \{Q^r_3\} \\ \{Q^i_1\} \\ \{Q^i_2\} \\ \{Q^i_3\} \end{Bmatrix}. \tag{3.92}$$

The vectors $\{\phi'_g\}_j$ can be replaced using the following equations in terms of $\{a\}$, $\{b\}$, $\{c\}$, and $\{d\}$:

$$\begin{aligned}
\{\phi'_g\}_1^r &= [\Phi]_1\{a^r\} + [\Phi]_1\{b^r\} & \{\phi'_g\}_1^i &= [\Phi]_1\{a^i\} + [\Phi]_1\{b^i\} \\
\{\phi'_g\}_2^r &= [\Phi]_2\{c^r\} & \{\phi'_g\}_2^i &= [\Phi]_2\{c^i\} \\
\{\phi'_g\}_3^r &= [\Phi]_3\{d^r\} & \{\phi'_g\}_3^i &= [\Phi]_3\{d^i\}.
\end{aligned} \tag{3.93}$$

Using Equation 3.80, the real and imaginary parts of the source vector $\{Q_1\}$ can be given by

$$\begin{aligned}
\{Q_1^r\} &= [A_1]\left(-[\Phi\omega^-]_1^r\{a^i\} - [\Phi\omega^-]_1^i\{a^r\} + [\Phi\omega^+]_1^r\{b^i\} + [\Phi\omega^+]_1^i\{b^r\}\right) \\
\{Q_1^i\} &= [A_1]\left(+[\Phi\omega^-]_1^r\{a^r\} - [\Phi\omega^-]_1^i\{a^i\} - [\Phi\omega^+]_1^r\{b^r\} + [\Phi\omega^+]_1^i\{b^i\}\right).
\end{aligned} \tag{3.94}$$

If the following matrices are defined

$$\begin{aligned}
[D_1^+]^r &= [A_1][\Phi\omega^+]_1^r & [D_1^+]^i &= [A_1][\Phi\omega^+]_1^i \\
[D_1^-]^r &= [A_1][\Phi\omega^-]_1^r & [D_1^-]^i &= [A_1][\Phi\omega^-]_1^i
\end{aligned} \tag{3.95}$$

then the real and imaginary parts of $\{Q_1\}$ become

$$\begin{aligned}
\{Q_1^r\} &= -[D_1^-]^r\{a^i\} - [D_1^-]^i\{a^r\} + [D_1^+]^r\{b^i\} + [D_1^+]^i\{b^r\} \\
\{Q_1^i\} &= [D_1^-]^r\{a^r\} - [D_1^-]^i\{a^i\} - [D_1^+]^r\{b^r\} + [D_1^+]^i\{b^i\}.
\end{aligned} \tag{3.96}$$

In a similar manner the real and imaginary parts of $\{Q_2\}$ and $\{Q_3\}$ can be given by

$$\begin{aligned}
\{Q_2^r\} &= [D_2^+]^r\{c^i\} + [D_2^+]^i\{c^r\} \\
\{Q_2^i\} &= -[D_2^+]^r\{c^r\} + [D_2^+]^i\{c^i\} \\
\{Q_3^r\} &= [D_3^+]^r\{d^i\} + [D_3^+]^i\{d^r\} \\
\{Q_3^i\} &= -[D_3^+]^r\{d^r\} + [D_3^+]^i\{d^i\}.
\end{aligned} \tag{3.97}$$

If the expressions for $\{\phi'_g\}_j$ from Equation 3.93 and for $\{Q_j\}$ from Equation 3.96 and Equation 3.97 are substituted into Equation 3.92 and the matrix E partitioned then

$$\begin{bmatrix} [E_{11}] & [E_{12}] & [E_{13}] & [E_{14}] & [E_{15}] & [E_{16}] \\ [E_{21}] & [E_{22}] & [E_{23}] & [E_{24}] & [E_{25}] & [E_{26}] \\ [E_{31}] & [E_{32}] & [E_{33}] & [E_{34}] & [E_{35}] & [E_{36}] \\ [E_{41}] & [E_{42}] & [E_{43}] & [E_{44}] & [E_{45}] & [E_{46}] \\ [E_{51}] & [E_{52}] & [E_{53}] & [E_{54}] & [E_{55}] & [E_{56}] \\ [E_{61}] & [E_{62}] & [E_{63}] & [E_{64}] & [E_{65}] & [E_{66}] \end{bmatrix} \begin{Bmatrix} [\Phi]_1\{a^r + b^r\} \\ [\Phi]_2\{c^r\} \\ [\Phi]_3\{d^r\} \\ [\Phi]_1\{a^i + b^i\} \\ [\Phi]_2\{c^i\} \\ [\Phi]_3\{d^i\} \end{Bmatrix}$$

$$= \begin{Bmatrix} -[D_1^-]^r\{a^i\} - [D_1^-]^i\{a^r\} + [D_1^+]^r\{b^i\} + [D_1^+]^i\{b^r\} \\ +[D_2^+]^r\{c^i\} + [D_2^+]^i\{c^r\} \\ +[D_3^+]^r\{d^i\} + [D_3^+]^i\{d^r\} \\ +[D_1^-]^r\{a^r\} - [D_1^-]^i\{a^i\} - [D_1^+]^r\{b^r\} + [D_1^+]^i\{b^i\} \\ -[D_2^+]^r\{c^r\} + [D_2^+]^i\{c^i\} \\ -[D_3^+]^r\{d^r\} + [D_3^+]^i\{d^i\} \end{Bmatrix}. \quad (3.98)$$

A matrix $[F]$ can the be defined by

$$[F] = [E] \begin{bmatrix} [\Phi]_1 & & & & & \\ & [\Phi]_2 & & & O & \\ & & [\Phi]_3 & & & \\ & & & [\Phi]_1 & & \\ & O & & & [\Phi]_2 & \\ & & & & & [\Phi]_3 \end{bmatrix} \quad (3.99)$$

where the elements outside the $[\Phi]_j$ sub-matrices in matrix on the right hand side of this equation are zeros.

If the matrix $[F]$ is partitioned and the terms containing the unknown vectors $\{b\}$, $\{c\}$ and $\{d\}$ moved to the left hand side of the equation and the terms

containing the known vector $\{a\}$ moved to the right hand side of the equation then

$$\begin{bmatrix} [F_{11}]-[D_1^+]^i & [F_{12}] & [F_{13}] & [F_{14}]-[D_1^+]^r \\ [F_{21}] & [F_{22}]-[D_2^+]^i & [F_{23}] & [F_{24}] \\ [F_{31}] & [F_{32}] & [F_{33}]-[D_3^+]^i & [F_{34}] \\ [F_{41}]+[D_1^+]^r & [F_{42}] & [F_{43}] & [F_{44}]-[D_1^+]^i \\ [F_{51}] & [F_{52}]+[D_2^+]^r & [F_{53}] & [F_{54}] \\ [F_{61}] & [F_{62}] & [F_{63}]+[D_3^+]^r & [F_{64}] \end{bmatrix}$$

$$\begin{bmatrix} [F_{15}] & [F_{16}] \\ [F_{25}]-[D_2^+]^r & [F_{26}] \\ [F_{35}] & [F_{36}]-[D_3^+]^r \\ [F_{45}] & [F_{46}] \\ [F_{55}]-[D_2^+]^i & [F_{56}] \\ [F_{65}] & [F_{66}]-[D_3^+]^i \end{bmatrix} \begin{Bmatrix} \{b^r\} \\ \{c^r\} \\ \{d^r\} \\ \{b^i\} \\ \{c^i\} \\ \{d^i\} \end{Bmatrix}$$

$$= \begin{Bmatrix} -[F_{11}]\{a^r\}-[F_{14}]\{a^i\}-[D_1^-]^r\{a^i\}-[D_1^-]^i\{a^r\} \\ -[F_{21}]\{a^r\}-[F_{24}]\{a^i\} \\ -[F_{31}]\{a^r\}-[F_{34}]\{a^i\} \\ -[F_{41}]\{a^r\}-[F_{44}]\{a^i\}+[D_1^-]^r\{a^r\}-[D_1^-]^i\{a^i\} \\ -[F_{51}]\{a^r\}-[F_{54}]\{a^i\} \\ -[F_{61}]\{a^r\}-[F_{64}]\{a^i\} \end{Bmatrix}$$

$$= -\begin{bmatrix} [F_{11}]+[D_1^-]^i & [F_{14}]+[D_1^-]^r \\ [F_{21}] & [F_{24}] \\ [F_{31}] & [F_{34}] \\ [F_{41}]-[D_1^-]^r & [F_{44}]+[D_1^-]^i \\ [F_{51}] & [F_{54}] \\ [F_{61}] & [F_{64}] \end{bmatrix} \begin{Bmatrix} \{a^r\} \\ \{a^i\} \end{Bmatrix}. \qquad (3.100)$$

This system of equations can then be solved to find the real and imaginary parts of $\{b\}$, $\{c\}$ and $\{d\}$ and thus determine the unknown reflected and transmitted modal mixtures.

3.1.7 Sound Power Transmission

The last topic to be discussed, to complete this section on the equation development, is the subject of sound power transmission. The basis of present

engineering methods for noise prediction in HVAC duct systems is to trace the sound power transmitted through the system. In the present work, on bends and duct junctions, many of the results are given in terms of the sound transmission loss of a duct component.

The presence of flow considerably complicates the equations for sound intensity. In the present work the generalized definition of acoustic intensity of Morfey [40] has been used. This definition can be used for irrotational isentropic flow in hard walled ducts and was used by Cabelli [10] when looking at the influence of flow on the acoustic characteristics of duct bends. As pointed out by Eversman [30], this definition does not give correct results for ducts with absorptive walls in the presence of flow.

3.1.7.1 Sound Power Transmission in a Straight Duct

For the case of uniform flow along the longitudinal x-axis of a straight duct Morfey's definition reduces to

$$I_x = \langle\langle \mathrm{Re}\,(p^*)\,\mathrm{Re}\,(u_x^*)\rangle\rangle + \frac{M}{\rho c_0}\langle\langle \mathrm{Re}\,(p^*)\,\mathrm{Re}\,(p^*)\rangle\rangle + M^2\langle\langle \mathrm{Re}\,(p^*)\,\mathrm{Re}\,(u_x^*)\rangle\rangle + \rho c_0 M\langle\langle \mathrm{Re}\,(u_x^*)\,\mathrm{Re}\,(u_x^*)\rangle\rangle \quad (3.101)$$

where $\langle\langle\ \rangle\rangle$ indicates the time average over the period of the harmonically varying quantity and Re( ) indicates the real part of the quantity. In the absence of flow, the last three terms of this equation are zero and the equation reduces to the standard definition of acoustic intensity—the time average of the product of the real acoustic pressure and acoustic particle velocity. The complex acoustic pressure $p*$ and acoustic particle velocity u_x^* can be written as

$$p^* = P^* e^{i\omega^* t^*} \quad \text{and} \quad u_x^* = U_x^* e^{i\omega^* t^*}. \quad (3.102)$$

For the case of uniform flow, the acoustic pressure can be related to the non-dimensional velocity potential using Equation 3.9 to give

$$P^* = -\rho M c_0^2 \left(\mathrm{i}\omega\phi' + M\frac{\partial \phi'}{\partial x} \right). \tag{3.103}$$

The mode shape functions are orthogonal so that the sound intensity can be calculated for each mode and added to give the total intensity at a given frequency. Substitution of Equation 3.103 and $U_x^* = Mc_0 \partial\phi'/\partial x$ and the solutions for forward and backward propagating waves from Equation 3.57, after considerable algebraic manipulation, gives the relatively simple relations

$$I_m^+ = \frac{1}{2}\rho c_0 (Mc_0)^2 \alpha_m \omega^2 \Phi_m^2 |A_{1m}|^2 \quad \text{and} \quad I_m^- = -\frac{1}{2}\rho c_0 (Mc_0)^2 \alpha_m \omega^2 \Phi_m^2 |A_{2m}|^2 \tag{3.104}$$

respectively for the intensities of the forward wave (positive x direction) and backward wave for the m^{th} mode when α_m is real. For the evanescent modes (α^m imaginary) the intensities can be shown to be zero. In deriving Equation 3.104 use was made of the relation

$$\langle\langle \mathrm{Re}(a)\,\mathrm{Re}(b) \rangle\rangle = \frac{1}{2}\left(A^r B^r + A^i B^i \right) \tag{3.105}$$

for the time average of the product of two harmonically varying quantities where $a = Ae^{\mathrm{i}\omega t}$ and $b = Be^{\mathrm{i}\omega t}$.

The transmitted sound power W_m^+ for the forward wave, can then be obtained by integrating the sound intensity I_m^+ over the cross-sectional area of the duct to give

$$\begin{aligned} W_m^+ &= \iint_A I_m^+ \, dA \\ &= \frac{1}{2}\rho c_0 (Mc_0)^2 \alpha_m \omega^2 |A_{1m}|^2 \iint_A \Phi_m^2 \, dA \\ &= \frac{1}{2}\rho c_0 (Mc_0)^2 \alpha_m \omega^2 |A_{1m}|^2 F_m A \end{aligned} \tag{3.106}$$

where F_m can be called the modal power factor and is defined by

$$F_m = \frac{\iint_A \Phi_m^2 \, dA}{\iint_A dA} \tag{3.107}$$

and A is the cross-sectional area of the duct. A similar expression can be derived for the backward wave.

3.1.7.2 Junction and Bend Sound Power Transmission and Reflection

The equations for transmitted sound power, developed in the previous section, can be applied to the straight ducts connected to the FEM model of a duct junction considered in Section 3.1.6.4. Equation 3.106 was based on quantities non-dimensionalized with the straight duct Mach number and characteristic dimension. This can be applied to the straight duct at Station 1, in which the incident modal mixture was specified and the reflected modal mixture determined, to give the total incident and reflected sound powers based on the FEM model quantities as

$$\begin{aligned} W^{\text{inc}_1} &= \frac{1}{2}\rho c_0 (M c_0)^2 \omega^2 A_1 \sum_{m=0}^{n_1} (\alpha_m)_1 (F_m)_1 \left[(a_m^r)^2 + (a_m^i)^2 \right] \\ W^{\text{refl}_1} &= \frac{1}{2}\rho c_0 (M c_0)^2 \omega^2 A_1 \sum_{m=0}^{n_1} (\alpha_m)_1 (F_m)_1 \left[(b_m^r)^2 + (b_m^i)^2 \right] \end{aligned} \tag{3.108}$$

where the subscript 1 refers to quantities evaluated at Station 1 and A_1 is the cross-sectional area of the connecting duct. Also a_m^r, a_m^i, b_m^r and b_m^i are the real and imaginary parts of the m^{th} elements of the modal mixture vectors $\{a\}$ and $\{b\}$ used in Section 3.1.6.3. Similarly the transmitted sound powers in the straight ducts connected at Station 2 and Station 3 are

$$\begin{aligned} W^{\text{trans}_2} &= \frac{1}{2}\rho c_0 (M c_0)^2 \omega^2 A_2 \sum_{m=0}^{n_2} (\alpha_m)_2 (F_m)_2 \left[(c_m^r)^2 + (c_m^i)^2 \right] \\ W^{\text{trans}_3} &= \frac{1}{2}\rho c_0 (M c_0)^2 \omega^2 A_3 \sum_{m=0}^{n_3} (\alpha_m)_3 (F_m)_3 \left[(d_m^r)^2 + (d_m^i)^2 \right] \end{aligned} \tag{3.109}$$

Based on the above, sound power reflection and transmission coefficients for individual modes can be written as

$$\begin{aligned} R_m^1 &= \frac{W_m^{\text{refl}_1}}{W^{\text{inc}_1}} = \frac{1}{W^{\text{inc}_1}}(\alpha_m)_1(F_m)_1\left[(b_m^r)^2+(b_m^i)^2\right] \\ T_m^2 &= \frac{W_m^{\text{trans}_2}}{W^{\text{inc}_1}} = \frac{A_2}{A_1 W^{\text{inc}_1}}(\alpha_m)_2(F_m)_2\left[(c_m^r)^2+(c_m^i)^2\right] . \\ T_m^3 &= \frac{W_m^{\text{trans}_3}}{W^{\text{inc}_1}} = \frac{A_3}{A_1 W^{\text{inc}_1}}(\alpha_m)_3(F_m)_3\left[(d_m^r)^2+(d_m^i)^2\right] \end{aligned} \tag{3.110}$$

The modal power factors F_m for each connecting duct were calculated based on the FEM model cross-section modal functions. The finite element approximation to the mode shape function Φ_m is

$$\Phi_m = \langle N\rangle\{q_m\} = \langle q_m\rangle\{N\} \tag{3.111}$$

which substituted into Equation 3.107 gives

$$\begin{aligned} F_m &= \frac{\langle q_m\rangle \iint_A \{N\}\langle N\rangle\, dy\, dz\{q_m\}}{\iint_A dy\, dz} \\ &= \langle q_m\rangle[P]\{q_m\}/A \end{aligned} \tag{3.112}$$

where $[P]$ is the acoustic "mass" matrix for the duct cross-section eigenvalue problem obtained by assembling the element matrices $[P_e]$ and A is the cross-section area obtained by adding the element areas A_e. The integrations in the element domain using the two-dimensional ISOHERM12 element are given by

$$\begin{aligned} [P_e] &= [J_g]^T \int_{-1}^{1}\int_{-1}^{1} \{F\}\langle F\rangle\, |J|\, d\xi\, d\gamma\, [J_g] \\ A_e &= \int_{-1}^{1}\int_{-1}^{1} |J|\, d\xi\, d\gamma \end{aligned} \tag{3.113}$$

In dealing with components with a single input and output the concept of transmission loss is commonly used. In this work, this concept will be extended to junctions with more than one output and will also include the reflected modes in

the duct with the specified incident modal mixture as an output. The transmission losses for the m^{th} reflected mode and the m^{th} transmitted modes in the output ducts have been defined as

$$TL_m^1 = -10\log_{10}R_m^1, \quad TL_m^2 = -10\log_{10}T_m^2 \quad \text{and} \quad TL_m^3 = -10\log_{10}T_m^3 \quad (3.114)$$

In most cases the incident modal mixture is restricted to a single mode and the transmission losses for all the individual output modes calculated. Also the combined output sound powers of all modes given by Equation 3.109 can be used to calculate an overall transmission loss for each duct outlet.

3.2 Tests of the FEM for Plane Waves in Straight Ducts

This section discusses tests of the finite element model to predict plane wave propagation in straight ducts with uniform flow using the FEM formulation developed in Section 3.1.5.

3.2.1 Propagation with the Inlet Acoustic Velocity Specified

The first problem to be considered, was a straight duct of length a modeled using ISOHERM12 quadrilateral elements. A duct width of a was used, however the model was constrained to a one dimensional problem, so that any width could be arbitrarily chosen. Models with one, two and four elements in a linear string were used. The same element mesh was used for both the flow and the acoustic problems and is shown as an example for the two element model in Figure 3.3. The group of the three global degrees of freedom at each corner of the elements corresponds to the velocity potential ϕ (acoustic or flow) and the partial derivatives $\partial\phi/\partial x$ and $\partial\phi/\partial y$ respectively. With reference to the velocity potential nodes of Figure 3.3, the constraint equations "[3]" = "[6]" = "[9]" = 0.0 were used to constrain the $\partial\bar{\phi}/\partial y$ and $\partial\phi'/\partial y$ to zero at nodes along the top and bottom edges of

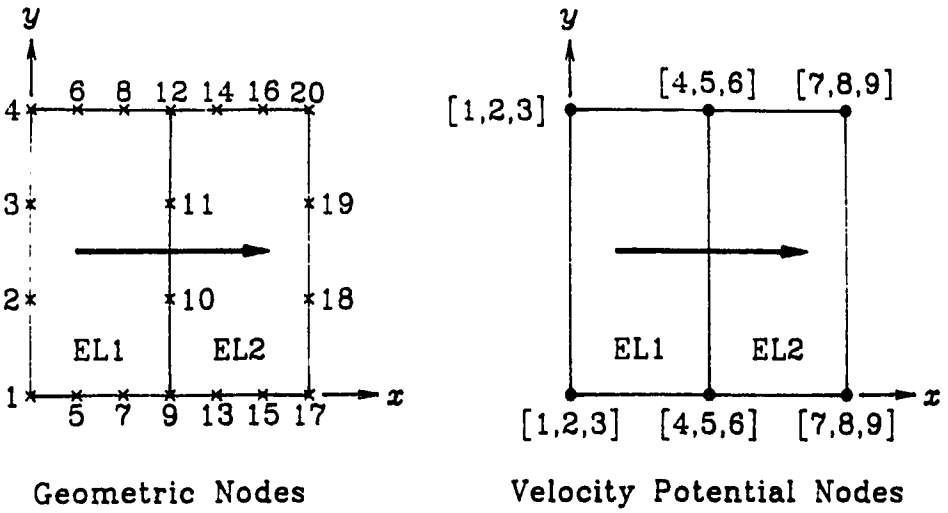

Figure 3.3 Two-Element Model for Plane Wave Propagation in a Straight Duct

the duct. For the flow problem an additional constraint equation "[1]" = 1.0 was used to assign a value of one to $\bar{\phi}$ at this node. Note that the same global degree of freedom has been assigned to nodes on the top and bottom of the duct with the same x coordinate, reducing the model to one-dimensional flow and plane wave propagation. Flow boundary conditions giving an inlet Mach ratio $M_{\text{inlet}}/M = -1$ and outlet Mach ratio $M_{\text{outlet}}/M = 1$ were used. An acoustic velocity of $U = 1$ was specified at the inlet (refer to Section 3.1.5.1) and anechoic termination at the outlet (refer to Section 3.1.5.2).

The flow problem was solved first (in this case giving the same result as the analytical solution) and the global vector $\{\bar{\phi}_g\}$ of flow velocity potential and derivative quantities then used in the solution of the flow-acoustic problem as described in Section 3.1.5.4.

The analytical solution of this problem can be obtained by using the above boundary conditions in the general solution (Equation 3.30) of the governing differential equation (Equation 3.29), which was derived from the convected wave

equation, and is given by

$$\phi'_{\text{conv.}} = \frac{M+1}{\omega} e^{-i\omega x/(1+M)} \tag{3.115}$$

The resulting FEM model acoustical velocity potential ϕ'_{FEM} at the outlet ($x = 1$) is compared to the above analytical solution in Table 3.1 for the one, two and four-element models, for a range of values of the non-dimensional frequency parameter ω (which equals ka) and Mach numbers of zero, 0.1 and -0.1. The magnitude and phase refer to the complex quantity given by the ratio of the FEM acoustic velocity potential and the convected wave equation velocity potential. The magnitude ratio (in decibels) was calculated on a logarithmic scale and is given by $10\log_{10}\left(|\phi'_{\text{FEM}}|/|\phi'_{\text{conv}}|\right)$.

For the case of no flow the errors generally increased with increasing ka and decreased as the number of elements in the model was increased. The one element model gave magnitude errors of less than 0.1 dB and phase errors of less than one degree up to a value of ka between 3 and 4. Two elements gave similar errors up to a value of ka between 6 and 8 and three elements gave magnitude errors of less than 0.1 dB at $ka = 12$. This would indicate that each element can model reasonably accurately one-half of a wavelength.

For the case of flow, Table 3.1 shows that the FEM models converged to nonzero error values and that the phase errors were generally higher at higher frequencies. It was suspected that this was due to the small Mach number approximation made in deriving the governing differential equation in terms of velocity potential used in the FEM model. The case of negative Mach numbers (the flow in the opposite direction to the acoustic propagation) exhibited higher phase errors than the positive Mach number case.

Table 3.1 Convergence for Plane Wave Propagation in a Straight Duct with Uniform Flow

ka	One element		Two elements		Four elements	
	Magnitude Error dB	Phase Error deg.	Magnitude Error dB	Phase Error deg.	Magnitude Error dB	Phase Error deg.
			$M = 0.0$			
0.5	0.0000	0.00	0.0000	0.00	0.0000	0.00
2	0.0021	0.02	0.0000	0.00	0.0000	0.00
4	-0.1220	1.08	0.0003	0.09	0.0000	0.00
6	-0.7219	29.34	0.0164	0.21	0.0001	0.03
8	0.2405	92.55	-0.2228	5.31	0.0017	0.18
10	3.1838	146.33	-0.0677	14.97	0.0026	0.72
12	1.7390	167.90	-1.9300	46.25	0.0590	0.70
			$M = 0.1$			
0.5	0.0050	0.24	0.0050	0.24	0.0050	0.24
2	0.0202	0.36	0.0177	0.36	0.0177	0.36
4	-0.1334	0.64	0.0132	1.12	0.0128	1.08
6	-0.8211	23.30	0.0198	0.90	0.0015	1.35
8	0.2280	79.23	-0.2491	4.69	0.0231	1.92
10	4.8110	128.58	-0.0562	8.56	0.0112	2.90
12	2.2140	98.55	-2.0196	27.70	0.0736	2.12
			$M = -0.1$			
0.5	0.0050	0.30	0.0050	0.30	0.0050	0.30
2	0.0194	0.65	0.0177	0.59	0.0177	0.59
4	-0.0865	5.29	0.0131	1.71	0.0128	1.55
6	-0.5807	42.68	0.0137	3.27	0.0014	2.09
8	0.1506	117.69	-0.1633	13.28	0.0223	3.10
10	1.9865	189.12	-0.0374	36.33	0.0098	4.98
12	1.2201	246.71	-1.5313	82.60	0.0509	6.75

The general solution to the small Mach number, potential flow equation for plane wave propagation with uniform flow was given by Equation 3.31 which for a wave propagating in the positive x-direction and $\partial\phi'/\partial x = 1$ at $x = 0$ reduces to

$$\phi'_{\text{vel.pot.}} = \frac{e^{-i\omega\left(\sqrt{M^2+1}-M\right)x}}{\omega\left(\sqrt{M^2+1}-M\right)} \tag{3.116}$$

With no flow, this solution is identical to the solution given in Equation 3.115. The magnitude and phase of this solution at $x = 1$ is compared to the convected wave equation solution of Equation 3.115 for Mach numbers of ± 0.1 in the first columns

of Table 3.2. The magnitude errors are shown to be independent of frequency and slightly higher for the negative Mach number case but less than one-fortieth of a decibel. The phase error is a linear function of frequency, again higher for the negative Mach number case, and reaching approximately two degrees at $ka = 6$. This is one aspect of the selected approximate flow model that was not initially appreciated. Even though the Mach number may be small, the resulting phase error can be significant if a large value of ka is used.

The FEM results given in Table 3.1 still do not converge exactly to the analytical small Mach number velocity potential solution given in Table 3.2. The finite element model was based on the same governing differential equation, however, there was a difference in boundary conditions used. The FEM model used the convected wave boundary condition to obtain the anechoic termination element matrix given by Equation 3.41 and Equation 3.42. The anechoic boundary condition could also be obtained by using the small Mach number potential flow solution of Equation 3.31. This leads to equations for the element matrix $[A_e]$ identical to Equation 3.41 and Equation 3.42 with the exception that the term $1/(1 + M_j)$ is replaced by $\sqrt{M_j^2 + 1} - M_j$. These terms differ by approximately half of one percent for M less than 0.1. The last four columns of Table 3.2 compare the FEM models with four elements using the small Mach number velocity potential anechoic termination to the analytical convected wave equation and small Mach number velocity potential solutions. For these cases the FEM model now converges to the analytical solutions. The results also show more clearly the effect of the flow on the accuracy of the phase error in the finite element solutions. The phase error increases with frequency and is larger for the negative Mach numbers. This is reasonable since the negative flow effectively decreases the speed of wave propagation, thus

Table 3.2 Comparison of Models for Plane Wave Propagation in a Straight Duct with Uniform Flow

ka	Exact vel.pot. compared to Exact conv.wave		FEM(vel.pot.b.c.) compared to Exact conv.wave		FEM(vel.pot.b.c.) compared to Exact vel.pot.	
	Magnitude Error dB	Phase Error deg.	Magnitude Error dB	Phase Error deg.	Magnitude Error dB	Phase Error deg.
			$M = 0.1$			
0.5	0.0196	0.12	0.0196	0.12	0.0000	0.00
2	0.0196	0.47	0.0196	0.47	0.0000	0.00
4	0.0196	0.94	0.0197	0.94	0.0000	0.00
6	0.0196	1.41	0.0198	1.42	0.0001	0.01
8	0.0196	1.88	0.0218	1.97	0.0022	0.09
10	0.0196	2.35	0.0237	2.77	0.0041	0.42
12	0.0196	2.82	0.0878	2.24	0.0682	-0.58
			$M = -0.1$			
0.5	0.0240	0.18	0.0240	0.18	0.0000	0.00
2	0.0240	0.70	0.0240	0.70	0.0000	0.00
4	0.0240	1.40	0.0240	1.40	0.0000	0.00
6	0.0240	2.11	0.0241	2.16	0.0001	0.06
8	0.0240	2.81	0.0255	3.15	0.0014	0.35
10	0.0240	3.51	0.0268	4.85	0.0028	1.33
12	0.0240	4.21	0.0695	6.88	0.0455	2.67

decreasing the wavelength so that each element is relatively longer compared to the wavelength.

At this stage one might suggest that it would be better to use the small Mach number velocity potential solution boundary condition. This can be easily done for plane wave propagation. For higher order mode propagation the solutions become more complicated and it was thought best to use the well known convected wave equation solutions for connecting ducts rather than deriving solutions to the approximate low Mach number potential flow equations. Also comparison of the FEM solutions with the two different boundary condition models in Table 3.1 and Table 3.2 shows that the difference between the two FEM models is small.

One consequence of choosing to use the convected wave equation in the

connecting ducts and the small Mach number velocity potential governing differential equation in the FEM domain is that the termination will not be truly anechoic. There will be a small reflection at the termination since the acoustic impedances at the connecting boundary will not match exactly if there is flow in the duct. This will be investigated in the following section.

3.2.2 Propagation with a Specified Incident Velocity Potential

The same straight duct with uniform flow modeled in Section 3.2.1 has been considered here. However, instead of a specified inlet acoustic velocity, the incident wave velocity potential has been specified at the inlet and implemented with the FEM using ISOHERM12 elements as discussed in Section 3.1.5.3. For convenience, a unit value was assigned to the incident acoustic velocity potential at the inlet ($B_{\text{inc}} = 1$ in Section 3.1.5.3). After solving for the FEM model nodal velocity potentials, the reflected velocity potential at the inlet, ϕ'_{refl} can be obtained by solving Equation 3.45 to give $\phi'_{\text{refl}} = \phi'_{\text{inlet}} - 1$ where ϕ'_{inlet} is the total velocity potential at the inlet obtained from the FEM model solution. Also the velocity potential for the transmitted wave at the outlet can be taken as ϕ'_{outlet}, the velocity potential at the outlet from the FEM solution. Applying the sound power definitions discussed in Section 3.1.7 to the plane wave mode leads to the following equations for the FEM model sound power reflection coefficient R and transmission coefficient T

$$R = |\phi'_{\text{inlet}} - 1|^2 \quad \text{and} \quad T = |\phi'_{\text{outlet}}|^2 \tag{3.117}$$

If the reflected wave is treated as a transmission path then the transmission loss TL of the FEM model and for lack of a better word, the reflection loss RL are then

$$TL = -10\log_{10}T \quad \text{and} \quad RL = -10\log_{10}R \tag{3.118}$$

In theory the total reflected and transmitted sound power should equal the incident sound power since there is no other dissipation within the rigid walled model. To compare the total reflected plus transmitted sound power to the incident sound power of the FEM model, a quantity called the total sound power loss PL will be defined, based on the ratio of the transmitted plus reflected sound power to the incident sound power and is given by

$$PL = -10\log_{10}(R + T) \tag{3.119}$$

Table 3.3 shows the reflection loss RL and the transmission TL for the straight duct of length a modeled with a string of one, two and four ISOHERM12 quadrilateral elements. Ideally the incident wave should propagate unattenuated with no reflected wave created so that $TL = 0$ and $RL = \infty$. The one element model gave errors in the transmission loss TL of less than 0.1 dB up to a value of ka between 4 and 6. Two elements give similar errors for a value of ka between 10 and 12. These are higher values of ka than observed for similar magnitude errors from Table 3.1 for the specified acoustic velocity problem of Section 3.2.1.

For the case of no flow, as the number of elements is increased, the TL does appear to converge to zero and the reflected wave becomes negligible. With flow, the models converge to a residual error value, presumably due to the small Mach number approximation in the governing differential equation in conjunction with using the convected wave equation boundary condition. For $M = \pm 0.1$ the residual error in TL was less than 10^{-4} decibels. The RL values converge to values of the order of 45 decibels or less for $M = \pm 0.1$ which means that the reflected wave sound power is less than 0.003 percent of the incident sound power. It was observed that the positive and negative Mach number cases give identical errors in TL but different errors in RL.

Table 3.3 Convergence for Plane Wave Propagation in a Straight Duct with the Incident Wave Specified

ka	One element		Two elements		Four elements	
	RL in dB	TL in dB	RL in dB	TL in dB	RL in dB	TL in dB
			$M = 0.0$			
0.5	148.3	0.000000	179.6	0.000000	212.7	0.000000
2	65.5	0.000001	99.0	0.000000	132.6	0.000000
4	28.5	0.006184	79.9	0.000000	127.0	0.000000
6	12.9	0.231286	37.5	0.000772	81.2	0.000000
8	6.4	1.136354	25.8	0.011462	67.9	0.000000
10	3.6	2.456823	25.9	0.011070	58.9	0.000006
12	2.3	3.797621	7.4	0.861033	32.0	0.002717
			$M = 0.1$			
0.5	54.2	0.000025	54.2	0.000025	54.2	0.000025
2	47.5	0.000110	48.6	0.000089	48.7	0.000088
4	29.4	0.004733	49.8	0.000068	50.1	0.000064
6	13.2	0.210475	36.7	0.000954	59.1	0.000008
8	6.5	1.096154	26.4	0.009410	47.1	0.000122
10	3.7	2.416534	28.4	0.006151	48.7	0.000078
12	2.4	3.759139	8.2	0.709997	31.2	0.003461
			$M = -0.1$			
0.5	50.7	0.000025	50.7	0.000025	50.7	0.000025
2	44.4	0.000110	45.2	0.000089	45.2	0.000088
4	29.8	0.004733	46.3	0.000068	46.6	0.000064
6	13.2	0.210475	36.4	0.000954	55.8	0.000008
8	6.5	1.096154	26.8	0.009410	43.9	0.000122
10	3.7	2.416534	28.5	0.006151	46.3	0.000078
12	2.4	3.759139	8.2	0.709997	30.8	0.003461

One measure of the accuracy of the model predictions, used for example by Cabelli [10], is the comparison of the transmitted plus reflected sound power to the incident sound power. The total sound power loss PL defined by Equation 3.119 for the current problem is given in Table 3.4 for the one, two and four-element models of the straight duct. Without flow, the PL values were less than 10^{-14} dB for all FEM models at all frequencies and thus the transmitted plus reflected sound power was exactly equal to the incident sound power (within computer round-off error). Certainly in this case the sound power check does not give a measure of the

Table 3.4 Total Sound Power Check for Plane Wave Propagation in a Straight Duct with the Incident Wave Specified

	Total sound power loss PL in dB		
ka	One element	Two elements	Four elements
	$M = 0.0$		
0.5	1.4465×10^{-15}	9.6432×10^{-16}	3.8573×10^{-15}
2	4.8216×10^{-16}	3.8573×10^{-15}	1.4465×10^{-15}
4	1.4465×10^{-16}	9.6432×10^{-16}	2.8929×10^{-15}
6	-2.8929×10^{-15}	9.6432×10^{-16}	-9.6432×10^{-16}
8	4.3395×10^{-15}	9.6432×10^{-16}	4.8216×10^{-16}
10	-3.8573×10^{-15}	-4.8216×10^{-15}	4.3395×10^{-15}
12	-3.8573×10^{-15}	-9.6432×10^{-15}	4.8216×10^{-16}
	$M = 0.1$		
0.5	8.2429×10^{-6}	8.2427×10^{-6}	8.2427×10^{-6}
2	3.3313×10^{-5}	2.9199×10^{-5}	2.9113×10^{-5}
4	-2.0537×10^{-4}	2.1826×10^{-5}	2.1055×10^{-5}
6	-7.2394×10^{-4}	3.5992×10^{-5}	2.4278×10^{-6}
8	4.1821×10^{-3}	-3.9213×10^{-4}	3.7950×10^{-5}
10	9.2923×10^{-3}	-6.8138×10^{-5}	1.8513×10^{-5}
12	1.1109×10^{-2}	-1.9794×10^{-3}	1.3194×10^{-4}
	$M = -0.1$		
0.5	-1.2313×10^{-5}	-1.2313×10^{-5}	-1.2313×10^{-5}
2	-4.7715×10^{-5}	-4.3576×10^{-5}	-4.3489×10^{-5}
4	1.9684×10^{-4}	-3.2194×10^{-5}	-3.1450×10^{-5}
6	7.2151×10^{-4}	-3.7403×10^{-5}	-3.5361×10^{-6}
8	-4.1962×10^{-3}	3.7646×10^{-4}	-5.4937×10^{-5}
10	-9.3191×10^{-3}	6.7392×10^{-5}	-2.4314×10^{-5}
12	-1.1129×10^{-2}	1.9743×10^{-3}	-1.3717×10^{-4}

accuracy of TL values which were in error by several decibels for the one element model at the largest ka values. With flow, the finite element models converged to small but nonzero values of PL in the order of 10^{-5} decibels, and the PL values were much smaller in many cases than the individual errors in the transmitted and reflected sound powers. Comparison of the PL values for $M = \pm 0.1$ shows that the values for a positive Mach number were roughly equal to those for the negative Mach number but of opposite sign. For the four-element model with positive

Mach number, the reflected plus transmitted sound power was slightly less than the incident sound power and for a negative Mach number slightly greater than the incident sound power.

3.3 Tests of the FEM Model Including Higher Order Modes

This section discusses tests of the finite element model to predict wave propagation in a straight duct with uniform flow and in a duct bend, including higher order modes using the FEM formulation developed in Section 3.1.6.

3.3.1 Mode Shapes and Eigenfrequencies for Rectangular Ducts

Part of the FEM developed for modeling higher order mode boundary conditions requires finding the mode shapes and eigenfrequencies of the duct cross-sections for the straight ducts linked to the bend or junction FEM models. The FEM model for the solution of this eigenvalue problem was considered in detail in Section 2.3. As the subsequent work will consider rectangular ducts, this section looks at rectangular duct cross-sections.

The exact mode shape function for the rectangular hard walled duct cross-section is

$$\Phi_m(y,z) = \cos(n_y \pi y) \cos\left(\frac{n_z \pi z}{r_z}\right) \tag{3.120}$$

and the exact non-dimensional frequency parameter given by

$$\omega_{cm}^2 = \pi^2 \left[n_y^2 + \left(\frac{n_z}{r_z}\right)^2 \right] \tag{3.121}$$

for the m^{th} mode, where n_y and n_z can have any integer value from zero to infinity. Also y and z have been non-dimensionalized based on the duct width in the y-direction and r_z is the ratio of the duct width in the z-direction to that in the y-direction. The modal power factor F_m, defined by Equation 3.107, calculated

from the exact mode shapes given by Equation 3.120 gives a value of $F_m = 1$ for the plane wave mode ($n_y = n_z = 0$), a value of $F_m = 1/2$ for modes with either $n_y = 0$ or $n_z = 0$ and a value of $F_m = 1/4$ for modes with both n_y and n_z nonzero.

Figure 3.4 shows the ISOHERM12 element meshes used to generate the eigenvalues, mode shapes and modal sound power factors. Most of the subsequent work deals with two-dimensional duct problems with one, two or three quadrilateral elements spanning the connecting duct interfaces so that only one-dimensional eigenvalue problems must be solved. The one-element model has been set up to illustrate the two-dimensional cross-section model needed to provide input into a three-dimensional duct model. The width of the duct in the z-direction has been taken as twice the width in the y-direction. The two and three-element models have been constrained to one-dimensional models in the y-direction.

The one-element model in Figure 3.4 assumes rigid walled ducts so that the derivatives $\partial\phi'/\partial y$ and $\partial\phi'/\partial z$ are taken to be zero at the corner nodes. These have been assigned to the last nodal quantity "[5]" of the one-element model in Figure 3.4. This nodal quantity was excluded from the global matrices in the element assembly procedure. The mode shape is thus defined in terms of an eigenvector of the four corner nodal acoustic velocity potentials only. The finite element solution to this ISOHERM12 one-element model gives the following modal matrix $[\Phi]$ (refer to Section 3.1.6.4, Equation 3.72)

$$[\Phi]_{1el} = \begin{bmatrix} 1 & 1 & 1 & 1 \\ 1 & -1 & 1 & -1 \\ 1 & 1 & -1 & -1 \\ 1 & -1 & -1 & 1 \end{bmatrix} \tag{3.122}$$

where each column is the eigenvector for a mode, ordered from the mode with the smallest eigenvalue in first column (the plane wave mode) to the mode corresponding to the largest eigenvalue in the last column. Note that in this case the evaluation

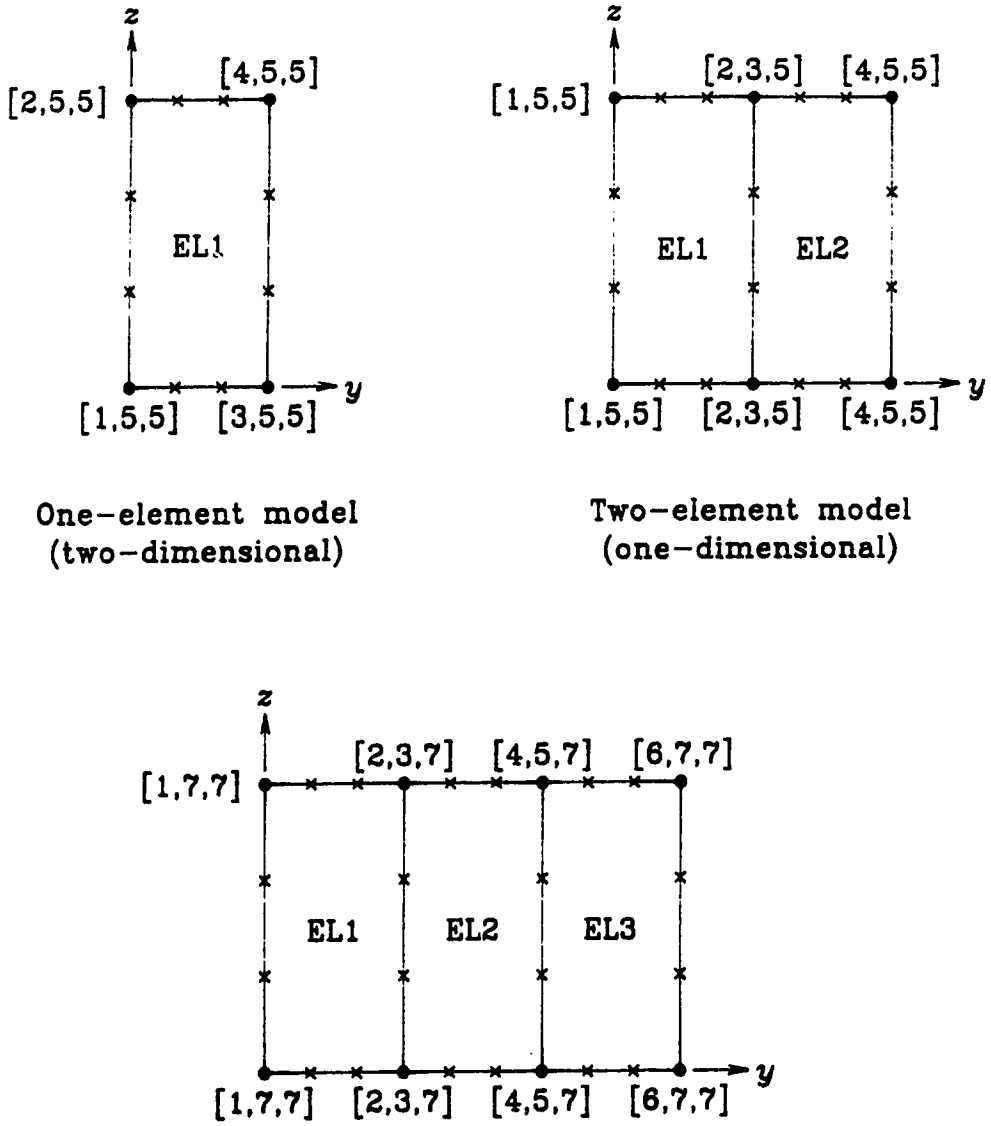

Figure 3.4 Rectangular duct cross-section models

of the exact mode shape functions given by Equation 3.120 at the corners of the duct gives modes identical to those in $[\Phi]$ obtained from the FEM model. If the one-element model is used to solve the one-dimensional eigenvalue problem then the modal matrix is given by

$$[\Phi]_{1el} = \begin{bmatrix} 1 & 1 \\ 1 & -1 \end{bmatrix} \tag{3.123}$$

where the first column corresponds to the plane wave mode and the second to the first cross mode.

The finite element solution to the ISOHERM12 two-element model shown in Figure 3.4 gives the following model matrix

$$[\Phi]_{2el} = \begin{bmatrix} 1 & 1 & 1 & 1 \\ 1 & 0 & -1 & 0 \\ 0 & -3.212 & 0 & 18.212 \\ 1 & -1 & 1 & -1 \end{bmatrix} \tag{3.124}$$

where the first, second and fourth elements of each column are the nodal velocity potentials and the third element of each column is the slope $\partial\phi'/\partial y$ midway across the duct. The nodal quantity "[5]" as for the one element model has been used for all nodal quantities constrained to zero. Note that in this case all elements of $[\Phi]$ are identical to the exact modal function evaluated at the nodes except for the slope quantities in the second and fourth columns. The exact value of $\partial\phi'/\partial y$ evaluated at this point for the first cross mode is $-\pi$ compared to a value of -3.212 in the FEM modal matrix, and for the third cross mode a value of 3π compared to a value of 18.212 in Equation 3.124.

Similarly the modal matrix $[\Phi]$ for three elements across the duct is given by

$$[\Phi]_{3el} = \begin{bmatrix} 1 & 1 & 1 & 1 & 1 & 1 \\ 1 & 0.5 & -0.5 & -1 & -0.5 & 0.5 \\ 0 & -2.736 & -5.739 & 0 & 17.079 & 36.444 \\ 1 & -0.5 & -0.5 & 1 & -0.5 & -0.5 \\ 0 & -2.736 & 5.739 & 0 & -17.079 & 36.444 \\ 1 & -1 & 1 & -1 & 1 & -1 \end{bmatrix} \tag{3.125}$$

where all velocity potential values are identical to the exact modal function evaluated at the nodes. The derivative values 2.736, 5.739, 17.079 and 36.444 in the third and fifth rows of this matrix correspond to the derivatives $d\Phi_m/dy$ of the exact modal function evaluated at one-third and two-third points across the duct. These are given by $\pi\sqrt{3}/2 = 2.720$, $\pi\sqrt{3} = 5.441$, $2\pi\sqrt{3} = 10.882$ and $5\pi\sqrt{3}/2 = 13.60$ for the first, second, fourth and fifth cross modes respectively.

In both the two and three-element models, the exact and FEM nodal derivative values differ significantly, with differences becoming greater as the mode number is increased. It is still best to use the FEM derivative values in the modal matrices rather than the exact values. Substitution of the exact values into the modal vectors leads to increased errors in the modal sound power factors and increased coupling between modes. The eigenvalues and modal sound power factors for the one, two and three element FEM models are compared to the exact values in Table 3.5. In terms of the one dimensional models, the one-element model predicts fairly accurately the first cross mode—the only cross mode that it considers. The two-element model predicts fairly accurately the first and second cross mode values and inaccurately predicts the third cross mode. The three element model gives fairly accurate predictions for the first, second and third cross modes, but less accurate predictions of the fourth and fifth cross modes.

The orthogonality of the modes can be checked by extending Equation 3.112 which defines the modal sound power factors F_m to give the matrix $[\Phi]^T[P][\Phi]/A$. The diagonal elements of this matrix are the modal sound power factors F_m. For the FEM models considered here, all off-diagonal elements had values of 10^{-14} or less which indicates insignificant coupling between the modes.

TABLE 3.5 Eigenvalues and Modal Power Factors for Duct Cross-sections

Mode No. m	Exact				ISOHERM12 FEM			
	n_x	n_y	ω_m^2	F_m	ω_m^2	Percent Error in ω_m^2	F_m	Percent Error in F_m
One-element, two-dimensional cross-section model								
0	0	0	0	1	0.0000	—	1.0000	0.000
1	0	1	$\frac{\pi^2}{4}$	$\frac{1}{2}$	2.4706	0.129	0.4857	-2.857
2	1	0	π^2	$\frac{1}{2}$	9.8824	0.129	0.4857	-2.857
3	1	1	$\frac{5\pi^2}{4}$	$\frac{1}{4}$	12.3529	0.129	0.2359	-5.632
Two-element, one-dimensional cross-section model								
0	0	0	0	1	0.0000	—	1.0000	0.000
1	1	0	π^2	$\frac{1}{2}$	9.8722	0.026	0.4954	-0.916
2	2	0	$4\pi^2$	$\frac{1}{2}$	39.5294	0.129	0.4857	-2.857
3	3	0	$9\pi^2$	$\frac{1}{2}$	94.2509	6.107	0.5974	19.49
Three-element, one-dimensional cross-section model								
0	0	0	0	1	0.0000	—	1.0000	0.000
1	1	0	π^2	$\frac{1}{2}$	9.8699	0.003	0.4988	-0.244
2	2	0	$4\pi^2$	$\frac{1}{2}$	39.5204	0.106	0.4895	-2.110
3	3	0	$9\pi^2$	$\frac{1}{2}$	88.9412	0.129	0.4857	-2.857
4	4	0	$16\pi^2$	$\frac{1}{2}$	162.858	3.131	0.5206	4.120
5	5	0	$25\pi^2$	$\frac{1}{2}$	273.558	10.87	0.8549	70.98

3.3.2 Propagation in a Straight Duct with Uniform Flow

The propagation within a rigid walled, two-dimensional, straight duct of width a has been considered in this section. A segment of the duct of length a has been modeled with one, two and three square ISOHERM12 elements across the duct width as shown in Figure 3.5. It was assumed that the straight duct extends to the left and right of the FEM model. The left side of the model has been taken

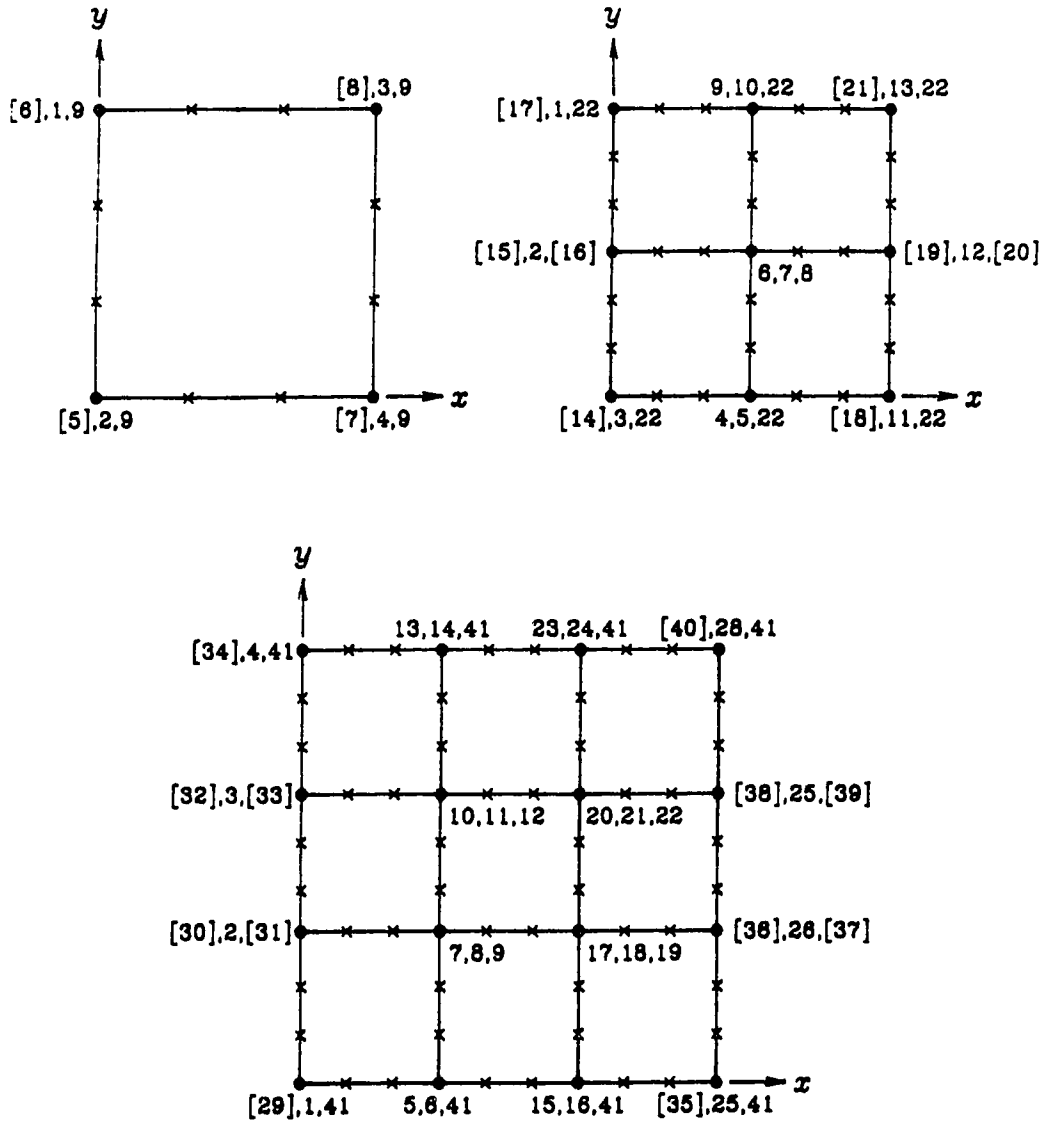

Figure 3.5 Finite Element Meshes for a Straight Duct

as the inlet at which an incident modal mixture is specified and an anechoic termination assumed at the outlet on the right side of the model. A uniform flow has been assumed for which a positive Mach number indicates flow from the left to the right.

The numbering of the global degrees of freedom in the models is shown in Figure 3.5. The highest numbered degree of freedom has been assigned to the $\partial\phi'/\partial y$ nodal quantities at the hard walls and has been constrained to a zero value. The numbers in square brackets indicate the quantities defining the inlet and outlet cross-section modal vectors. For the one-element model these involve only acoustic velocity potential quantities. For the other models these include $\partial\phi'/\partial y$ terms as well.

Either a plane wave, or the first, second or third cross modes have been chosen for the incident modal mixture vector $\{a\}$ defined in Section 3.1.6.4. A real unit value was assigned to the element of $\{a\}$ corresponding to the selected mode and zeros assigned to all other elements. The outlet modal mixture vector $\{c\}$ was then calculated from the exact convected wave equation solution and the FEM model over a range of ka values. The elements of $\{a\}$ and $\{c\}$ correspond respectively to the incident acoustic velocity potential at the inlet and the transmitted acoustic velocity potential at the outlet, taken at the lower wall of the duct for each mode.

The resulting plane wave acoustic velocity potential at the outlet with a unit incident plane wave velocity potential is shown in Figure 3.6 for the case of no flow. The real and imaginary parts of the outlet velocity potential for the FEM models with one, two and three elements across the duct are compared to the exact solution as a function of ka. The exact solution has been plotted at intervals in ka of 0.125 and the FEM values at twice this interval. All three models show good agreement with the exact solution up to ka of 3.5 at which point the one-element

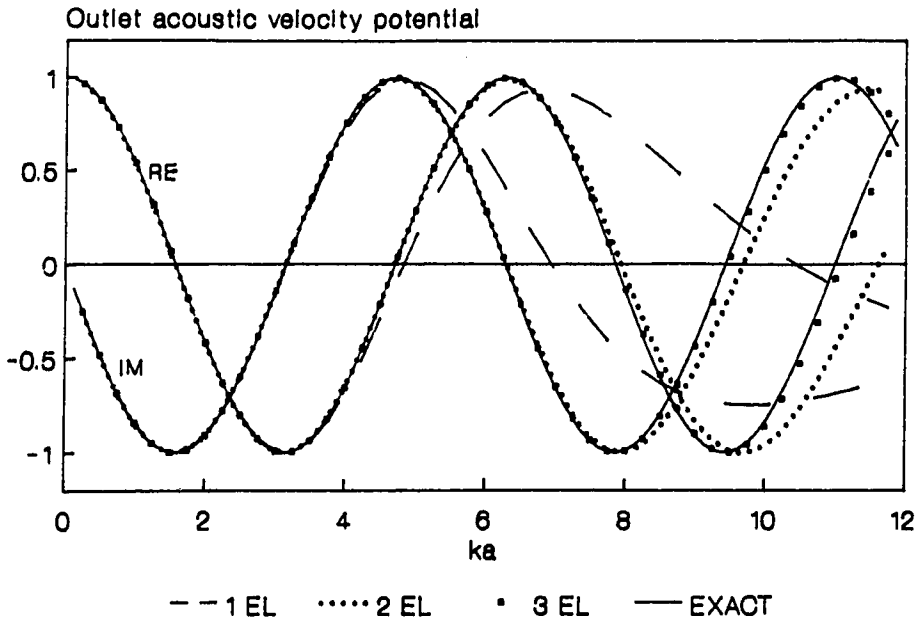

Figure 3.6 Plane Wave Acoustic Velocity Potential for a Straight Duct with no Flow

prediction starts to deviate visibly from the exact curves. With two elements across the duct width, the FEM prediction visibly starts to deviate from the exact curve at a ka value of about 7 and with three elements at a ka value of 10.

A similar graph for the first cross mode is shown in Figure 3.7. Below the cut-on frequency for this mode, the imaginary part of ϕ' is zero and the real part of ϕ' at the outlet is less than the unit incident value at the input. This demonstrates the decay of this evanescent mode from inlet to outlet and shows how the amount of decay is reduced as the frequency parameter ka increases and approaches the cut-on value of $ka = \pi$. The deviation between the exact and FEM model curves near the cut-on frequency is caused by differences in intervals at which the exact and FEM model points are plotted. The convergence of the FEM models to the exact solution appears to be similar to that for the plane wave.

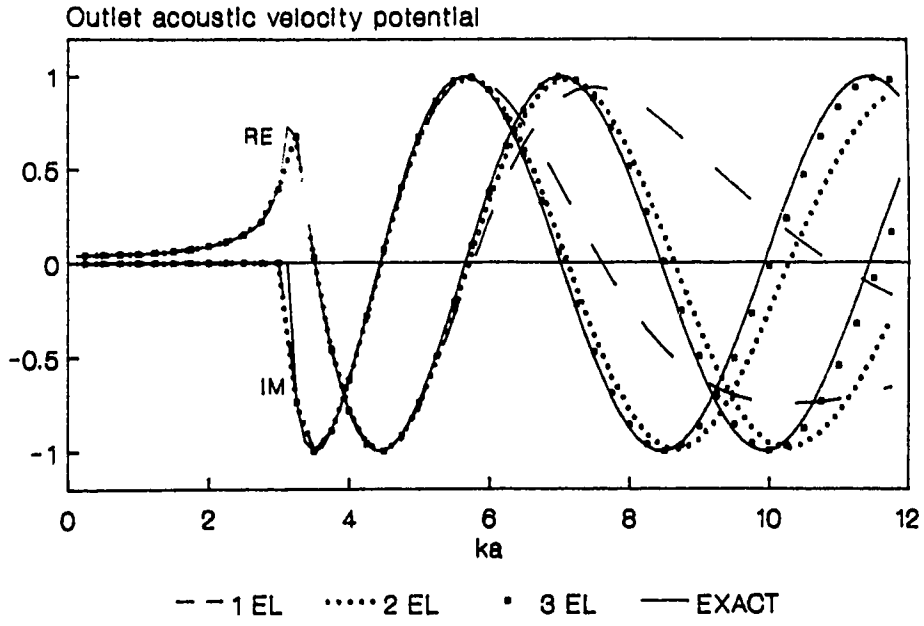

Figure 3.7 First Cross Mode Acoustic Velocity Potential for a Straight Duct with No Flow

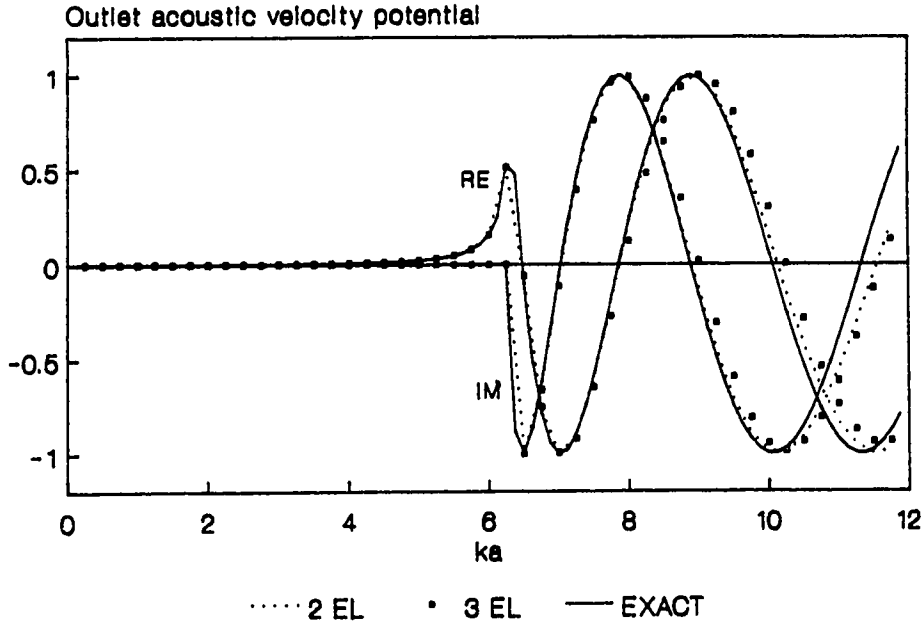

Figure 3.8 Second Cross Mode Acoustic Velocity Potential for a Straight Duct with No Flow

The graph of the second cross mode velocity potential at the outlet, for a unit inlet second cross mode potential, is shown in Figure 3.8. Note that the one-element model only predicts the plane wave and first cross mode and thus is not shown on this graph. The FEM model with two elements across the duct width starts to visibly deviate from the exact curve at a ka value of about 8. Note that the FEM model with three elements across the duct width gives greater errors than with two elements. This unexpected result may be partially explained by the observation that each element in the two-element model models exactly one half of a wavelength of the cross-section mode shape. It was noted in the last paragraph of Section 2.3.2.2, that the eigenvalues of a one-dimensional tube were predicted more accurately when each element modeled exactly half a wavelength. Table 3.5 shows, however, that the three-element model gives marginally smaller errors than the two-element model when predicting the eigenvalue ω_2 and modal power factor F_2 for the second cross mode. Thus, one would have expected the model with three elements across the duct width to give at least as good a prediction as with two elements across the width.

The results for the third cross mode are shown in Figure 3.9 for the case of no flow. The noticeable "clipping" of the exact solution, in this and other figures, is caused by the coarseness of the intervals at which the solution was evaluated. The FEM model with two elements across the duct width deviates considerably from the exact solution above the cut-on frequency of $ka = 3\pi$ for this mode. The model with three elements across the duct width on the other hand gives a very accurate prediction up to ka approaching 12—in fact more accurate than the predictions of the plane wave and lower cross modes with this model. For this mode each element models exactly one half of a wavelength of the cross-section mode shape.

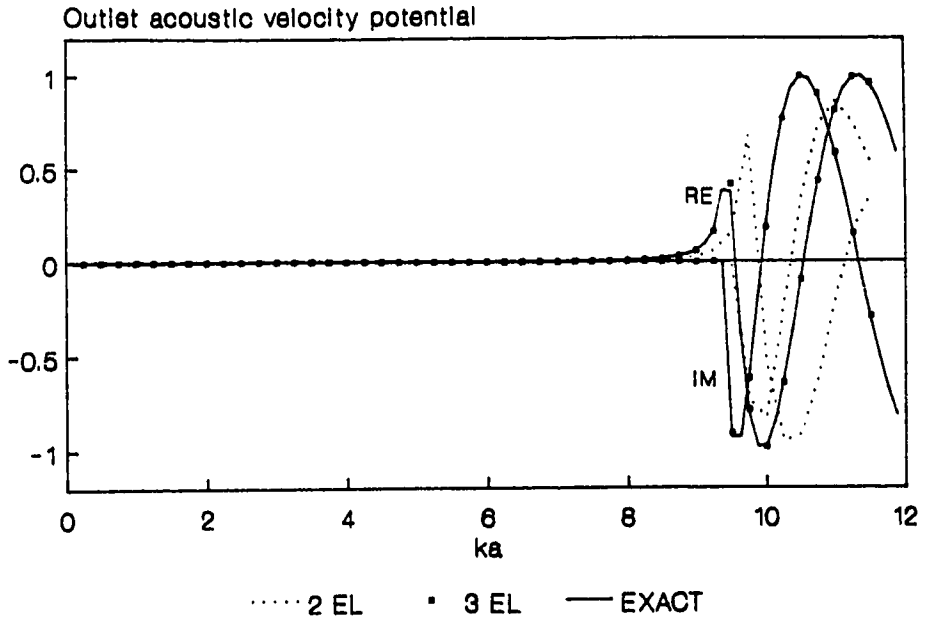

Figure 3.9 Third Cross Mode Acoustic Velocity Potential for a Straight Duct with No Flow

The results with flow are given in Figure 3.10, Figure 3.11, Figure 3.12 and Figure 3.13 for Mach numbers of 0.1 and −0.1 where a positive Mach number indicates the flow is in the same direction as the acoustic wave propagation and a negative Mach number indicate that the flow in the opposite direction. The results for the plane wave are shown in Figure 3.10 and are similar to the curves obtained for the no-flow case. For the positive Mach number case, the sinusoidal shaped curves have been "stretched out" and for the negative Mach number case "compressed" along the ka axis in comparison to the no-flow case. Also it was observed that flow in the opposite direction of the acoustic propagation increased the prediction error at a given ka value. Similar observations can be made concerning the first cross-mode results given in Figure 3.11. One difference noted here, compared to the no-flow case, is that below the cut-on frequency, the imaginary part of the velocity potential is nonzero and positive for the positive Mach number case and negative

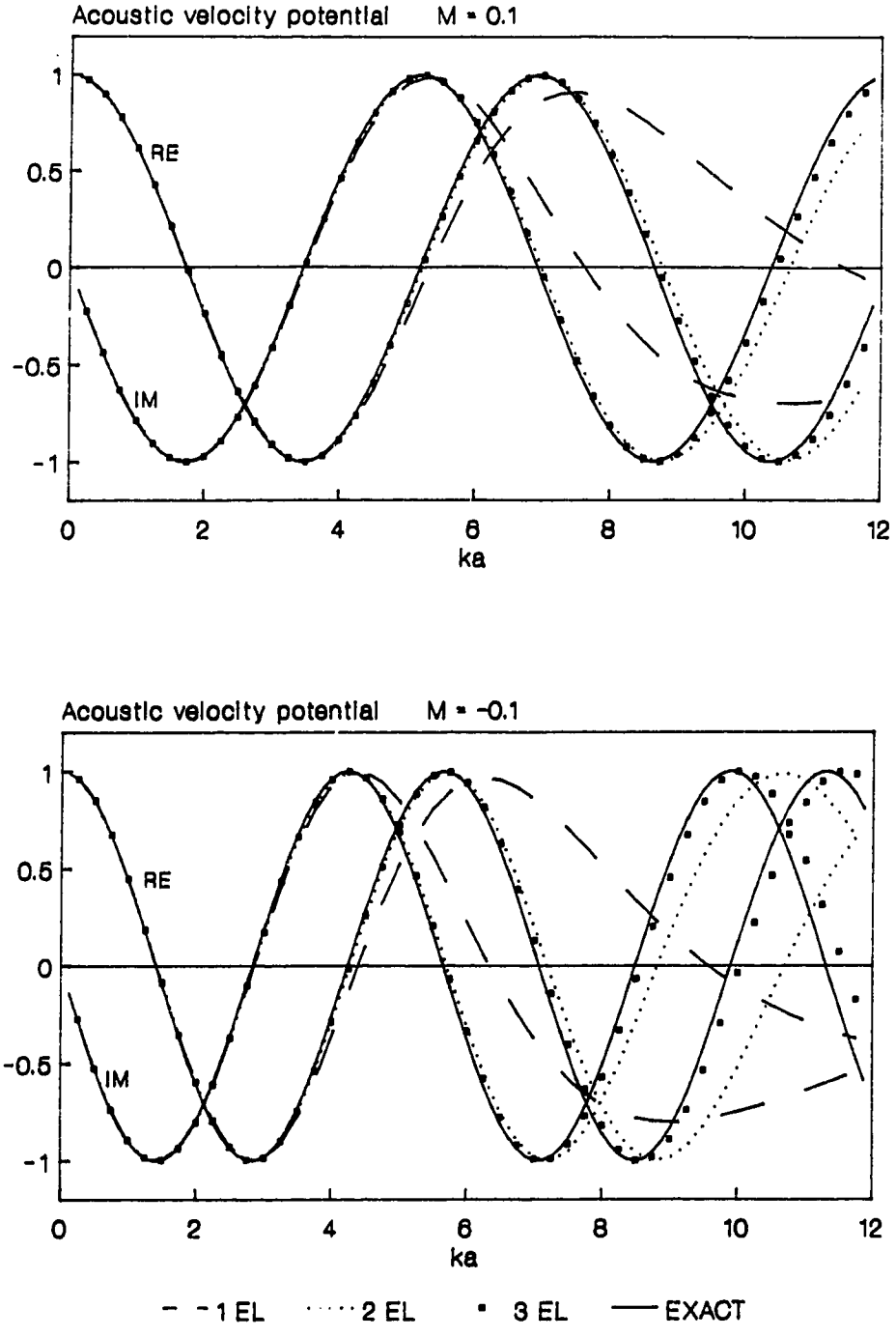

Figure 3.10 Outlet Plane Wave Acoustic Velocity Potential for a Straight Duct with a Uniform Flow

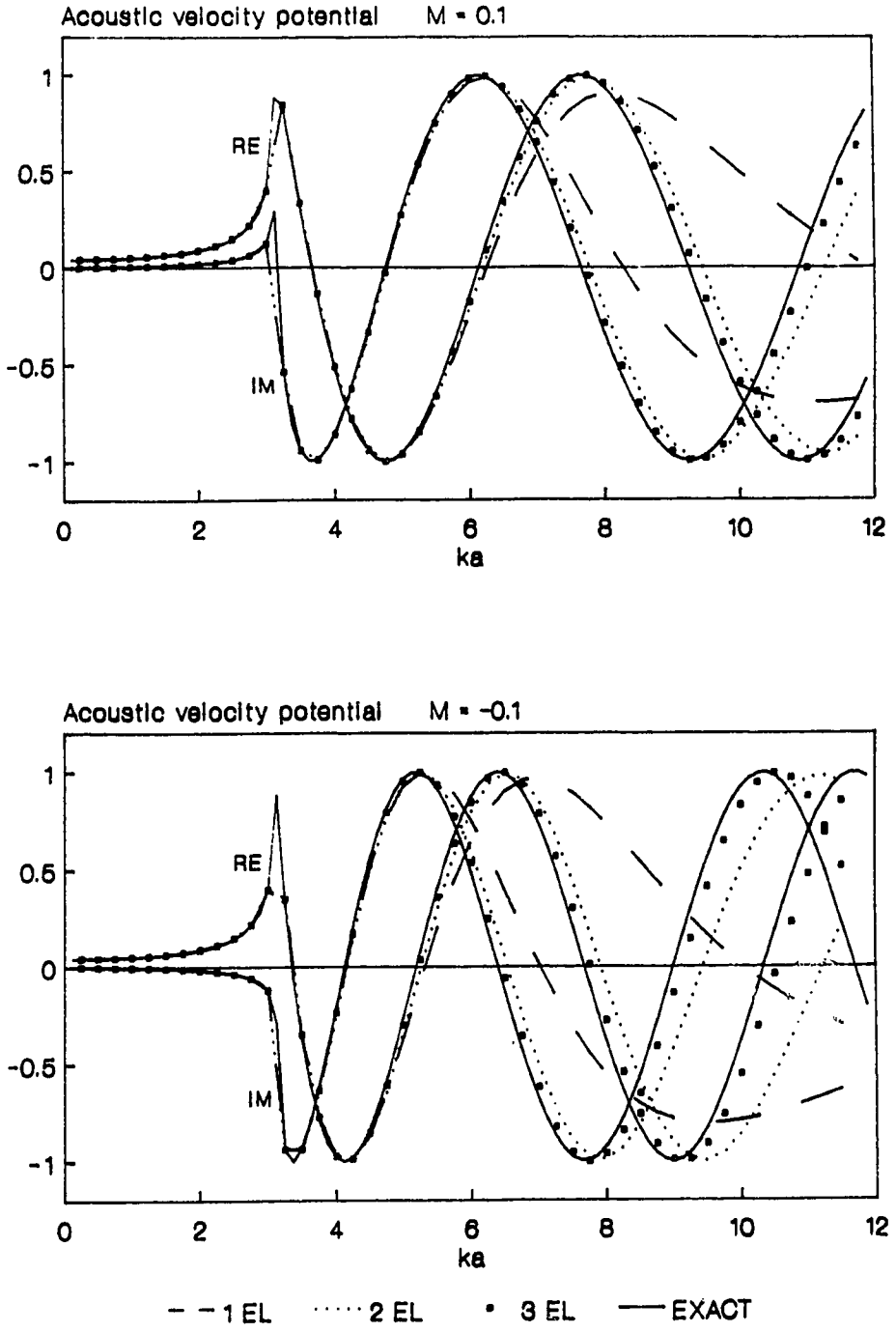

Figure 3.11 Outlet First Cross Mode Acoustic Velocity Potential for a Straight Duct with a Uniform Flow

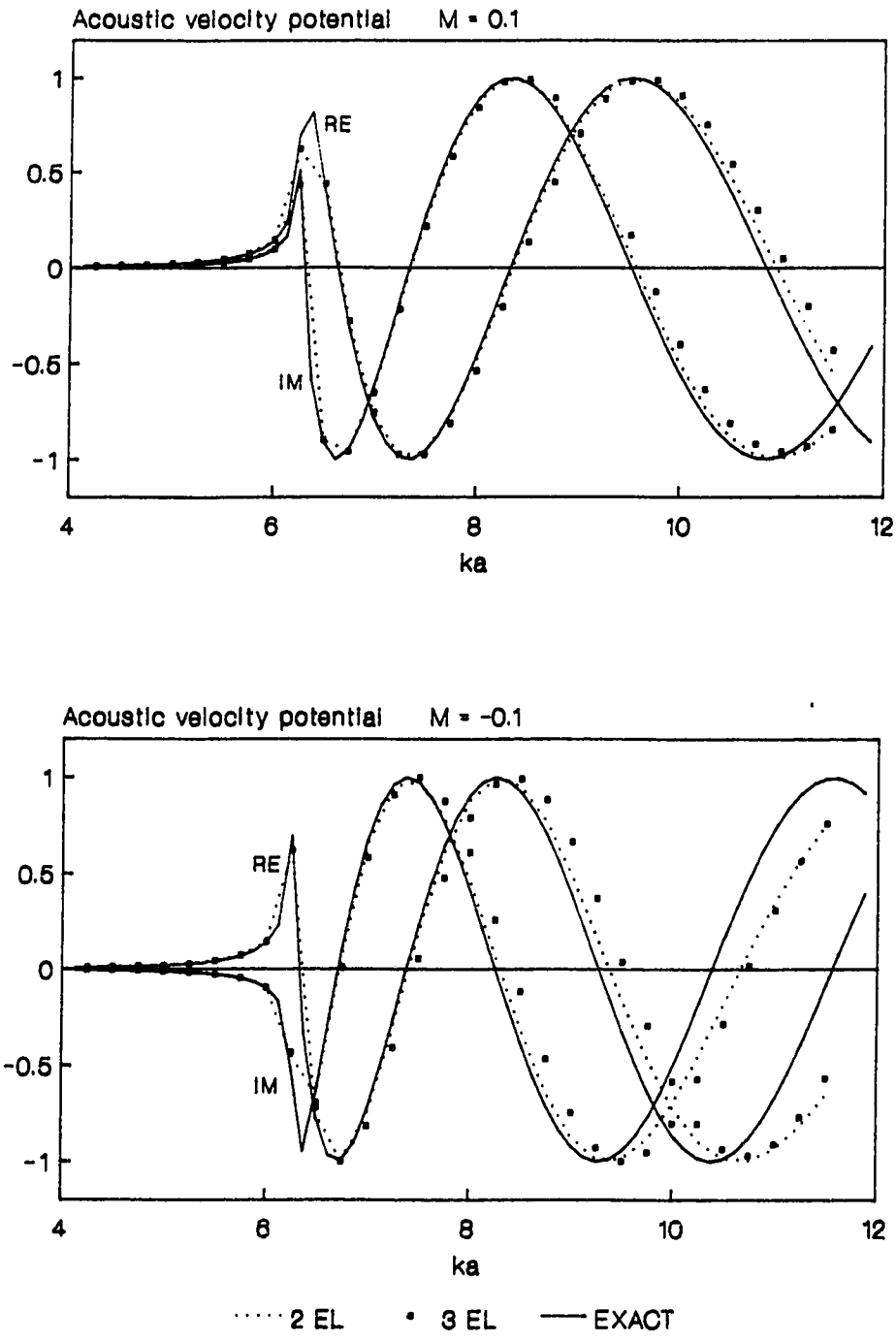

Figure 3.12 Outlet Second Cross Mode Acoustic Velocity Potential for a Straight Duct with a Uniform Flow

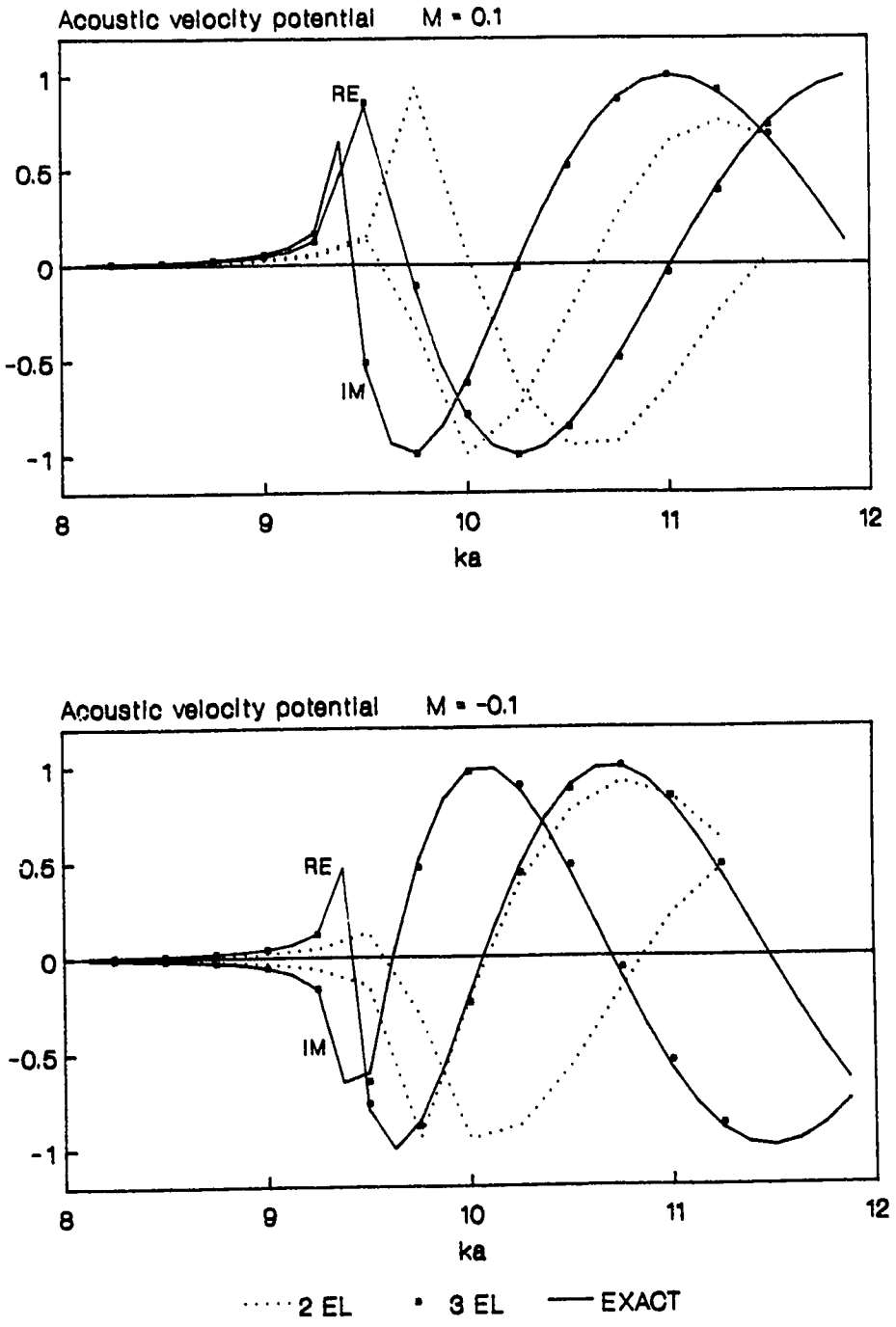

Figure 3.13 Outlet Third Cross Mode Acoustic Velocity Potential for a Straight Duct with a Uniform Flow

for the negative Mach number case. As with no flow, the results for the second cross mode are generally more accurate with two elements across the duct width than with three. Also the model with three elements across the duct width gives accurate results for ka approaching 12 for Mach numbers of 0.1 and -0.1.

In the next chapter considerable work is done in terms of prediction of sound power transmission loss and reflection loss for plane waves and the first cross modes in duct system components. The computer program used has been checked here for the straight duct problem considered above. The results for the reflected and transmitted plane wave with a plane wave incident were identical (to the number of significant digits shown) to that given in Table 3.3 which were based on constraining inputs and outputs to plane waves only. The predicted transmission loss TL and reflection loss RL of the first cross mode with the first cross mode incident are shown in Table 3.6 for the FEM models with one, two and three elements across the duct width. Comparing Table 3.3 and Table 3.6 shows that the one element model gives slightly smaller errors in TL and RL for the first cross mode than for the plane wave. The model with three elements across the duct width generally gave smaller errors for the plane wave than for the first cross mode. The results for the model with two elements across the cross-section were mixed and varied depending on the frequency parameter ka. One puzzling difference between these two tables is that in Table 3.3 for the plane wave propagation, the transmission losses for positive and negative Mach numbers were identical. For the first cross mode case, this is also true for the models with one element and three elements across the duct width. For the case of two elements across the duct width for ka of 10 and 12 (above the cut-on of the third cross mode) the results differ for positive and negative Mach numbers. The following paragraph sheds some light on the reason for this difference.

TABLE 3.6 Convergence for First Cross Mode Propagation in a Straight Duct with the First Cross Mode Incident

ka	One element		Two elements		Three elements	
	RL in dB	TL in dB	RL in dB	TL in dB	RL in dB	TL in dB
$M = 0.0$						
4	53.4	0.000020	53.2	0.000021	59.7	0.000005
6	18.2	0.066406	24.5	0.015551	55.4	0.000013
8	7.9	0.773874	17.2	0.082667	33.8	0.001802
10	4.1	2.110010	35.1	0.090083	21.7	0.029458
12	2.6	3.524120	9.7	0.549310	21.8	0.028759
$M = 0.1$						
4	47.6	0.000111	90.5	0.000000	59.1	0.000015
6	18.9	0.055575	24.1	0.017700	45.7	0.000167
8	8.1	0.730077	17.8	0.071480	32.4	0.002716
10	4.2	2.061800	35.0	0.211718	21.9	0.028250
12	2.6	3.480470	10.6	0.482457	22.6	0.023499
$M = -0.1$						
4	44.3	0.000111	54.3	0.000000	50.4	0.000015
6	19.0	0.055575	23.7	0.017700	42.6	0.000167
8	8.1	0.730077	17.9	0.071480	31.7	0.002716
10	4.2	2.061800	35.3	0.030151	21.9	0.028250
12	2.6	3.480470	10.7	0.441922	22.8	0.023499

In duct components, such as elbows for example, a specified single incident mode can be scattered, contributing sound power to many transmitted and reflected modes. In a straight rigid duct of uniform cross-section a given incident mode will continue to propagate as a single mode with no contributions to other modes. To check how well this was predicted with the straight duct FEM models, the TL and RL values were predicted for the first, second and third cross modes with the plane wave incident and for the plane wave, second and third cross modes with the first cross mode incident. With only one exception the TL and RL gave what appeared to be more or less random values between 280 dB and 320 dB with little dependence on the frequency, Mach number or number of elements. The one exception was the case of two elements across the duct cross-section when looking

at the TL and RL for the third cross mode with the first cross mode incident. For this case with ka greater than the third cross mode cut-on frequency, the RL values ranged from between 10 and 30 dB and TL ranged from 20 to 50 dB depending on frequency and Mach number. Thus, for this case, significantly more sound energy was transferred from the incident first cross mode to the transmitted and reflected third cross mode. This would explain the observation in the previous paragraph concerning different transmission losses for positive and negative Mach numbers at ka values of 10 and 12 in Table 3.6 for the case of two elements across the duct width.

The reason for this apparent transfer of sound energy to a higher mode in this FEM model is not completely understood. Certainly based on Figure 3.9, the model with two elements across the duct width predicts rather poorly the outlet third cross mode velocity potential with the third cross mode incident. With reference to the modal matrix for the two element cross-section model given by Equation 3.124, the modal vectors for the first and third cross modes are given by the second and fourth columns of this matrix. The only difference between these modes is the slope terms given in the third row. However the check of the orthogonality of the mode shapes, discussed in the last paragraph of Section 3.3.1 where the matrix $[\Phi]^T[P][\Phi]$ was evaluated, did not show any higher values for the off-diagonal terms involving the first and third cross modes than for other modes.

Subsequent work concentrates on predictions for the plane wave and first cross mode in duct components up to $ka = 6$. Based on the results for the straight duct problem with undistorted elements, the use of one element across the duct width should give acceptable results up to $ka = 4$, and two elements across the width should give acceptable results up to $ka = 6$ even with a Mach 0.1 flow opposite the direction of acoustic propagation.

3.3.3 Propagation in a Duct Bend

The previous straight duct problem tested the acoustic-flow model with undistorted elements. In this section, the propagation in a duct bend using distorted elements is considered. The bend selected is basically a 90 degree mitred elbow in which the inner corner of the bend has been rounded with a radius of one half the duct width. This bend was considered by Cabelli [10] using eight-noded quadrilateral isoparametric elements.

Meshes with four to thirty-one ISOHERM12 elements were used as shown in Figure 3.14. The normal derivative of ϕ' was constrained to zero at nodes on the bend walls to reduce the number of global DOF. The 113 DOF model was close to the maximum size model that could be handled on the desktop computer system used. The results with no flow for a plane wave incident are shown in Figure 3.15. $R_{\phi'}$ is the acoustic velocity potential reflection coefficient defined as the ratio of the reflected mode velocity potential to the incident mode velocity potential both taken at the duct wall. The transmission coefficient $T_{\phi'}$ is defined similarly base on the ratio of the transmitted and incident modes. The upper and lower graphs on the left hand side of the figure are for the reflected and transmitted plane wave modes and the graphs on the right side are for the reflected and transmitted first cross modes. This also applies to Figure 3.16 in which the results for the first cross mode incident are shown.

Cabelli's results [10] were digitized from a blown up photocopy of the figure and thus may not be reproduced precisely. There is, however, good agreement with the 113 DOF model. There are significant differences between the 113 DOF model and the 52 DOF model for some of the graphs above $ka = 4$, indicating that three elements are needed across the duct in this case to accurately model up to

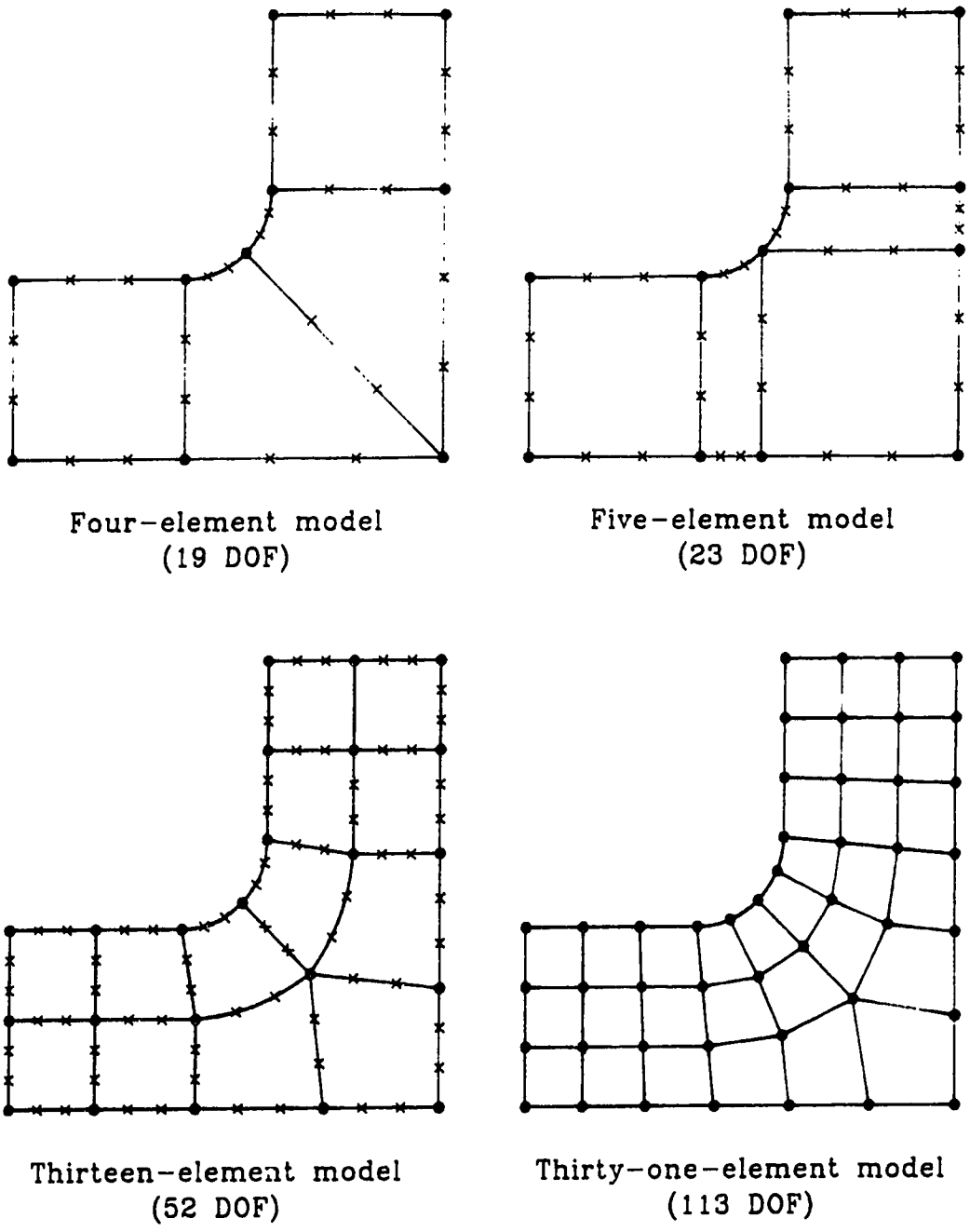

Figure 3.14 ISOHERM12 Finite Element Models for a Duct Bend

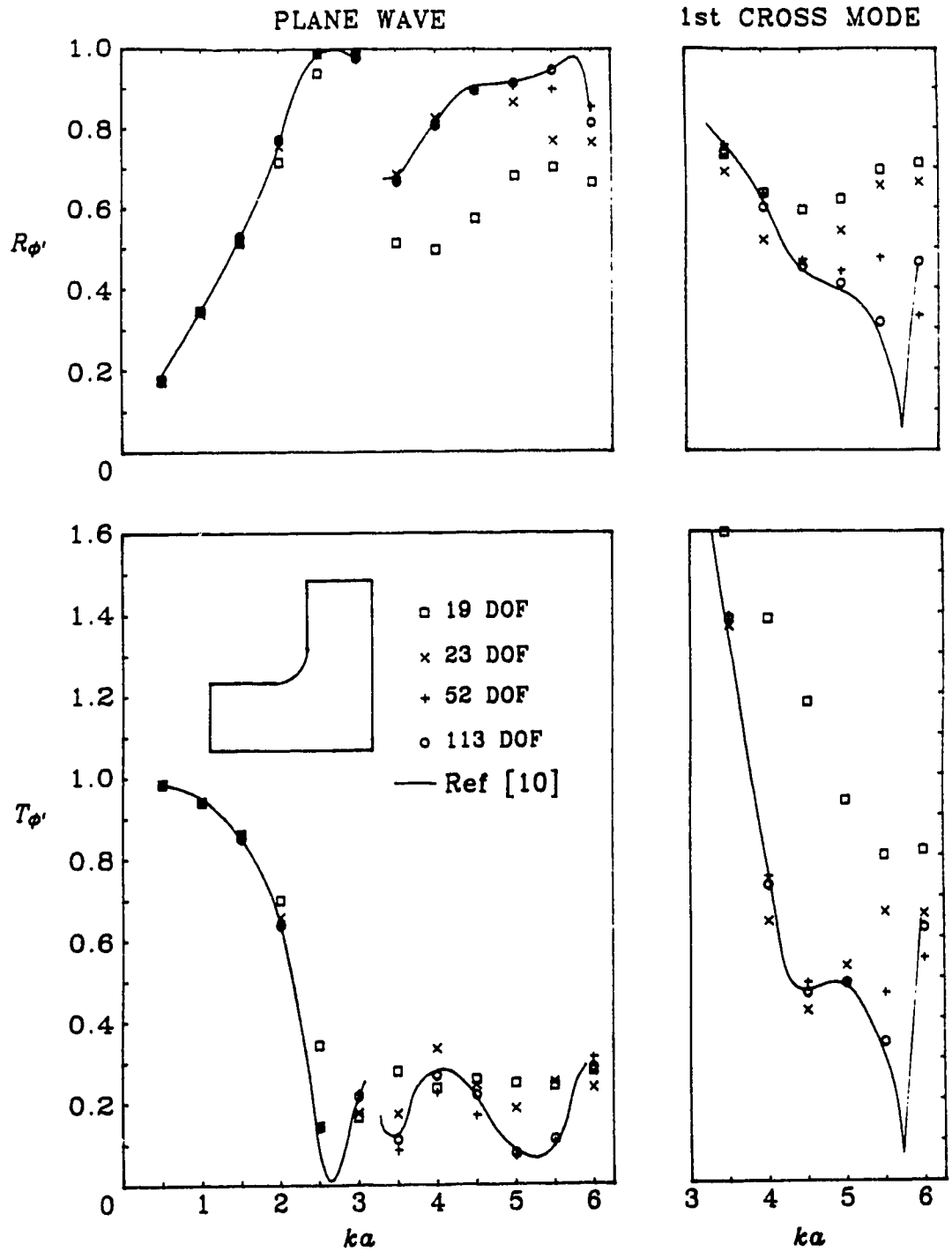

Figure 3.15 Bend Reflection and Transmission Coefficients with a Plane Wave Incident

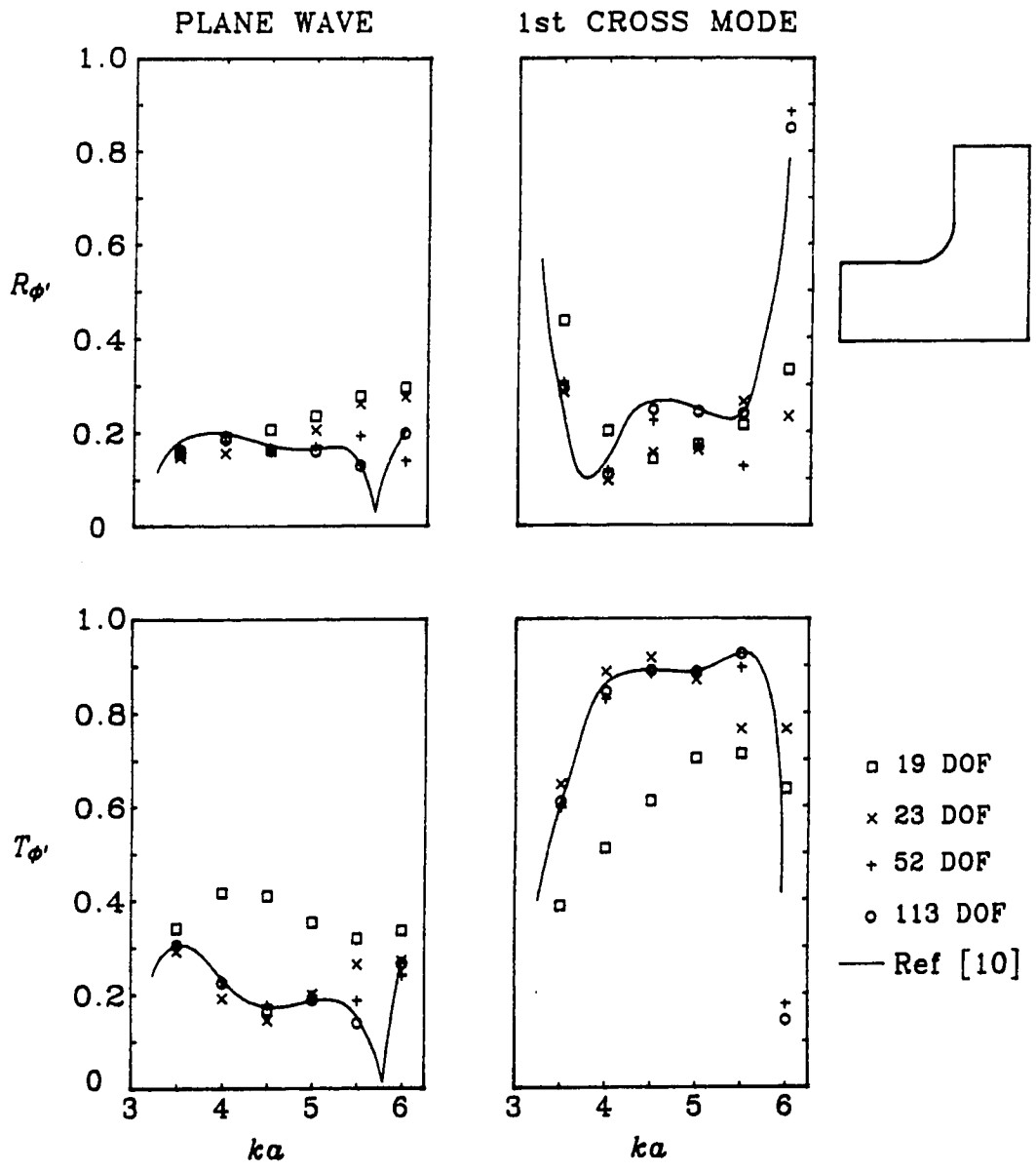

Figure 3.16 Bend Reflection and Transmission Coefficients with the First Cross Mode Incident

$ka = 6$. The need to use a finer mesh compared to that required for the straight duct problem is probably due to the decreased accuracy of the distorted elements but may also be partly due to the more complex acoustic field within the bend.

Two of the four elements in the 19 DOF model were severely distorted and this model gave poor results even at some points below the first cross-mode cut-on at $ka = \pi$. The five-element 23 DOF model, on the other hand, gave generally good agreement up to $ka = \pi$ and in fact reasonable agreement up to $ka = 4$ with the plane wave incident and to $ka = 5$ with the first cross mode incident. In this model three of the five elements are square and two elements long rectangles distorted along one of the short boundaries.

Cabelli also gave results for compressible potential mean flows, with inlet Mach numbers of 0.25 and 0.4, and local Mach numbers reaching 0.39 and 0.66 respectively at the inner curved corner. Some results were obtained for this elbow at these Mach numbers even though the incompressible flow model used was probably not very accurate at these velocities. The resulting transmission and reflection coefficients obtained typically showed smaller effects of flow and poor correlation with Cabelli's results.

The work of Peat [45] uses the same incompressible flow equations as used in this thesis and gives results for a duct expansion chamber for $M = 0.1$. The results are however for an axisymmetric cylindrical expansion chamber, assume plane wave inputs and outputs, given in terms of the muffler four-pole parameters and given only up to $ka = 1.5$. Peat's paper does not give any results for the no-flow case and thus does not indicate how significantly the flow influences the four-pole parameters at this Mach number. It was decided that the limited verification that might be obtained was not at this stage worth the effort necessary to modify

the current computer programs to handle this problem. Thus the straight duct results with flow and the bend results with no flow have been relied on as sufficient verification of the prediction model.

CHAPTER IV

PROPAGATION OF SOUND THROUGH DUCT BENDS AND JUNCTIONS

4.1 Introduction

This chapter is mainly concerned with sound propagation through duct junctions—a subject which has been given relatively little attention in the research literature. The physical problem to be considered is a duct bend or junction connected to infinitely long or anechoically terminated straight ducts. It is assumed that the incident mode or modes in one of the connecting ducts is known. The resulting reflected modes in this duct and the transmitted modes in the other connecting ducts are then to be determined. For example, with a plane wave incident, reflection and diffraction effects within the duct bend or junction can cause the scattering of the plane wave acoustic energy into higher order reflected and transmitted modes.

Considerable work has been done by Cabelli [9], [10] and Cabelli and Shepherd [13], [14], [51] on duct bends of various geometries using both the FDM and the FEM. Two bends are considered in this chapter to examine certain aspects of application of the ISOHERM12 element. The remainder of the chapter is concerned with application of this element to duct junctions or branch points.

4.2 A Mitred 90 Degree Bend

In Section 3.3.3 the propagation of sound through a duct bend requiring the use of distorted ISOHERM12 elements was considered. Three elements were required across the duct cross-section to accurately model the elbow reflection and transmission coefficients up to $ka = 6$ where a is the duct width. This model contained 31 elements and was close to the maximum size model that could be handled on the desk top computer system used for this work. In the subsequent work on duct junctions, it was anticipated that models with three elements across the duct width would be too large for the computer system used. A mitred 90 degree bend has been considered here to test the accuracy of the undistorted element for modeling this type of problem.

The finite element meshes which were used are shown in Figure 4.1. These are identified based on the number of elements across the duct width. In the earlier work of Craggs and Stredulinsky [23] and Stredulinsky, Craggs and Faulkner [55], on elbows and bends within a piping network, finite element models were constrained to plane waves at the interface to connecting straight ducts. The finite element meshes were extended one duct width from the bend or junction to allow some distance for the evanescent modes generated at the bend or junction to decay so that a plane wave boundary condition could be applied at the interfaces. For the case of flow it is also necessary to extend the finite element domains into the connecting straight ducts to model the inlet and outlet flow fields. The prediction method developed in Chapter III includes the evanescent modes in the boundary conditions at the connecting duct interfaces so that, in the absence of flow, it should be possible to shorten the inlet and outlet finite element domains and thus reduce the size of the finite element model. A model with a shortened inlet and outlet called

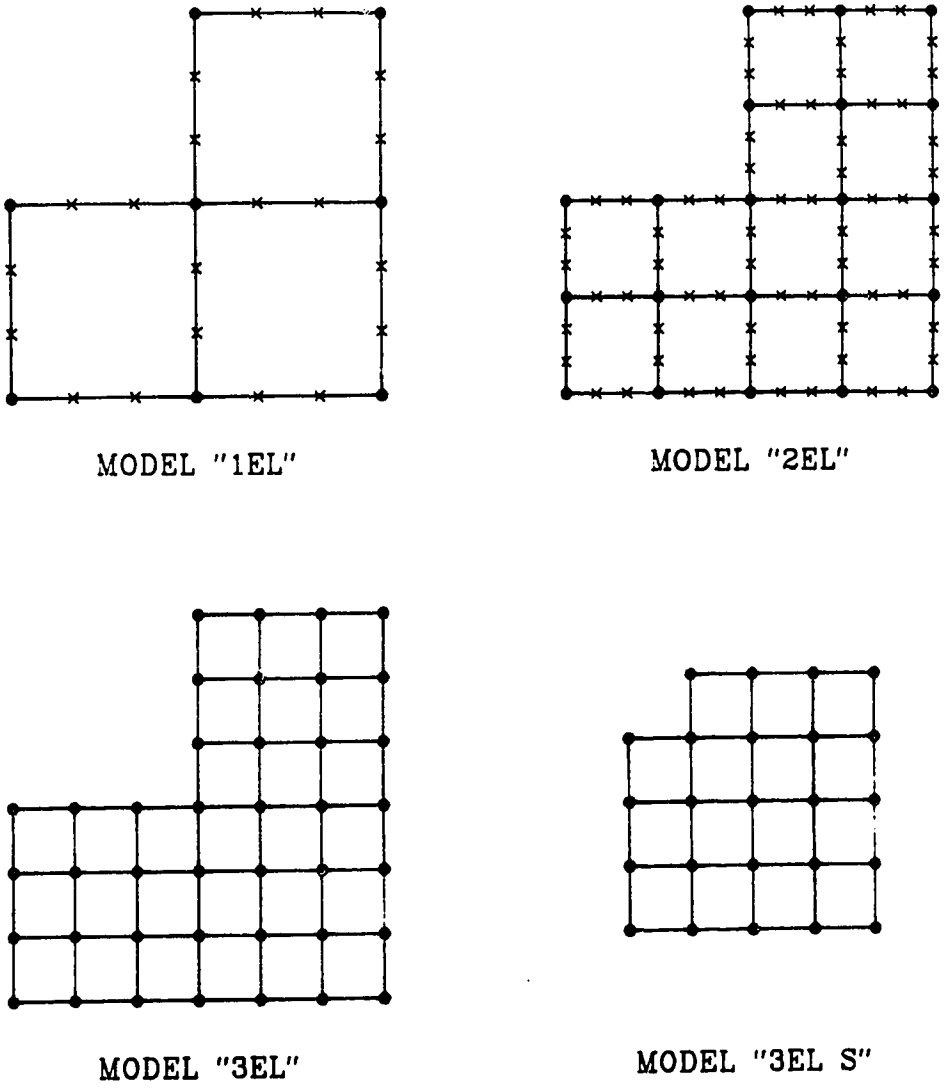

Figure 4.1 ISOHERM12 Meshes for a 90 Degree Mitred Duct Bend

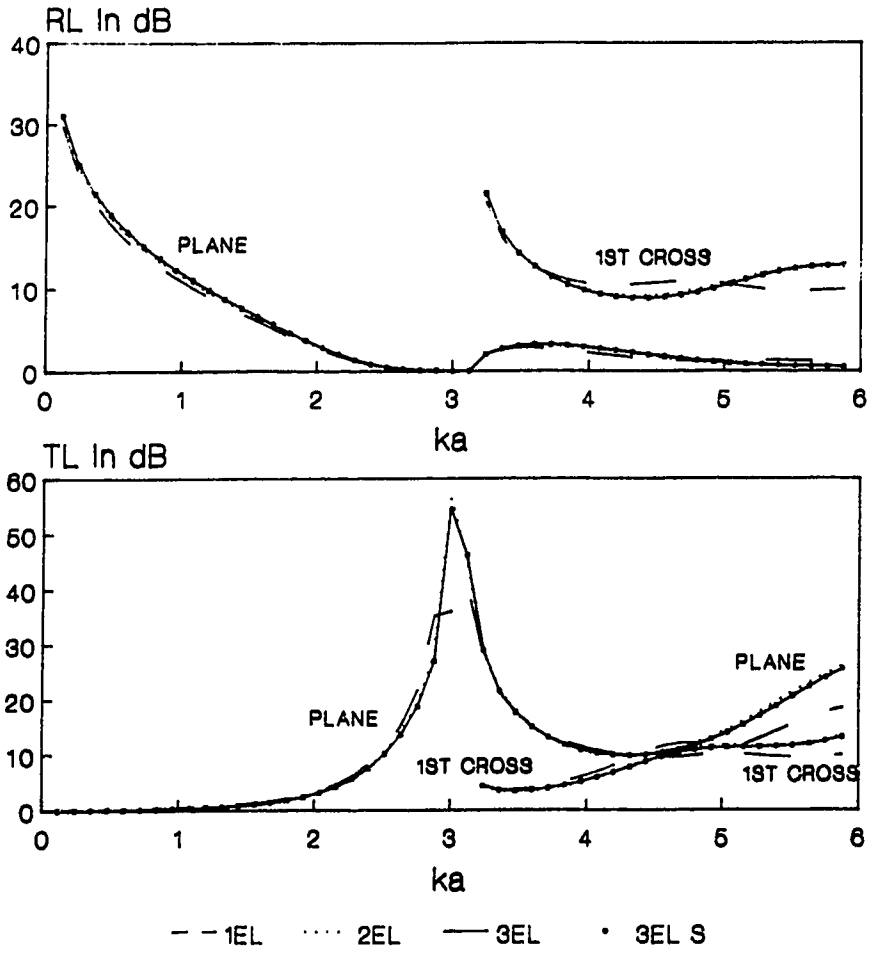

Figure 4.2 Convergence of FEM Models of a 90 Degree Mitred Bend with No Flow and a Plane Wave Incident

model "3EL S" is given in Figure 4.1. It may be possible to reduce this model further to a square composed of nine elements. This would require that the inlet and outlet boundaries be linked at one node—a condition not included in the prediction method development of Chapter III.

The results obtained using these models are compared, for the case of no flow, in Figure 4.2 for a plane wave incident and in Figure 4.3 with the first cross mode incident. Both the reflection loss RL and the transmission loss TL for the plane wave and first cross mode components are shown. The results for

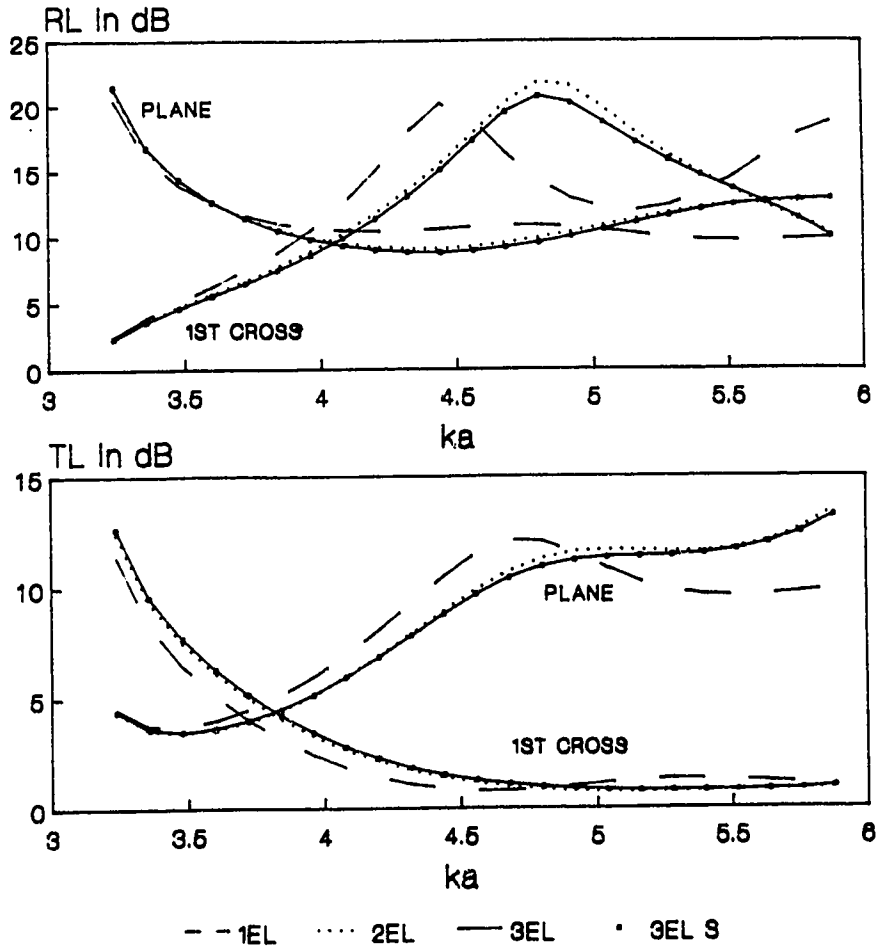

Figure 4.3 Convergence of FEM Models of a 90 Degree Mitred Bend with no Flow and the First Cross Mode Incident

the model "1EL" with one element across the duct width differ significantly from the other models. The "2EL" and "3EL" models differ generally by less than one decibel with differences reaching a maximum of 1.3 dB for the reflection loss with the first cross mode incident and ka between 4.5 and 5. The differences between the "3EL" and reduced "3EL S" models was 0.03 dB or less over the frequency range considered. Thus these results would indicate that undistorted element models with two elements across the duct cross-section should give acceptable results for $ka < 6$. Also in the absence of flow the results indicate that it is not necessary to extend the

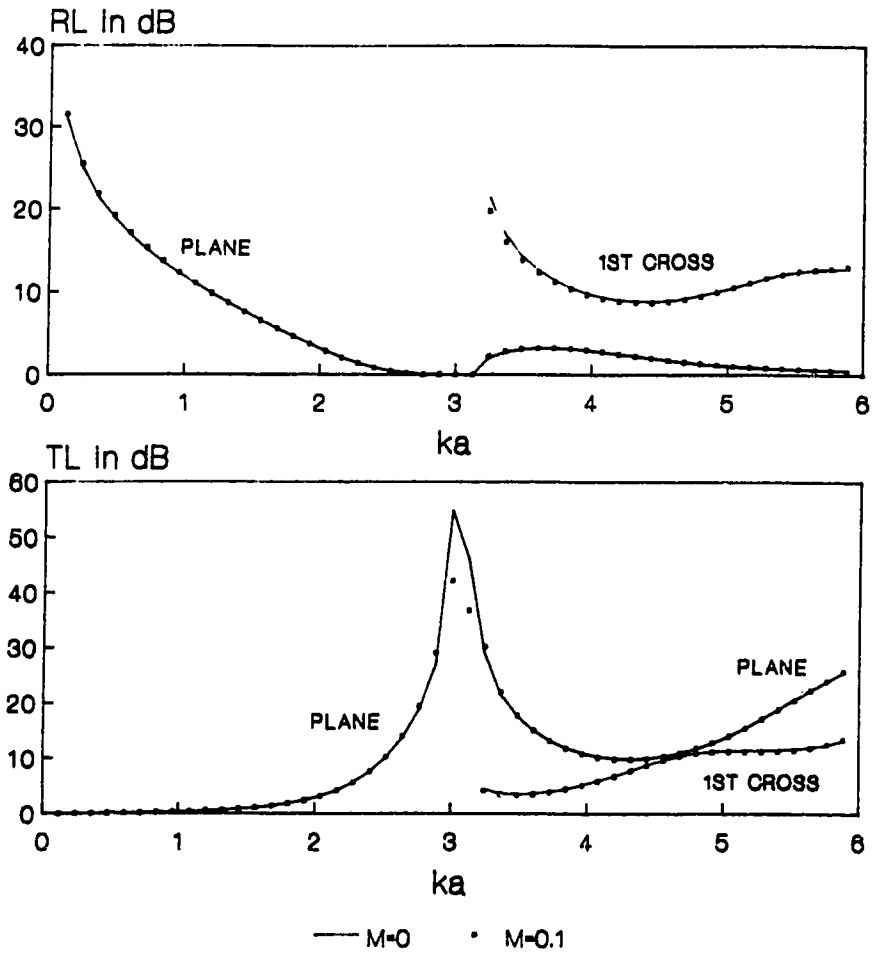

Figure 4.4 Propagation Characteristics of a 90 Degree Mitred Bend with Flow and a Plane Wave Incident

finite element models into the connecting straight ducts (with the restriction that the current prediction method requires that the connecting duct surfaces must be separated).

The velocity potential flow solution for this bend is likely to differ significantly from the actual flow field, since in a real flow, separation is likely to occur at the mitred inner corner. The effect of the potential flow on the propagation characteristics of the bend is shown in Figure 4.4 for a plane wave incident and in Figure 4.5 for the first cross mode incident. In these graphs the reflection loss *RL*

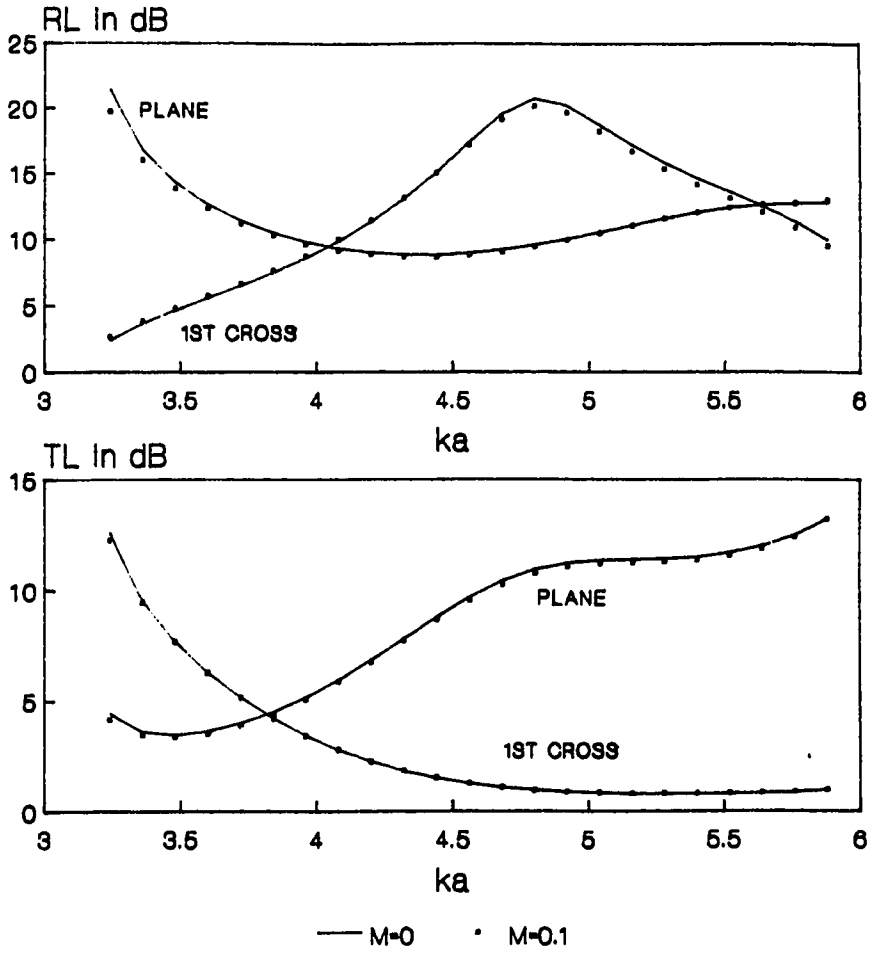

Figure 4.5 Propagation Characteristics of a 90 Degree Mitred Bend with Flow and the First Cross Mode Incident

and the transmission loss TL for no flow are compared to the case with flow with an inlet and outlet Mach number of 0.1 moving in the same direction as the acoustic wave. The effect of flow appears to be very small except near the cut-on frequency of the first cross mode where the plane wave transmission loss with a plane wave incident has changed by approximately 10 dB. The largest differences seem to occur where RL and TL are large—where relative differences in small sound power values are compared.

4.3 A Curved 90 Degree Bend with Turning Vane

The bend to be considered in this section is a 90 degree curved bend with an inner radius of $0.5a$ and an outer radius of $1.5a$, so that the width of the connecting straight ducts is a. A thin rigid turning vane subtending an angle of 90 degrees has been included in the bend for the case with the vane at a radius of $0.875a$ and for the case of the vane at $1.125a$. This bend was considered by Cabelli [9] using the FDM for values of ka up to 3. Without the vane in place, this type of bend has a small transmission loss over this frequency range. With the vane in place, the bend shows a significant peak in transmission loss at a frequency well below the cut-on frequency for the first cross mode in the connecting straight duct.

The finite element meshes used to model these bends are shown in Figure 4.6. Initially models with two elements across the duct width were used. Also, along the turning vane including the end nodes of the vane, the boundary condition that the acoustic velocity normal to vane be zero was used to constrain the acoustic velocity potential derivative nodal degrees of freedom. The reflection and transmission loss results for this model are shown in Figure 4.7 for a turning vane at a radius of $0.875a$, and in Figure 4.8 for a turning vane at a radius of $1.125a$ under the legend item "2ELC". It was then noted that there were significant differences between the predictions with this model and the results of reference [9]. Predictions were then obtained leaving the derivative nodal degrees of freedom at the ends of the vane unconstrained, increasing the number of global degrees of freedom from 74 to 76 and giving the results referred to as "2EL" in Figure 4.7 and Figure 4.8. A third result was obtained using three elements across the cross-section with shortened inlet and outlet FEM domains and again leaving the nodal quantities at the ends of the vanes unconstrained. This result is referred to as "3EL" in Figure 4.7 and Figure 4.8.

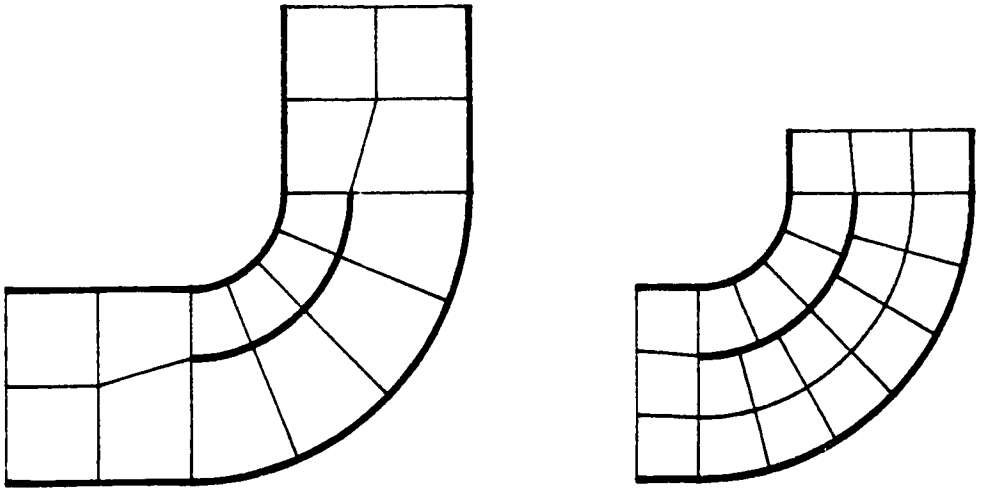

Bend with a turning vane at a radius of 0.875a

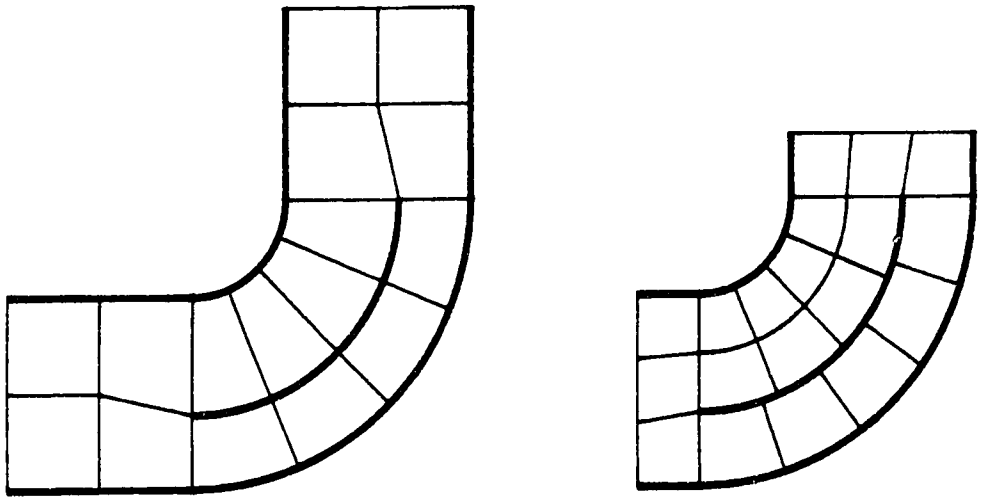

Bend with a turning vane at a radius of 1.125a

Figure 4.6 ISOHERM12 meshes for Curved 90 Degree Bends with an Inner Radius of 0.5*a* and an outer radius of 1.5*a*

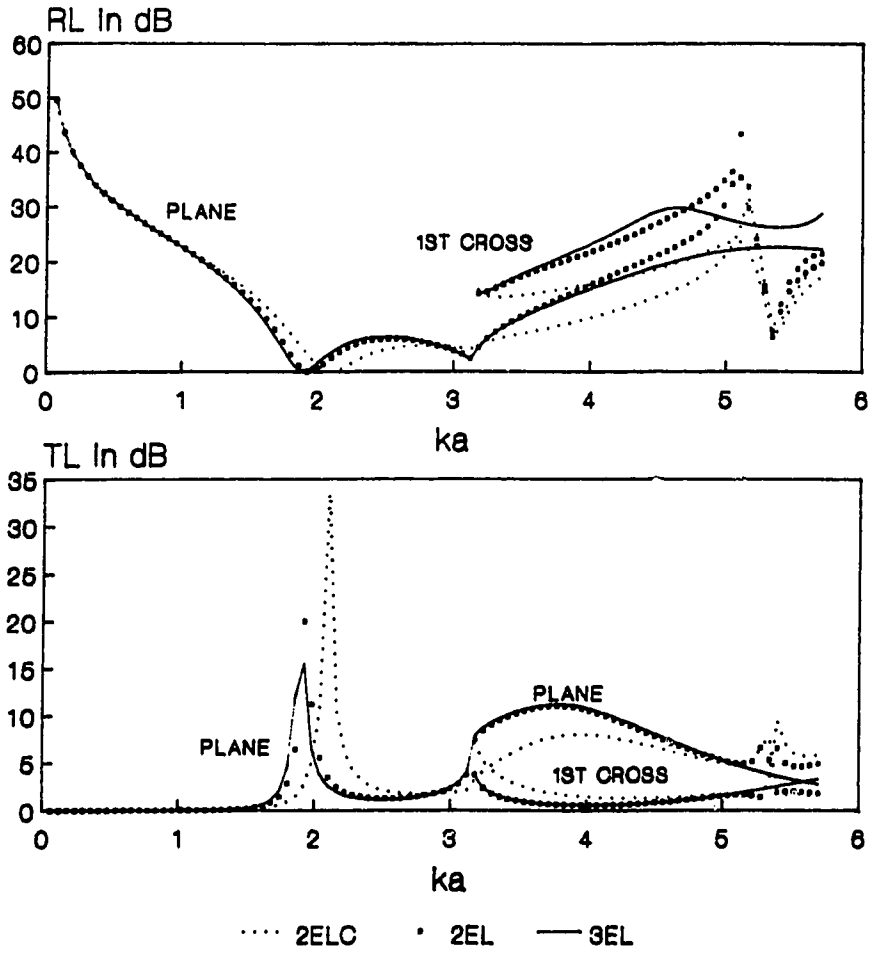

Figure 4.7 Convergence of FEM models for a curved 90 degree bend with a turning vane radius of $0.875a$ and a plane wave incident

These figures show an eight percent shift in ka for the peak in the plane wave transmission loss located at approximately $ka = 2$ in Figure 4.7 and a slightly smaller shift in Figure 4.8 when comparing the "2ELC" and "2EL" results. Also there are significant differences in transmission loss values for these two models above $ka = 1.5$. The "2EL" and "3EL" results are much closer, but still show some shift in the first TL peak and significant differences in the RL values above $ka = 4$ and in TL above $ka = 5$.

These results indicate that even in the range of ka between 1.5 and 2,

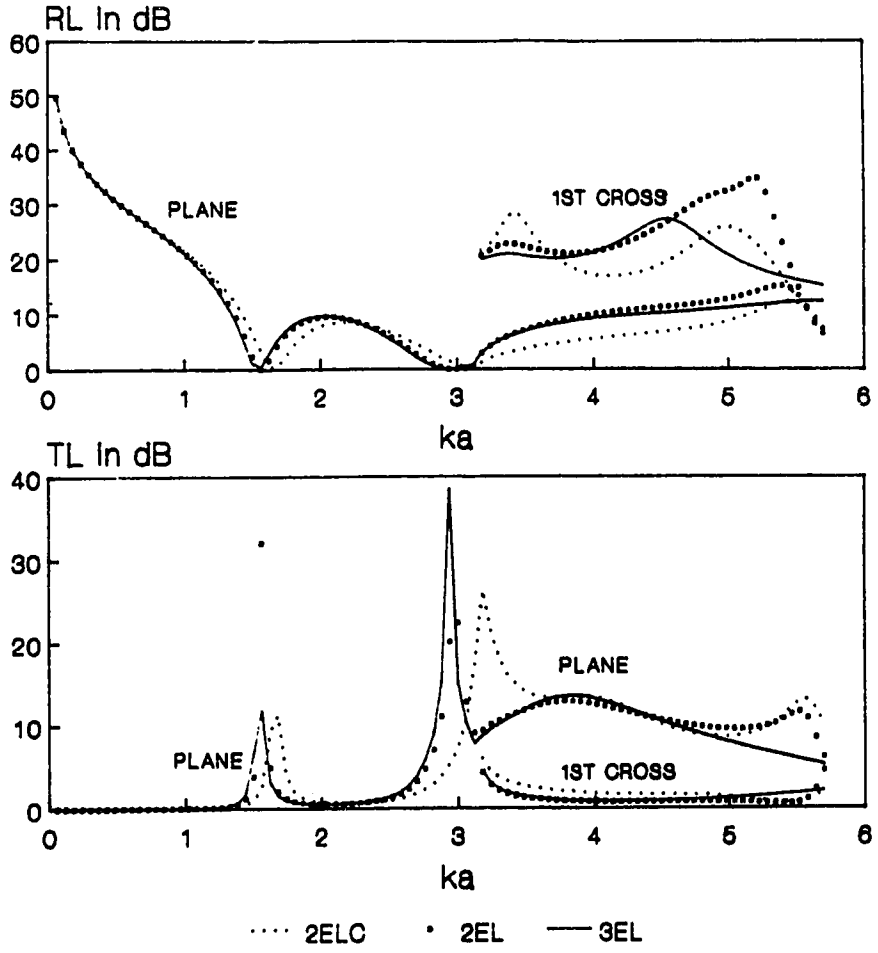

Figure 4.8 Convergence of FEM models for a curved 90 degree bend with a turning vane radius of $1.125a$ and a plane wave incident

the finite models have still not converged, even with three elements across the inlet and outlet width. Based on the previous elbows considered, this was unexpected. The bend with a curved inner corner shown in Figure 3.15, which involved distorted elements, showed good agreement between models with one and two elements across the duct width and insignificant differences between models with two and three elements across the duct width in this frequency range. At present it is not known whether the poorer result for this bend is due to the nature of the distortion of the elements or possibly the more complex sound field created by the presence

of the turning vane. These results alsc confirm, as found in modeling a complex shaped enclosure in Section 2.3.4, that constraining the derivative nodal quantities at boundary discontinuities can over-constrain the FEM models leading to increased errors. Even though the acoustic velocity normal to the vane is zero at end of the vane, in the fluid just beyond the end of the vane there could be a significant acoustic velocity perpendicular to the vane and therefore it is best to leave this node unconstrained and let the implicit boundary condition determine the normal acoustic velocity at the ends of the turning vane.

The FDM predictions of Cabelli [9] and the ISOHERM12 model with three elements across the duct cross-section are compared in Figure 4.9 and Figure 4.10 respectively for the turning vane at a radius of $0.875a$ and $1.125a$. These graphs show the plane wave transmission loss for a plane wave incident. Cabelli's results were digitized from a small figure which was given in terms of the reflection coefficient and the converted to transmission loss values and thus may not be reproduced precisely. Cabelli's results show the first transmission loss peak at a significantly lower frequency than the ISOHERM12 results and probably lower than values to which ISOHERM12 models with finer meshes are likely to converge. It was noted in Cabelli's paper, that using the FDM, the ends of the vane could only be determined to within one mesh space and for the vanes considered, the angle subtended by the vane was between 72 and 90 degrees. His experimental work on other bends with turning vanes consistently showed that the best approximation corresponded to the upper limit. In view of the above, some additional experimental results were obtained using an existing facility at the University of Alberta for measuring duct component transmission loss using the transfer function method of Chung and Blaser [15], [16].

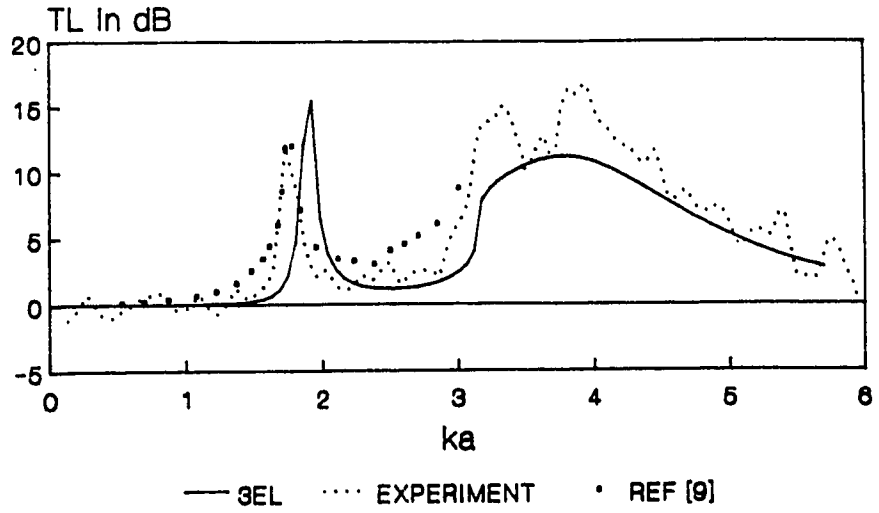

Figure 4.9 Comparison of the FEM with Experiment and the FDM of Reference [9] for the Plane Wave Transmission Loss of a Curved 90 Degree Bend with a Turning Vane at a Radius of $0.875a$

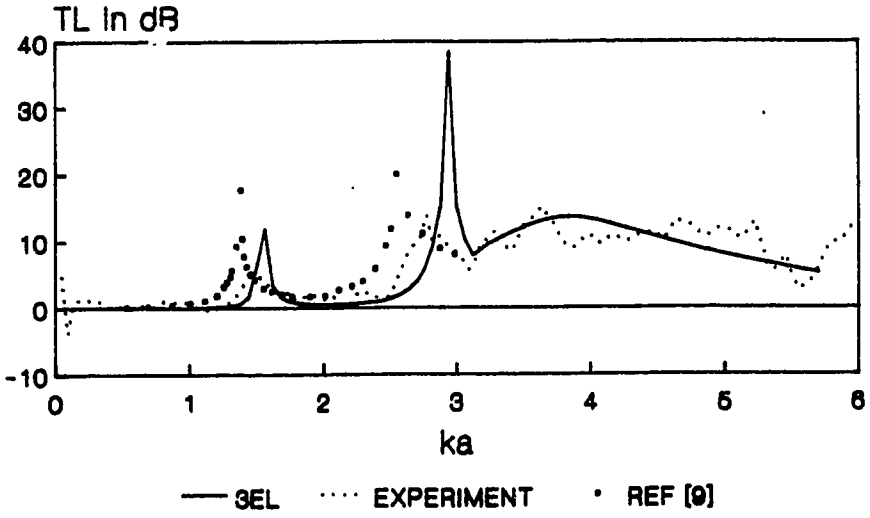

Figure 4.10 Comparison of the FEM with Experiment and the FDM of Reference [9] for the Plane Wave Transmission Loss of a Curved 90 Degree Bend with a Turning Vane at a Radius of $1.125a$

The noise generation apparatus used in this experimental work consisted a white noise source, and amplifier driving an array of four small loudspeakers at the entrance of a straight inlet duct. This inlet duct was connected to the test bend which in turn connected to an outlet duct with an anechoic termination. The measurement apparatus consisted of two 1/4 inch B&K 4145 microphones, a B&K 2807 microphone power supply and a dual channel Nicolet 660A FFT spectrum analyser controlled by an HP Integral computer.

The experimental procedure was developed for measurement of plane wave transmission loss. The speaker array could be configured as a monopole, dipole or quadrapole—for the present measurement the monopole configuration was used to excite mainly the plane wave mode in the inlet duct. Measurement test stations were located upstream and downstream of the test bend. The microphones were located flush to the inner duct wall and spaced 24 mm apart along the axis of the duct, midway across the duct face in the plane of the bend. These measuring points were chosen to be at the nodal plane of the first cross mode so that the plane wave transmission loss measurement could be extended above the cut-on of the first cross mode [1,0] at $ka = \pi$ where a is the width in the plane of the bend. The actual bend considered, had an inner corner radius of 100 mm and outer radius of 300mm, with the turning vane located at either a radius of 175mm or 225mm. The vane was assumed to have zero thickness in the FEM predictions but actually had a thickness of 5mm. The rectangular connecting ducts had an inside dimension of 200 mm in the plane of the bend and 150 mm in the perpendicular dimension. Thus additional cut-on frequencies of $ka = 4.19$ for the [0,1] mode and of $ka = 5.23$ for the [1,1] modes were in the frequency range considered.

The experimental procedure consisted of measuring the acoustic transfer function and auto-spectrum with the two microphones at the upstream measure-

ment station (averaging 192 FFT traces) and then repeating the measurements at the downstream station. This data was transferred and used by the HP Integral computer to calculate transmission loss values. The results for the bend at a radius of $0.875a$ are shown in Figure 4.9. The location of the first experimental transmission loss peak is closer to Cabelli's result than the "3EL" ISOHERM12 model result. For the case of the vane at a radius of $1.125a$ the first peak in the transmission loss is shifted to a lower frequency and both Cabelli's prediction and the ISOHERM12 "3EL" prediction show a second peak at roughly double the frequency at which the first peak occurs. Again Cabelli's FDM result is lower than the FEM result. The peaks in the measured transmission loss curve are smaller than either predicted result and located midway between the predicted peaks.

There is certainly further work needed to resolve the above differences, including using the FEM models with finer meshes (probably requiring the use of a larger computer system) and comparing with FEM models using, for example, the HEX12 element. The actual thickness of the vane could also be modeled, although since this thickness is less than 3% of the duct width this is not expected to have a significant influence.

4.4 Propagation Through Duct Junctions

Compared to the amount of research done on duct bends, there has been relatively little work done on duct junctions where three or more ducts join at a common junction (restricted to three ducts in the present work). Some analytical work has been done for "T" junctions and 90 degree side branches for simple two dimensional rectangular geometries which involve solution of the Helmholtz equation in Cartesian coordinates and boundaries parallel to the coordinate axes. Miles [39] considered a "T" joint of equal width tubes using an electrical circuit analogy which

limited his approach to plane waves and assumed higher order modes decayed over short distances. In Miles' formulation any tube leading into the "T" could be chosen for the incident wave. The plane wave reflection coefficient and the transmission coefficients for the other branches could then be determined. This "T" junction was also considered by von Said [57]. In von Said's work, higher order modes were considered. An incident plane wave or the first cross mode were considered entering the stem of the "T" and the total reflection coefficient and transmission coefficient for the symmetric outlet ducts determined up to the cut-on of the fourth cross mode. He did not give individual mode reflection and transmission coefficients.

A different approach is taken by Redmore and Mulholland [46] who used a mode coupling theory to predict the sound pressure in a 90 degree side branch attached to a semi-infinite straight rectangular duct, with a source distribution at one end. This approach assumes that the modal sound field in the main duct is not affected by the presence of the side branch, and that the disturbances caused by this sound field at the common plane between the side branch and the main duct become the source for the sound field in the branch duct.

The subsequent work in this chapter considers the junction problem in which three semi-infinite straight ducts meet at a junction. The incident wave modal mixture approaching the junction along one of the ducts is specified and the reflection loss (the transmission loss for the reflected wave) and the transmission losses for each mode in the two outlet ducts determined. Before considering some specific applications two low frequency approximations will be considered in the next section. These are used in subsequent sections for comparison purposes.

4.4.1 Low Frequency Approximations for Duct Junctions

At very low frequencies, the classical approach to plane wave propagation in pipes can be used to predict the reflection and transmission losses for pipes connected at a common junction point. The acoustic pressure is assumed to be constant in the vicinity of the junction so that the combined incident wave plus reflected wave acoustic pressures in the inlet duct can be taken as equal to the acoustic pressures of the transmitted plane waves in the two outlet ducts (only valid at low frequencies). These conditions and the continuity condition that the incident plus reflected wave volume velocities must equal the combined outlet wave volume velocities, can be used to determine the reflected and transmitted plane waves for a given incident plane wave. The reflection loss RL for the reflected wave in the inlet duct and the transmission losses TL_1 and TL_2 for the two outlet ducts are then given by

$$RL = 10\log_{10}\left(\frac{1}{R}\right) = 10\log_{10}\left[\left(\frac{S_{\text{in}} + S_{\text{out1}} + S_{\text{out2}}}{S_{\text{in}} - S_{\text{out1}} - S_{\text{out2}}}\right)^2\right] \tag{4.1}$$

$$TL_1 = 10\log_{10}\left(\frac{1}{T_1}\right) = 10\log_{10}\left[\frac{(S_{\text{in}} + S_{\text{out1}} + S_{\text{out2}})^2}{4S_{\text{in}}S_{\text{out1}}}\right] \tag{4.2}$$

$$TL_2 = 10\log_{10}\left(\frac{1}{T_2}\right) = 10\log_{10}\left[\frac{(S_{\text{in}} + S_{\text{out1}} + S_{\text{out2}})^2}{4S_{\text{in}}S_{\text{out2}}}\right] \tag{4.3}$$

where R and T are the reflection and transmission coefficients respectively and S_{in}, S_{out1}, and S_{out2} are the cross-sectional areas of the inlet and two outlet ducts. Note that the results are only dependent on the duct cross-sectional areas and are independent of the junction geometry and frequency.

The work of Miles [39] for a "T" junction leads to ninefold infinity of simultaneous equations. If all higher order modal terms are dropped from these

equations, as a first approximation the following equations are obtained for a 90 degree side branch with ducts all of width a. A matrix Y can be formed as

$$[Y] = \begin{bmatrix} \frac{1}{\tan ka} & \frac{1}{\sin ka} & -\frac{1}{ka} \\ \frac{1}{\sin ka} & \frac{1}{\tan ka} & -\frac{1}{ka} \\ -\frac{1}{ka} & -\frac{1}{ka} & \frac{1}{\tan ka} \end{bmatrix} \tag{4.4}$$

where k is the wave number and a is the duct width, then let $[Z] = [Y]^{-1}$. A matrix $[C]$ can then be defined by

$$[C] = \begin{bmatrix} [I] & -[Z] \\ [Z] & [I] \end{bmatrix} \tag{4.5}$$

where [I] is the identity matrix. Also a column vector $\{D\}$ can be defined by

$$\{D\} = \begin{Bmatrix} -1 \\ 0 \\ 0 \\ Z_{11} \\ Z_{12} \\ Z_{13} \end{Bmatrix} \tag{4.6}$$

where Z_{11}, Z_{12} and Z_{13} are elements of the first column of $[Z]$. These can be used to form the linear system of equations

$$[C]\{\beta\} = \{D\} \tag{4.7}$$

which can be solved for the vector β containing the real and imaginary parts of the pressure reflection and transmission coefficients. The reflection loss and transmission loss value TL_{br} for the side branch and TL_{ct} for the continuing straight duct are then

$$RL = 10\log_{10}\left(\frac{1}{(\beta_1)^2 + (\beta_4)^2}\right) \tag{4.8}$$

$$TL_{\mathrm{br}} = 10\log_{10}\left(\frac{1}{(\beta_3)^2 + (\beta_6)^2}\right) \tag{4.9}$$

$$TL_{\mathrm{ct}} = 10\log_{10}\left(\frac{1}{(\beta_2)^2 + (\beta_5)^2}\right). \tag{4.10}$$

4.4.2 FEM Predictions for a 90 Degree Equal Width Side Branch

The first duct junction to be considered was a 90 degree side branch in a rectangular duct with a side branch having the same cross-section dimensions as the main straight duct. This junction was modeled in two dimensions using the ISOHERM12 meshes show in Figure 4.11. Based on the ninety degree mitred elbow results of Section 4.2, it was anticipated that the use of two elements across the cross-section would give acceptable accuracy up to $ka = 6$. The computer used did not have sufficient memory to handle the problem with three elements across the duct width if the finite element domain was extended one duct width into each connecting straight duct. The model "3EL S", with shortened inlet outlet finite element domains was used to check the convergence of the FEM models for the no-flow case. With reference to Figure 4.11, the incident wave was taken to enter the left hand duct. A wave could then be reflected back down this inlet duct and waves could be transmitted out the side branch and the continuing main duct to the right of the FEM model.

The RL and TL values predicted by the ISOHERM12 models with no flow and a plane wave incident are shown in Figure 4.12 as a function of ka based on the duct width. "PL" in the legend refers to the reflected and transmitted plane wave components and "1X" refers to the first cross mode components. Except close to the cut-on of the first cross mode at $ka = \pi$ for the reflection loss RL, the difference between the "2EL" and "3ELS" curves is less than one decibel. Thus the "2EL" models could be used to give a reasonable indication of the junction sound propagation. Similar convergence of FEM models was obtained in Figure 4.13 for the case of the first cross mode incident.

Figure 4.14 compares the plane wave results for the "3EL S" model to the simple low frequency (frequency independent) approximation and Miles [39] first

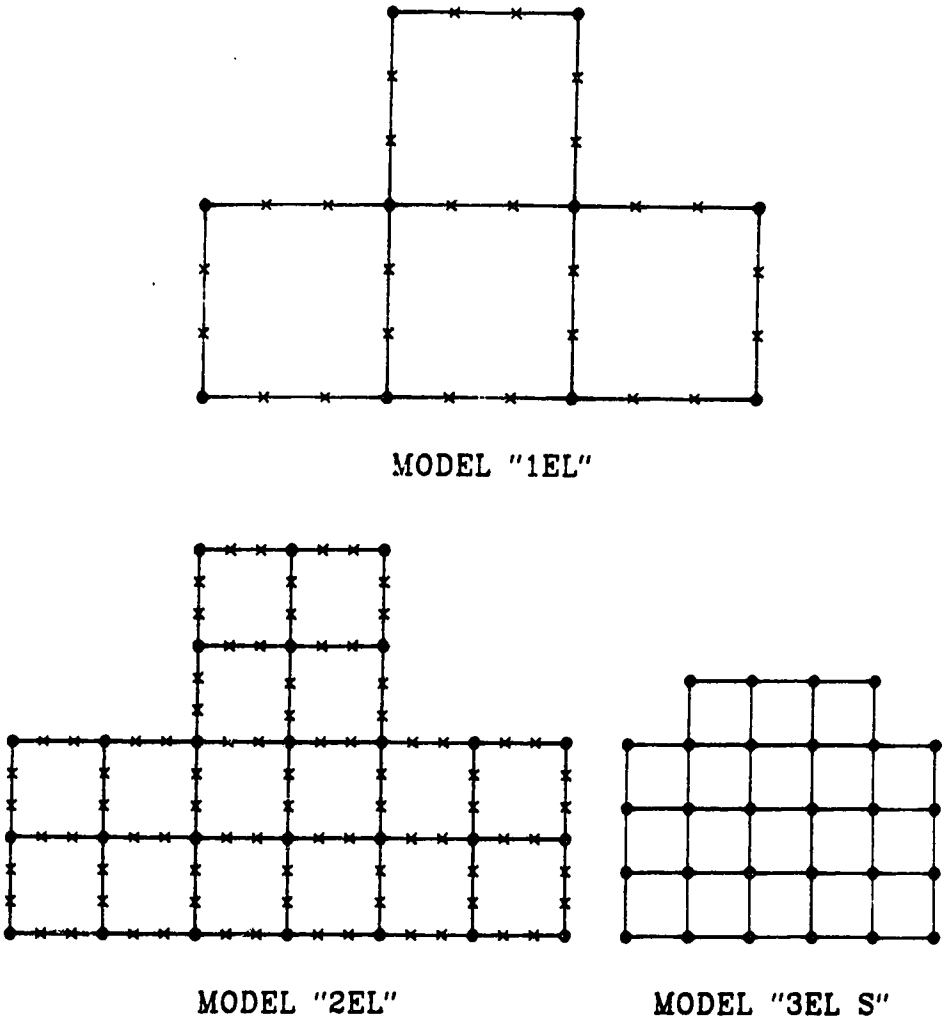

Figure 4.11 ISOHERM12 Meshes for a 90 Degree Side Branch with Equal Width Ducts

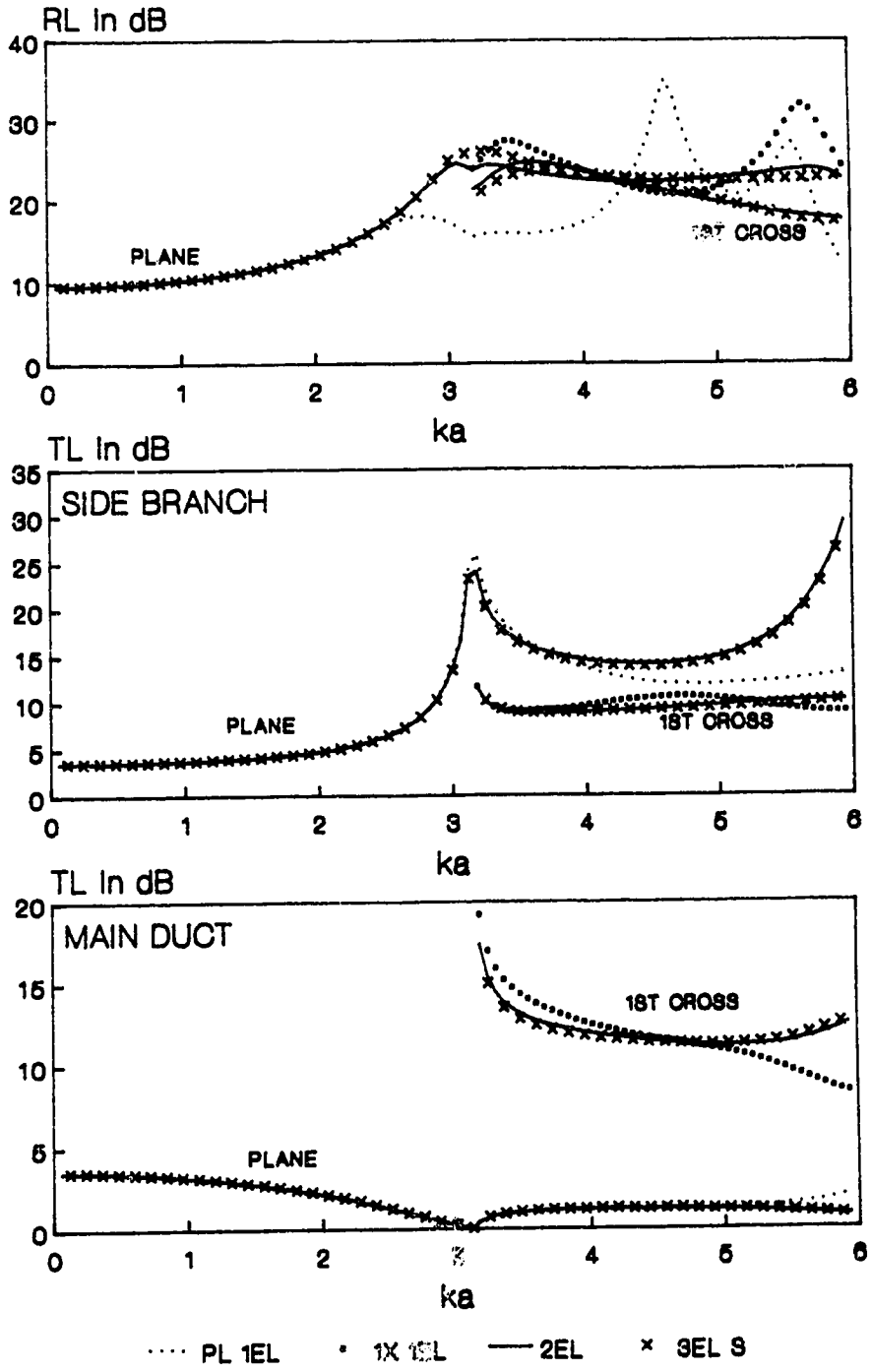

Figure 4.12 Convergence of FEM Models for a 90 Degree Side Branch with the Same Width as the Main Duct and a Plane Wave Incident with No Flow

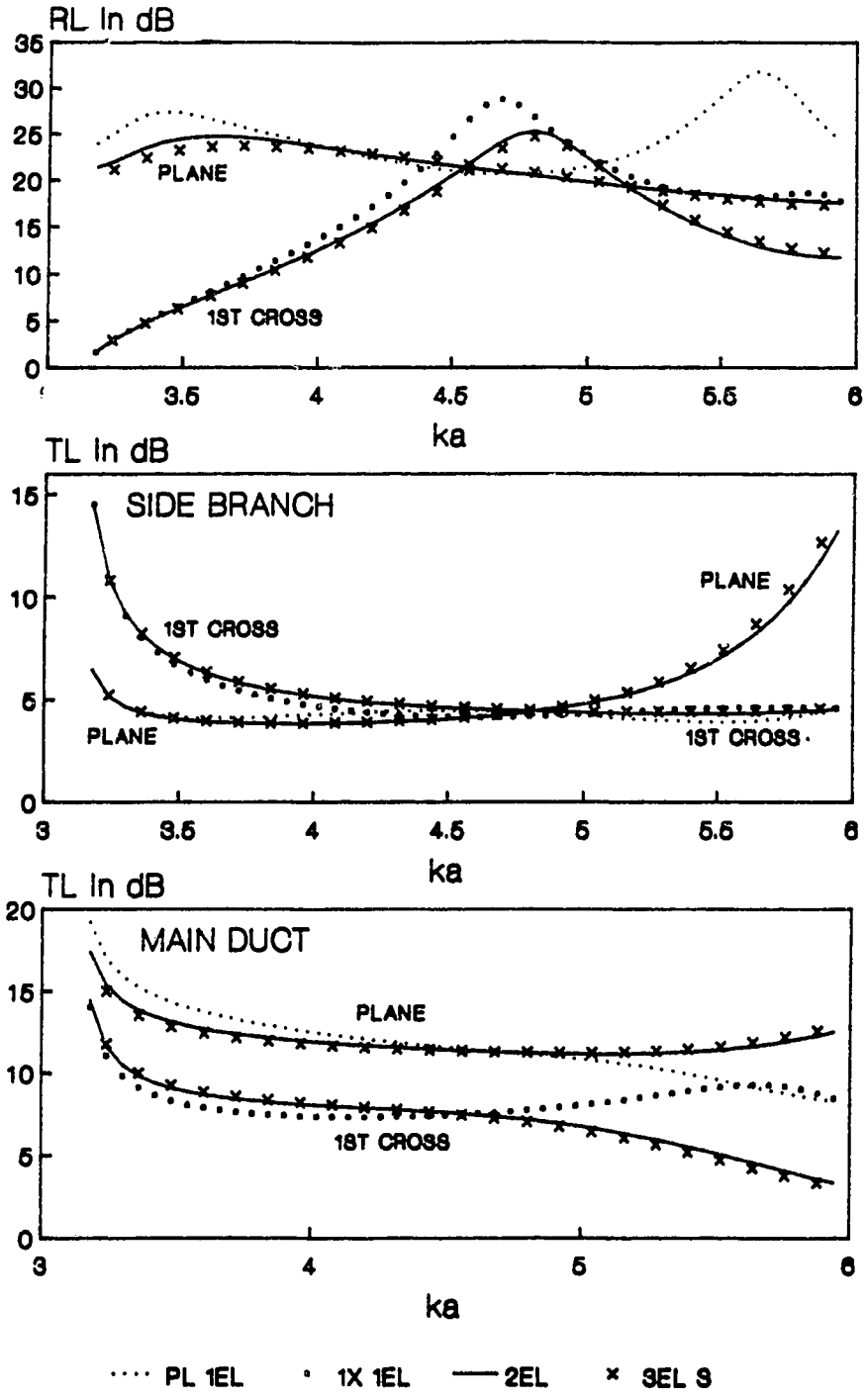

Figure 4.13 Convergence of FEM Models for a 90 Degree Side Branch with the Same Width as the Main Duct and the First Cross Mode Incident with No Flow

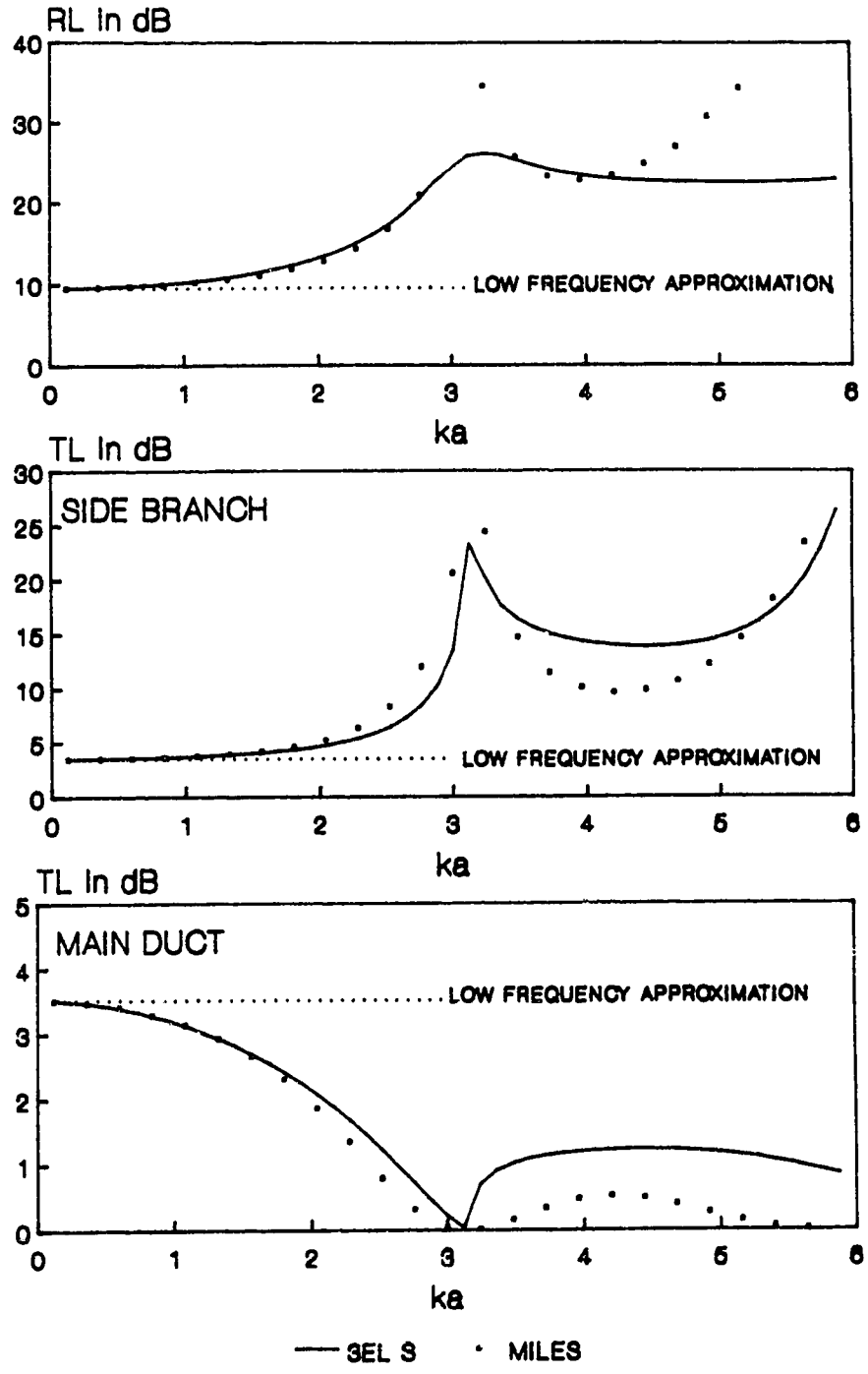

Figure 4.14 Comparison with Other Approximate Solutions for a 90 Degree Side Branch with the Same Width as the Main Duct and a Plane Wave Incident with No Flow

approximation discussed in the previous section. At $ka = 0.06$ the three predictions agree within 0.002 dB. This figure indicates that the simple low frequency result can be used to predict the RL and TL values to within one decibel up to a ka of between 1 an 1.5. Miles results shows good agreement up to $ka = 2$ and generally shows similar trends as the FEM prediction over most of the frequency range considered.

The effect of flow at Mach 0.1 on the propagation characteristics of a 90 degree mitred bend was found to be small as discussed in Section 4.2. For the case of a duct junction its was anticipated that perhaps greater changes due to flow could occur because of the more complex flow field. Certainly a junction leads to many more flow possibilities, including different combinations of flow direction in the connecting ducts and variation of flow rates in the ducts. Two flow configurations have been considered here. In the first (M indicated as positive), the flow has been taken to be in the same direction as the acoustic propagation—into the inlet duct with the incident wave and the out the side branch and the continuing duct. In the second case (M indicated as negative), the flow has been taken in the opposite direction—into the junction from the side branch and the main continuing duct and out the acoustic inlet duct—opposite to the direction of the incident and transmitted acoustic waves.

The ISOHERM12 mesh used to model this junction with flow was the model "2EL" shown in Figure 4.11. As indicated in Section 4.2 for the mitred bend, the potential flow through this junction which contains sharp mitred corners may not be very realistic but hopefully will provide some indication of the flow effects. Also it would have been desirable to also use models with three elements across the duct width in order to check the convergence of the predictions. It was not possible, however, to run a model of this size on the computer system used in this work. The

results for inlet Mach numbers of 0, 0.1 and -0.1 are shown in Figure 4.15 for a plane wave incident, and in Figure 4.16 for the first cross incident, for the case of an equal flow split. With an inlet Mach number of 0.1, since the connecting ducts have the same cross-sectional area, the branch and continuing main duct flows were at Mach 0.05. Excluding the region near the cut-on frequency for the first cross-mode at $ka = \pi$, the changes due to flow were less 0.2 decibel below this frequency and less than one decibel above it.

Figure 4.17 graphs the differences in RL and TL for the cases with flow compared to the no-flow case for a plane wave incident. The graph for the reflection loss shows the most complex variation with frequency. The graphs indicate that the flow has a greater influence on the plane wave transmitted in the branch than on the first cross mode. The opposite appears to occur for the transmission down the continuing main duct—here the flow appears to have little effect on the plane wave transmission but a significant effect on the first cross mode transmission particularly at higher frequencies. Additional results were obtained for the case of only 10% of the flow out the side branch and for the case of 90% of the flow out the side branch. The results for these cases with a plane wave incident are given in Figures 4.18 and 4.19. The comments made concerning the case with 50% branch flow apply for these cases as well. In comparing the 10% and 90% branch flow cases, significant changes were noted in the RL values, most noticeable for the first cross mode. The transmission down the side branch changed very little. The transmission of the plane wave out the continuing main duct did not change significantly however in going from a 10% branch flow to a 90% branch flow there was generally a decrease in transmission of the 1st cross mode down the continuing main duct.

For the first cross mode incident the results for the three flow cases are given in Figure 4.20, Figure 4.21 and Figure 4.22. Again as a function of frequency,

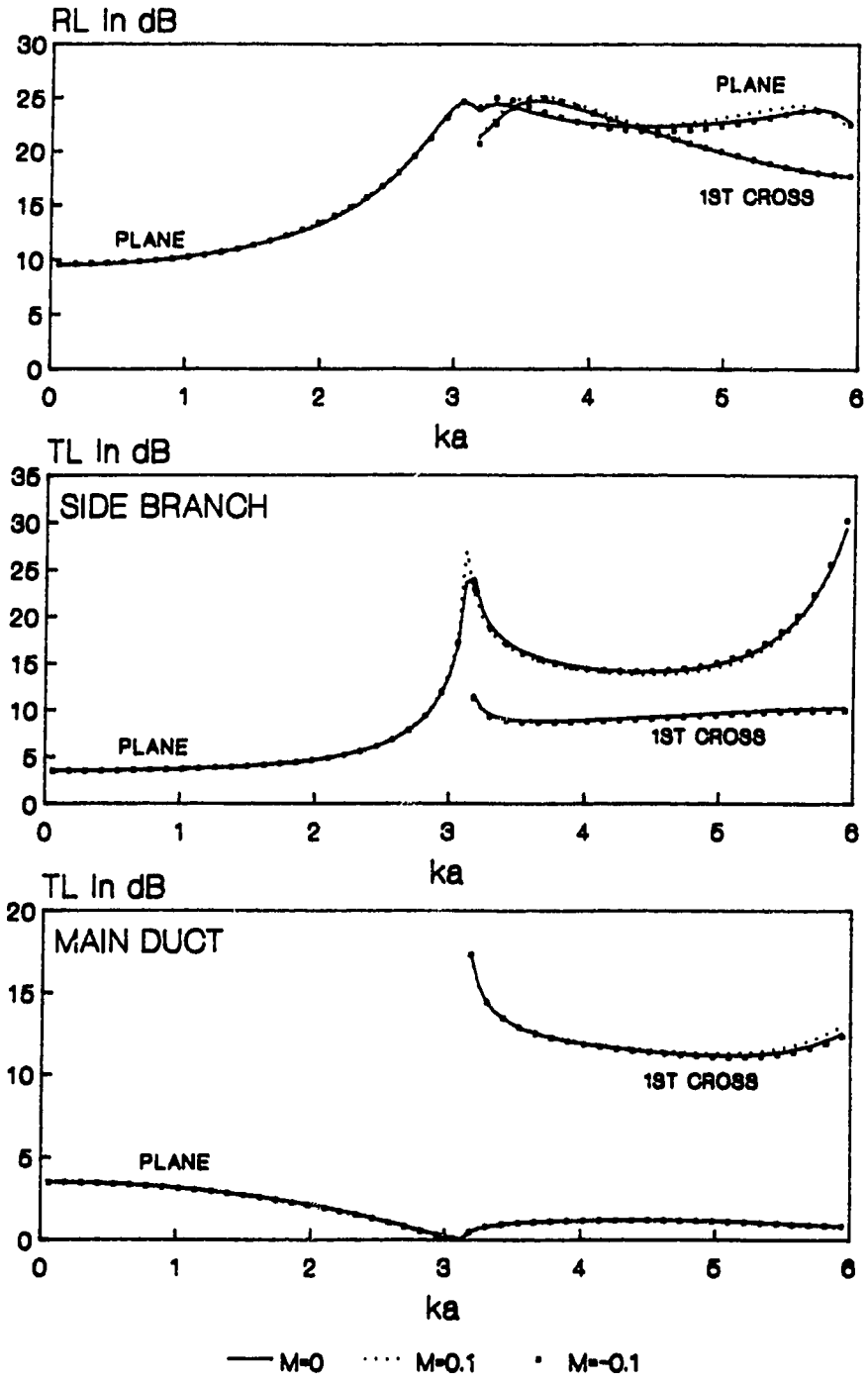

Figure 4.15 The Effect of Flow on Sound Propagation for a 90 Degree Side Branch with the Same Width as the Main Duct and an Equal Flow Split with a Plane Wave Incident

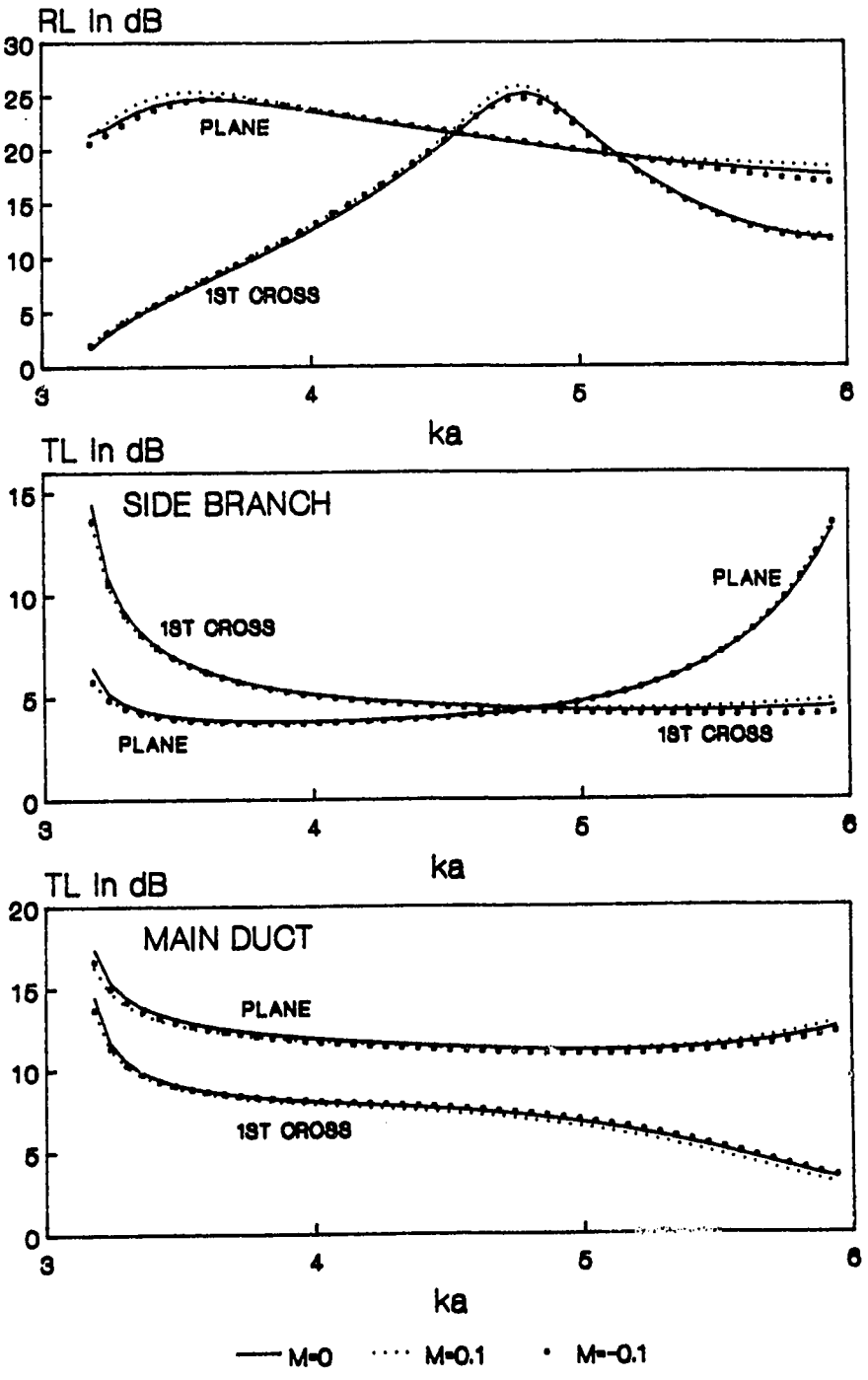

Figure 4.16 The Effect of Flow on Sound Propagation for a 90 Degree Side Branch with the Same Width as the Main Duct and an Equal Flow Split with the First Cross Mode Incident

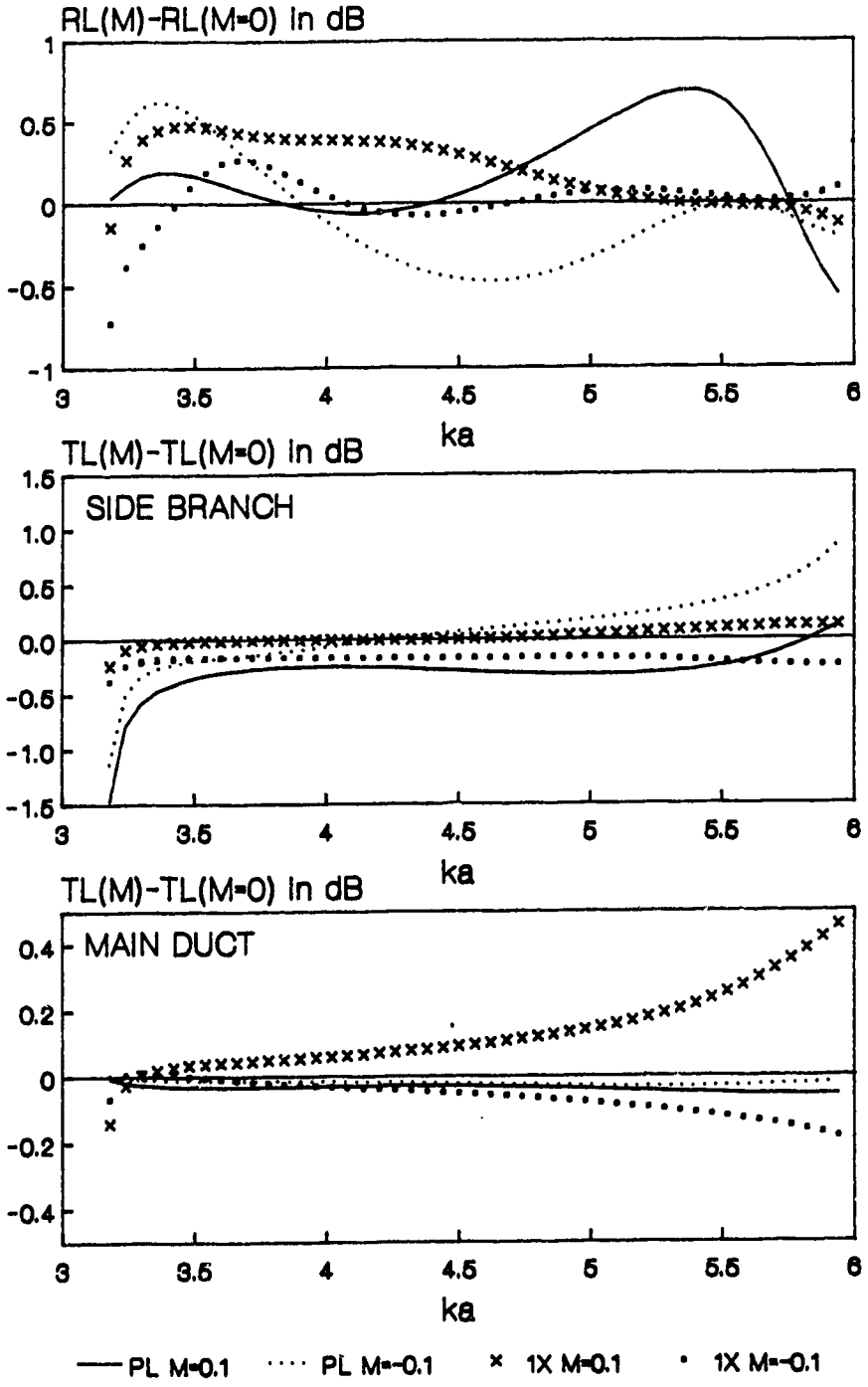

Figure 4.17 Change in RL and TL with respect to the No-flow Case for a 90 Degree Side Branch with the Same Width as the Main Duct and an Equal Flow Split with a Plane Wave Incident

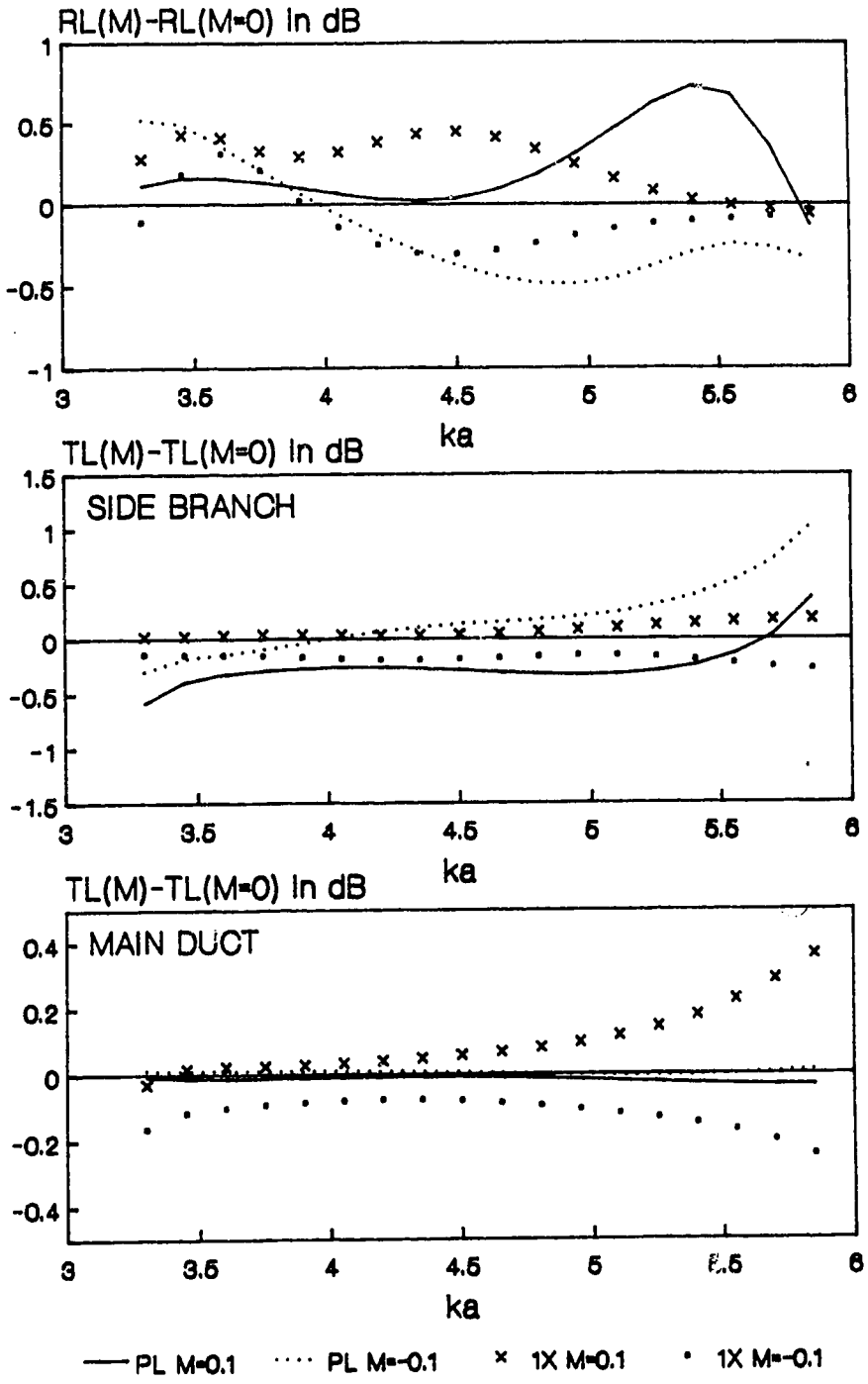

Figure 4.18 Change in *RL* and *TL* with respect to the No-flow Case for a 90 Degree Side Branch with the Same Width as the Main Duct and 10% of the Flow Out the Side Branch with a Plane Wave Incident

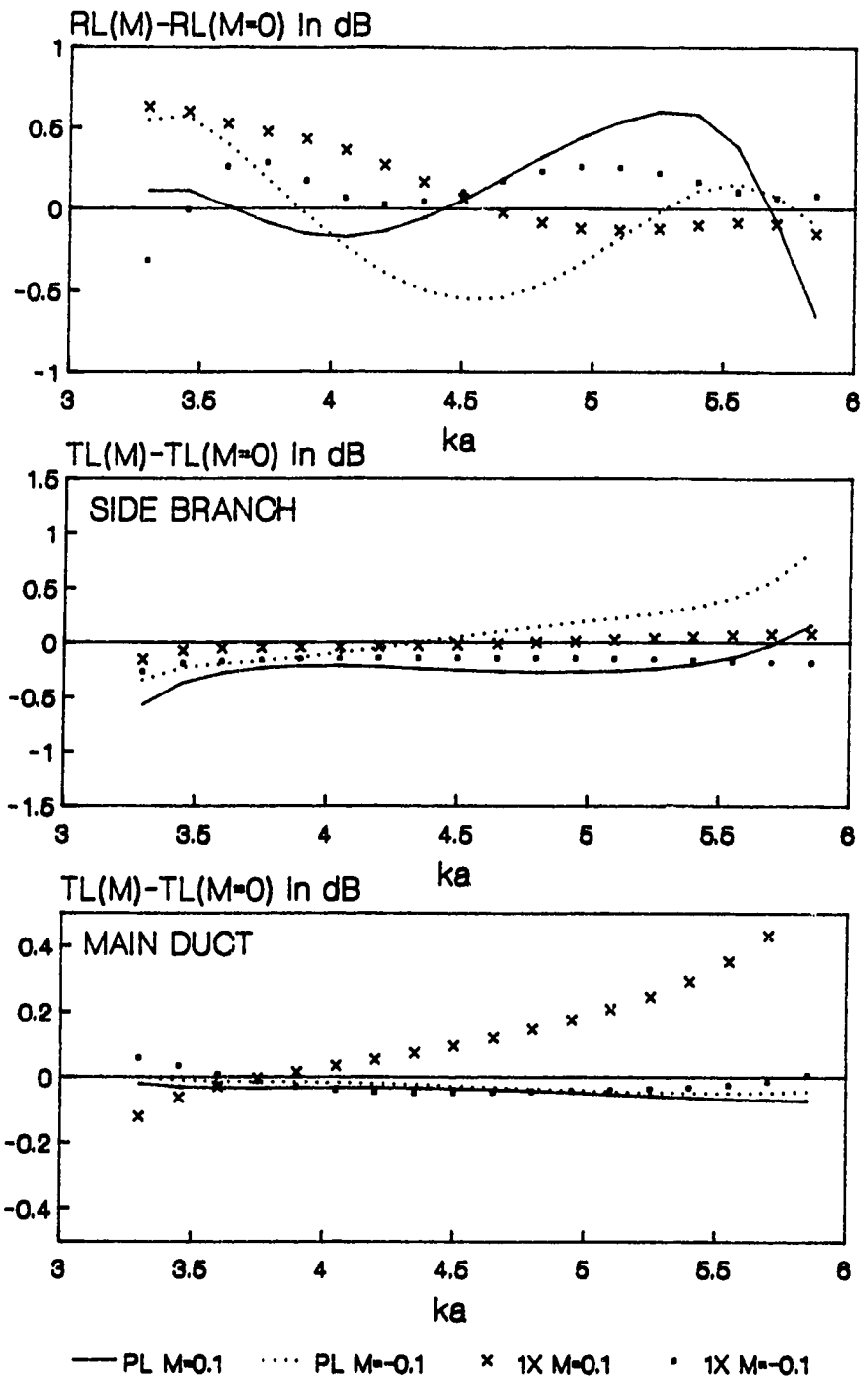

Figure 4.19 Change in RL and TL with respect to the No-flow Case for a 90 Degree Side Branch with the Same Width as the Main Duct and 90% of the Flow Out the Side Branch with a Plane Wave Incident

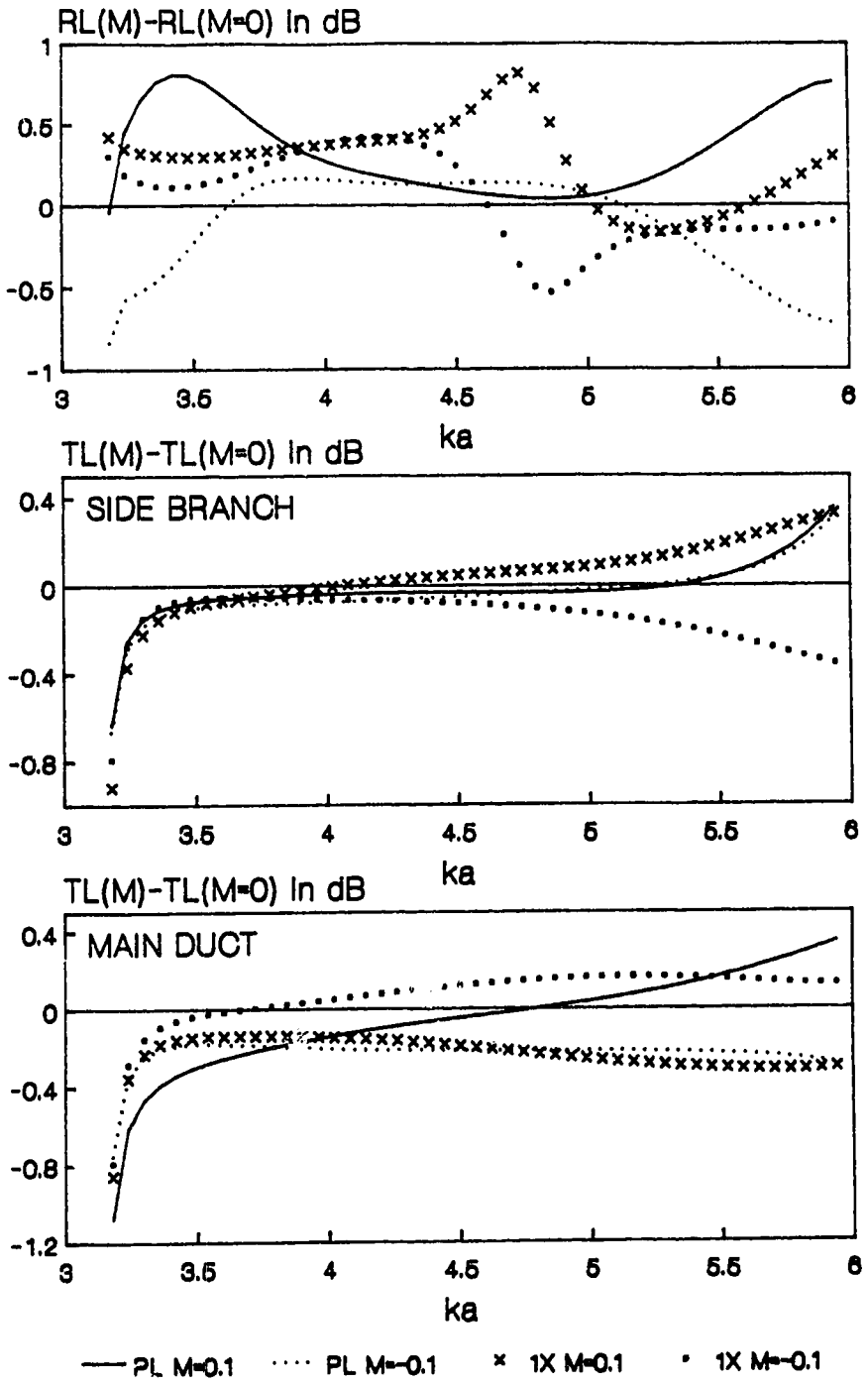

Figure 4.20 Change in RL and TL with respect to the No-flow Case for a 90 Degree Side Branch with the Same Width as the Main Duct and an Equal Flow Slit with the First Cross Mode Incident

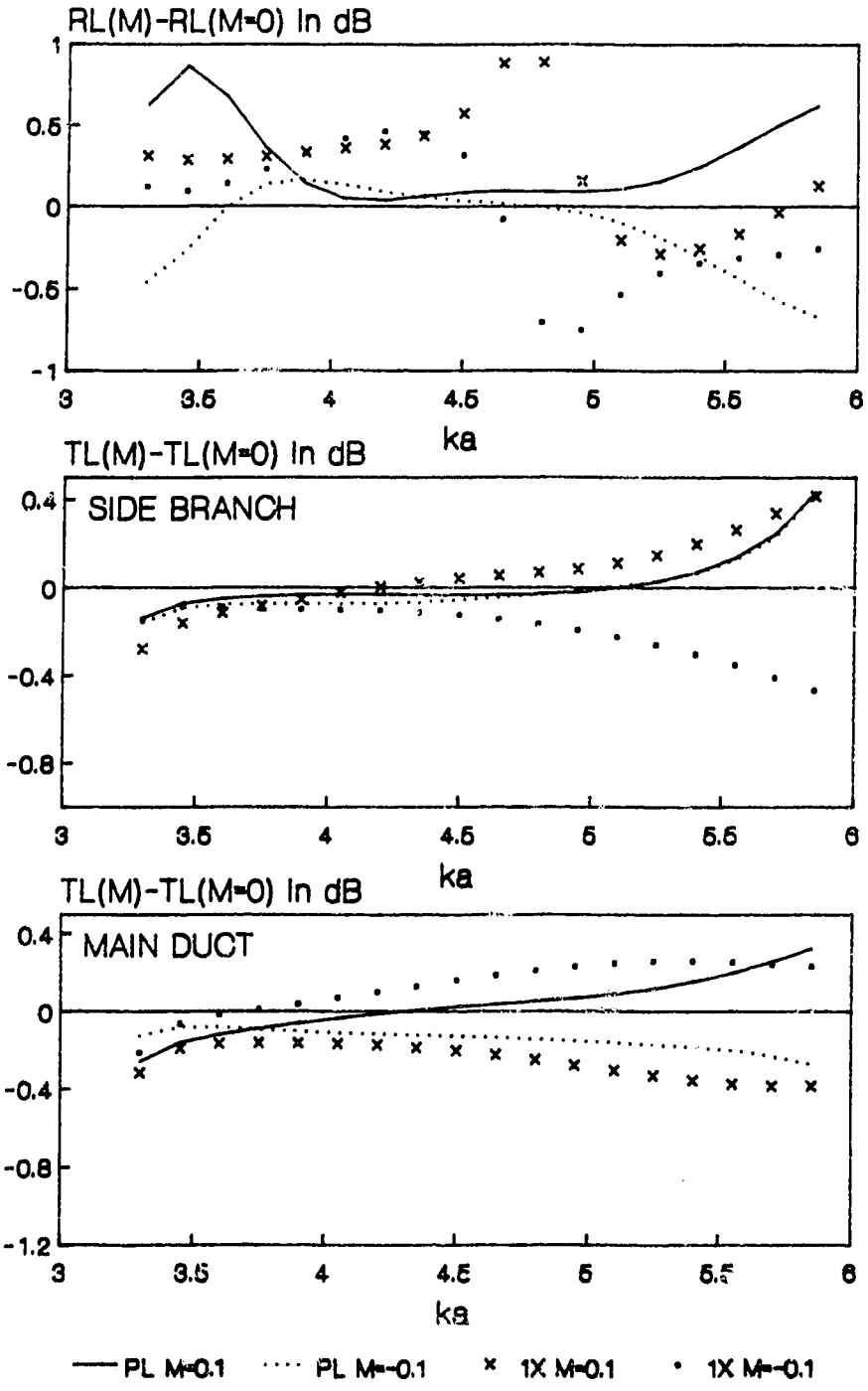

Figure 4.21 Change in RL and TL with respect to the No-flow Case for a 90 Degree Side Branch with the Same Width as the Main Duct and 10% of the Flow Out the Side Branch with the First Cross Mode Incident

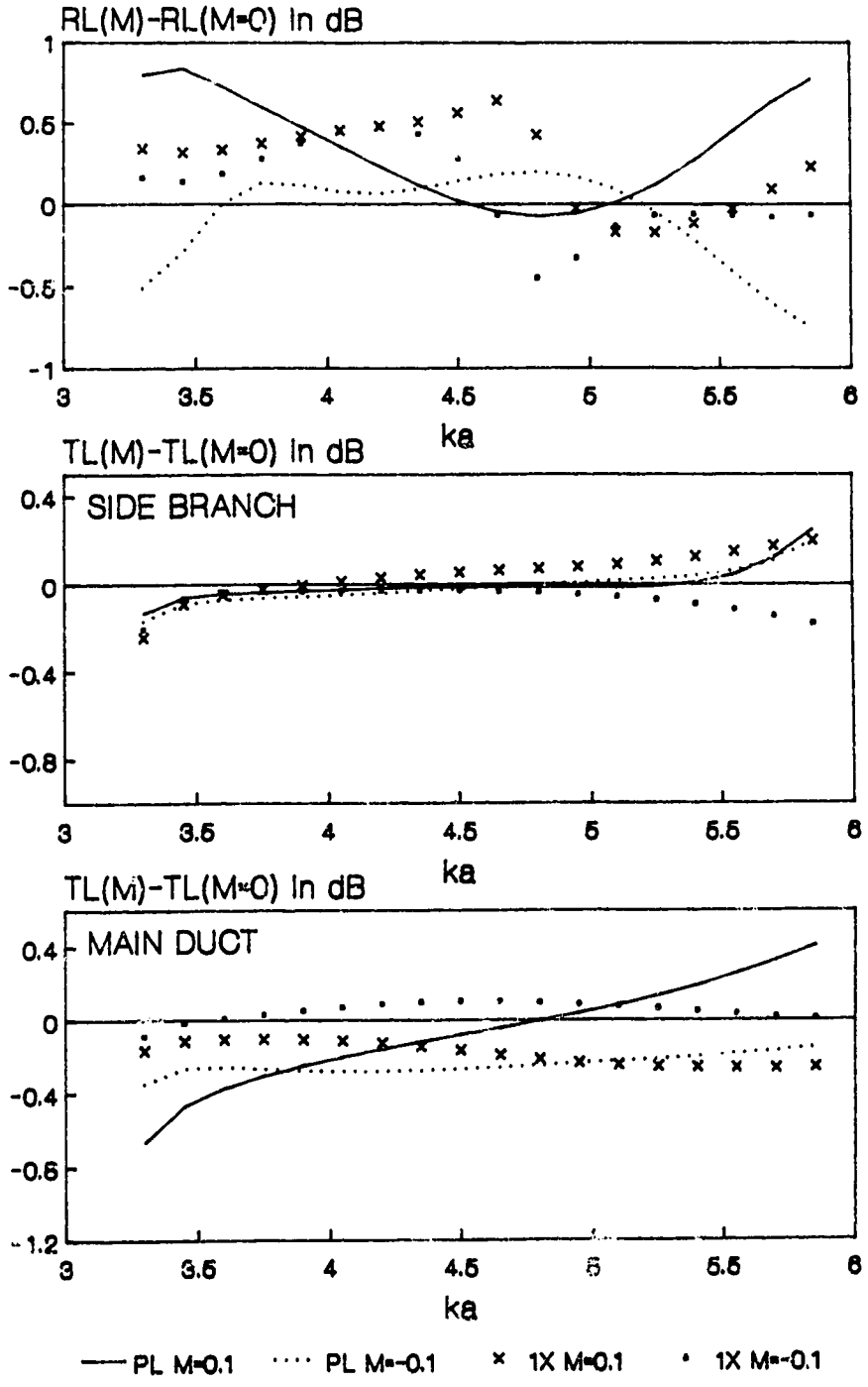

Figure 4.22 Change in *RL* and *TL* with respect to the No-flow Case for a 90 Degree Side Branch with the Same Width as the Main Duct and 90% of the Flow Out the Side Branch with the First Cross Mode Incident

the curves are most complicated for the reflection loss RL. In these cases, the side branch plane wave transmission loss is unaffected by the flow except near the cross mode cut-on frequencies while first cross mode shows greater changes with flow.

As indicated above, it would be desirable to use finer mesh models to confirm the above results with flow. Probably the major conclusion that can be drawn from this is that for Mach numbers of 0.1 or less the convective effect of flow has a relatively small influence on duct bend and junction transmission losses.

4.4.3 FEM Predictions for a 90 Degree Half Width Side Branch

This section considers a duct junction with a 90 degree side branch which has half the width of the inlet and continuing duct. The ISOHERM12 mesh used to model this junction is shown in Figure 4.23. The results for this junction are shown for the no-flow case and for the case of an inlet Mach number of 0.1 and equal flow velocities of Mach 0.0667 in the continuing main duct and side branch. The non-dimensional frequency parameter ka is based on the inlet duct width.

The RL and TL values predicted for this junction with a plane wave incident are shown in Figure 4.24. The graphs are generally similar to that obtained for the full width side branch shown in Figure 4.15 and show similar effects of flow. One difference is the decreased plane wave reflection and side branch transmission at low frequencies due to the decrease in cross-sectional area of the branch. There is also a sharper peak in the reflection loss graph near the cut-on of the first cross mode at $ka = \pi$. The other major difference is the absence of the first cross mode in the transmission loss graph for the side branch. The cut-on of the first cross mode in the branch occurs at $ka = 2\pi$ for no flow.

The results with the first cross mode incident, shown in Figure 4.25 for the half width branch, also show significant changes in the curves as a function of

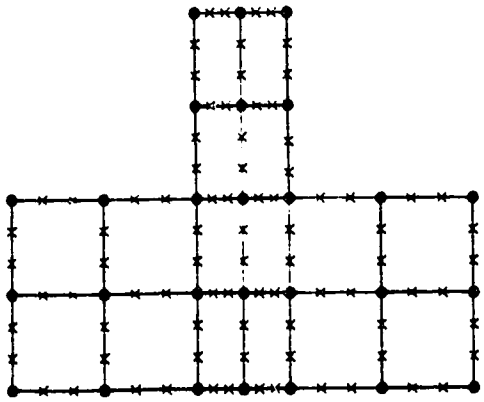

Figure 4.23 ISOHERM12 Element Mesh for a 90 degree Side Branch with Half the Width of the Main Duct

frequency compared to the results for a full width side branch shown in Figure 4.16. The most significant change was for the first cross mode reflection loss curve which for the full width side branch showed a peak in RL near $ka = 4.8$. For the half width branch the corresponding RL curve continually increased over the frequency range considered, shifting the peak (if it still occurs) to a point above $ka = 6$. The effect of flow with an inlet Mach number of 0.1 was small and generally similar to that found for the full width branch.

4.4.4 FEM Predictions for a 45 Degree Side Branch

The last junction to be considered in this chapter is a more complex junction containing a 45 degree side branch and a tapered section reducing the cross-sectional area of the continuing duct—probably more typical of junctions occurring in HVAC systems than the 90 degree side branches considered previously.

The finite element mesh used for this junction is shown in Figure 4.26. Note that a mesh with only one element across the duct width had be used. This leads to one of the limitations of the present prediction method as developed in

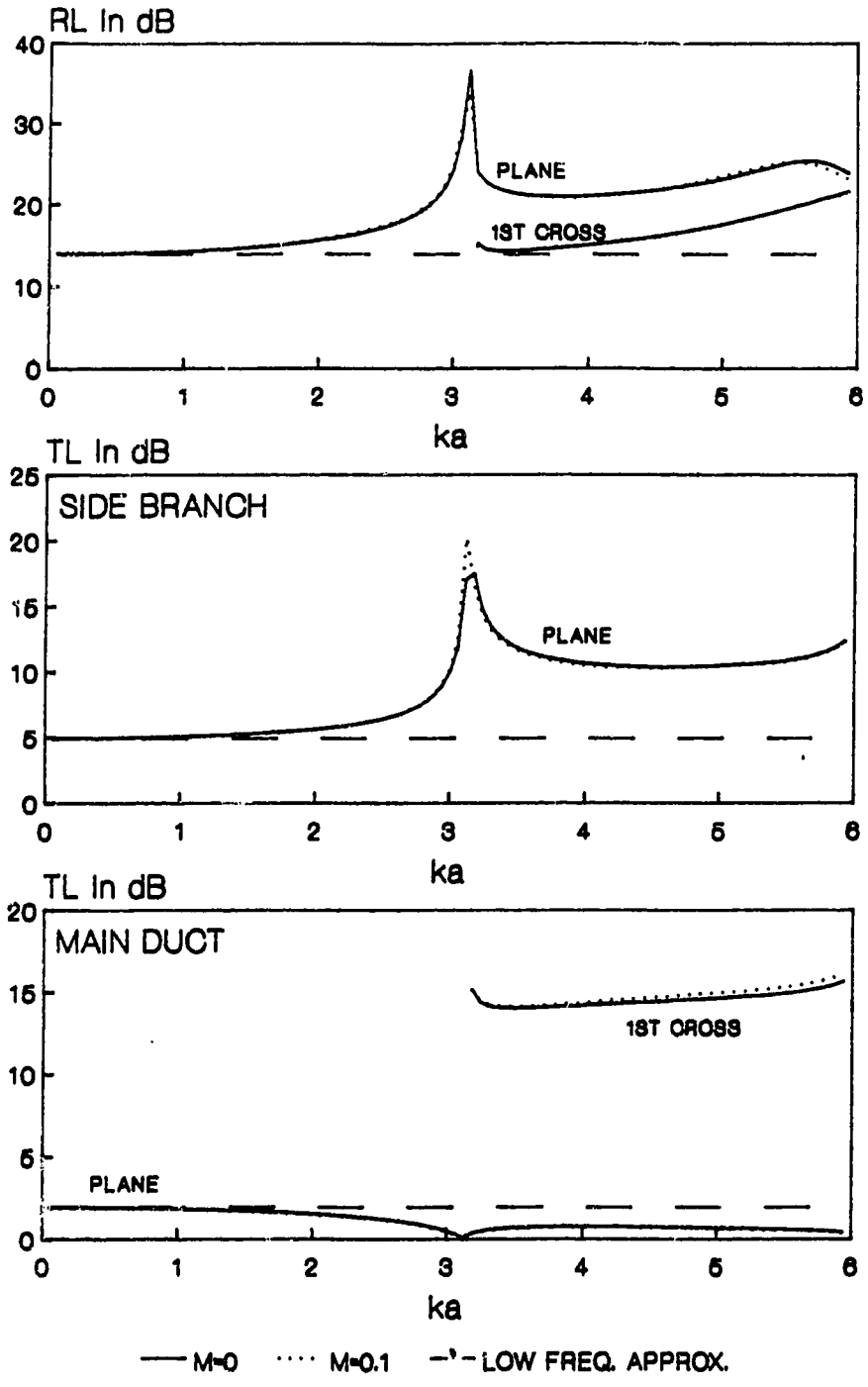

Figure 4.24 The Effect of Flow on Sound Propagation for a 90 Degree Side Branch with Half the Width of the Main Duct and 1/3 of the Flow Out the Side Branch with a Plane Wave Incident

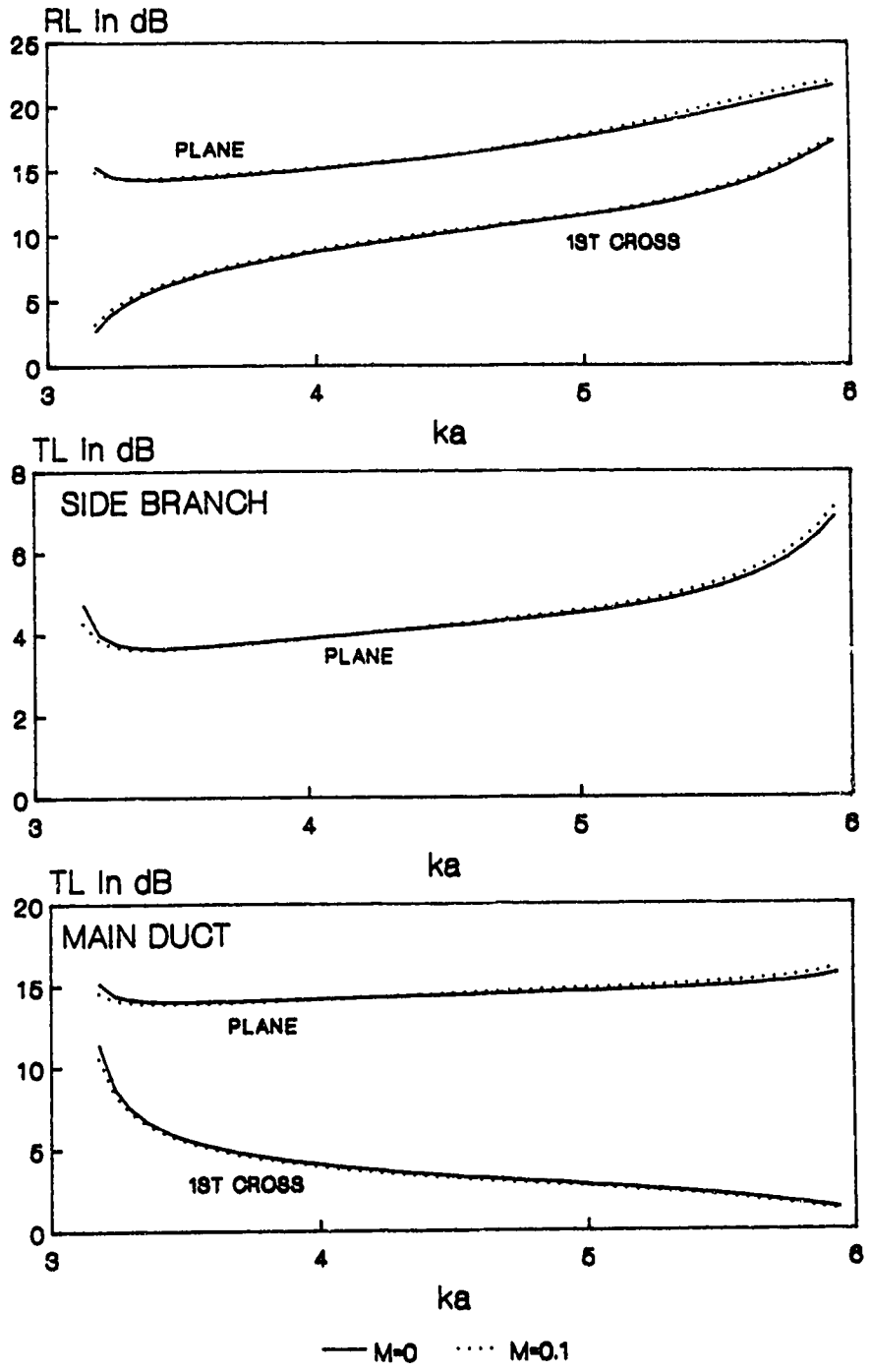

Figure 4.25 The Effect of Flow on Sound Propagation for a 90 Degree Side Branch with Half the Width of the Main Duct and 1/3 of the Flow Out the Side Branch with the First Cross Mode Incident

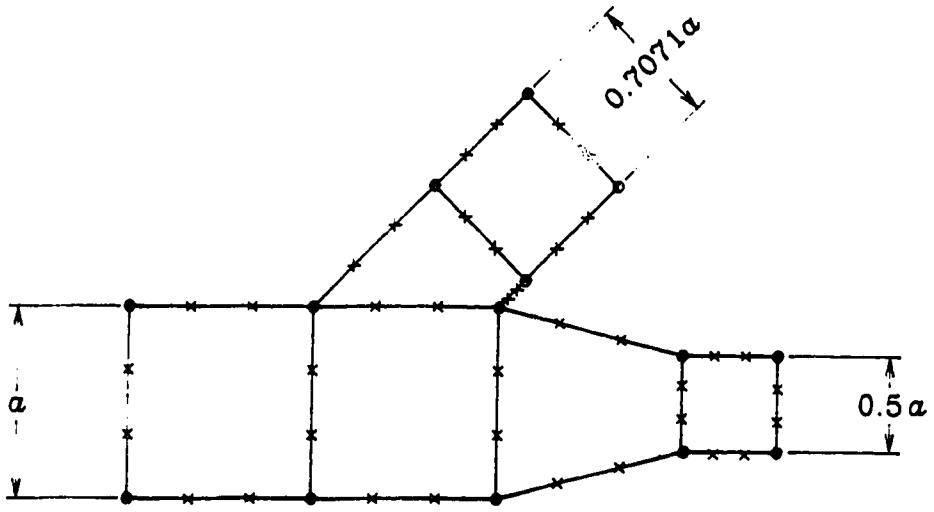

Figure 4.26 ISOHERM12 Element Mesh for a Junction with a 45 Degree Side Branch

Chapter III. The global finite element model, given by the global matrix equation shown in Equation 3.52, is in terms of acoustic velocity potential and derivative nodal quantities. These derivative nodal quantities are with respect to the global spatial coordinates. The duct cross-section modal matrices introduced in Section 3.1.6.4 for the modes occurring at the connecting straight duct interfaces are in terms of velocity potential nodal quantities and derivative nodal quantities tangent to the connecting duct interfaces. These can only be used directly in the current method if the normal to the interface surface is parallel to one of the global coordinate axes. The one exception is the case when only one element is used across the duct cross-section. In this case, for a hard walled duct the derivative quantities were constrained to zero so that the nodal quantities were in terms of the velocity potential only and connecting interfaces at any angle could be used. The conventional isoparametric elements such as HEX12 and HEX32 discussed in Chapter II do not have this problem since the nodal quantities used with these elements do not involve derivative quantities and thus could be used with the present method

for connecting duct interfaces at any angle.

The resulting predictions for this 45 degree junction are shown in Figure 4.27. In view of the coarseness of the mesh used, the results may not be very accurate especially above $ka = 3$. The side branch and continuing duct plane wave TL curves are similar to that obtained for a similar but not identical junction studied by Stredulinsky, Craggs and Faulkner [55] using two quadratic HEX8 elements across the duct widths and constraining connecting duct interfaces to plane waves. The side branch plane wave TL curve contains a "hump" reaching a maximum at roughly half the cut-on frequency of the first cross mode. This hump did not occur in the simple 90 degree branch results shown in Figure 4.14 and 4.24. It is similar to that occurring in a simple 1/4 wavelength expansion chamber with a length a. Along the path from the inlet to the branch outlet there is an expansion and contraction occurring roughly over a length a which may be working effectively like a 1/4 wavelength expansion chamber.

The results tend to diverge more rapidly from the low frequency approximation than for the simpler 90 degree elbows. For example, the results for the 90 degree branch shown in Figure 4.24 follow the horizontal line representing the low frequency approximation closely up to $ka = 1$, whereas the results of Figure 4.27 for the 45 degree side branch diverge significantly for ka of between 0.2 and 0.4.

As indicated above, due to the coarseness of the finite element mesh, the results for first cross mode are probably not very accurate. They do, however, show the different ka cut-on values for the different width branches, which are analytically π for the reflected wave, $\pi\sqrt{2}$ and 2π for the branch and duct continuing straight on. Further work is required to modify the prediction method so that finer meshes could be used to confirm the above results for branches at 45 degrees or any other desired angle.

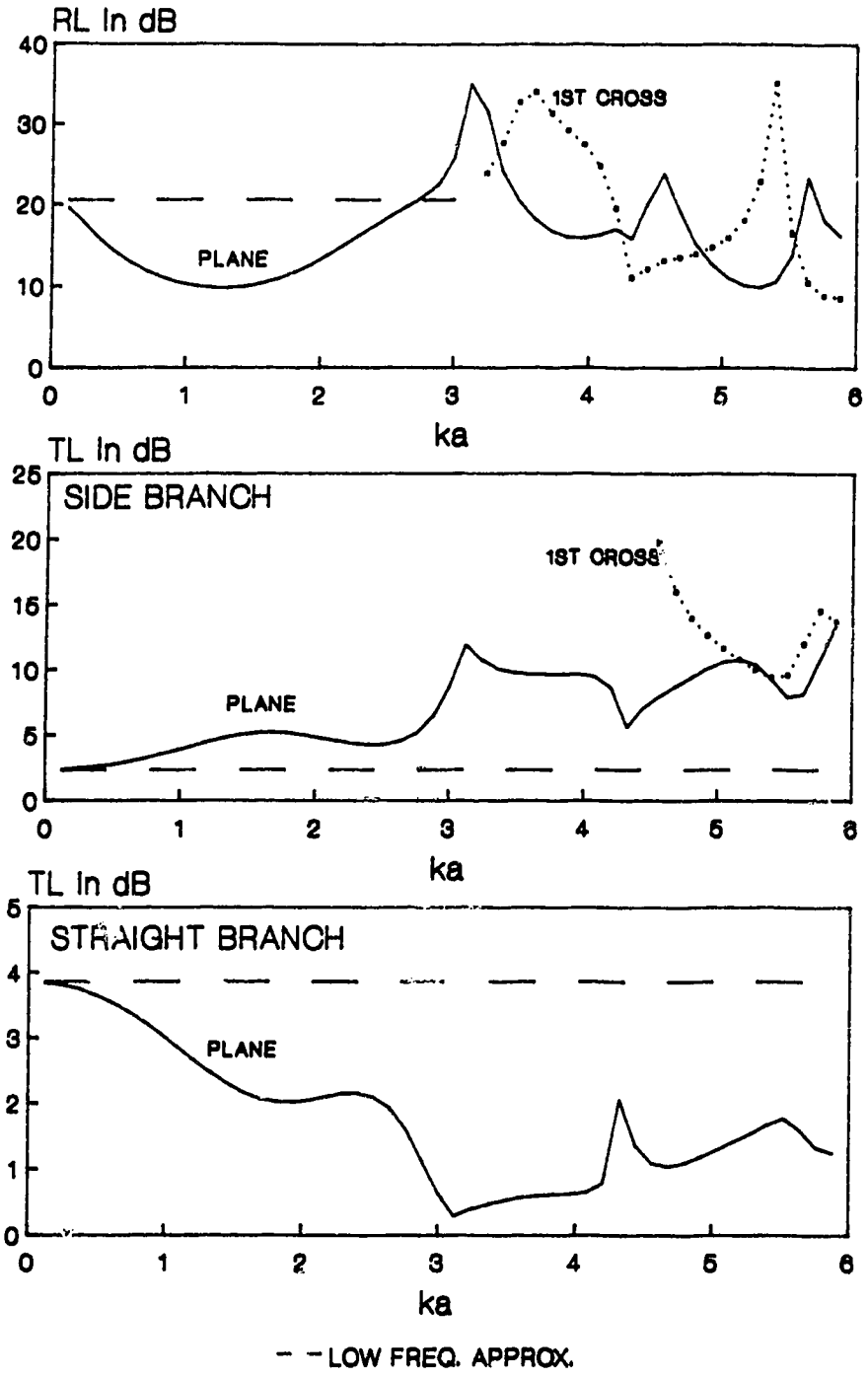

Figure 4.27 Propagation of Sound Through a Duct Junction with a 45 Degree Side Branch and No Flow for a Plane Wave Incident

CHAPTER V

CONCLUDING REMARKS

5.1 Summary

This thesis has considered the development of a cubic isoparametric Hermitian hexahedral finite element to efficiently model the propagation of sound through rigid walled duct bends and junctions. With the goal of improved technology transfer, the computer programs developed have been implemented on a desk top computer.

The element was initially tested by considering the acoustic enclosure eigenvalue problem, governed by the Helmholtz equation, and the incompressible potential fluid flow problem governed by Laplace's equation. The results for this new element have been compared to results for the conventional cubic isoparametric element which uses Serendipity shape functions and has the same number of degrees of freedom as the new Hermitian element. The new element leads to fewer degrees of freedom in global models compared to the conventional cubic isoparametric element models having the same number of elements (typically giving 40% fewer degrees of freedom). This is achieved by concentrating nodal quantities at the corners of the element and also explicitly constraining derivative nodal quantities at the rigid walled boundaries. It was demonstrated that the new element generally gave more accurate results on a degree of freedom basis. This improved accuracy was greatest for the case where the cuboid parent elements remained rectangular. Under certain

twisting distortions of the element boundaries, the new element gave much higher errors than the conventional isoparametric element.

A finite element model using this element was then developed to study the propagation of sound through duct bends and junctions including the convective effect of low Mach number steady fluid flow through the bend or junction. Due to memory limitations of the computer, a two-dimensional version of the element was used for this part of the work. The fluid flow was modeled using incompressible potential flow theory. The flow field was obtained first and then used in the equation governing the acoustic model. The same element mesh was used for both the acoustic and flow models. The initial development was tested with boundary conditions limiting the sound propagation to plane waves in straight ducts connected to the bend or junction models. This was then extended to consider higher order mode boundary conditions. An undistorted element model was first used to model propagation with flow in a straight duct. Propagation of modes up to and including the third cross mode was considered, and accurate results obtained up to $ka = 12$ with three elements across the duct cross-section. A distorted element model was tested for the problem of a mitred duct bend with a curved inner corner. This problem required three elements across the duct cross-section to accurately model plane wave and first cross mode propagation up to $ka = 6$.

Following the development and testing of the acoustic-flow model, the procedure was used to consider two additional duct bend problems and to study sound propagation in duct junctions. The first bend considered was a 90 degree mitred bend which could be modeled with undistorted elements. In this case it was found that models with only two elements across the duct width could accurately model plane wave and first cross mode propagation up to $ka = 6$. It was also

demonstrated that in the absence of flow, with the present procedure, it is not necessary to extend the FEM model very far into the connecting straight ducts since the evanescent modes were included in the boundary conditions.

The second bend considered was a curved 90 degree bend with a turning vane. Modeling this bend required distorted elements and there were significant differences, above $ka = 4$, between models with two elements and three elements across the cross-section and some difference between these models at a transmission loss peak between $ka = 1.5$ and $ka = 2$. This predicted peak was in one case roughly 10% higher than measured and predicted by another researcher using a FDM model. This problem also demonstrated, as found earlier when studying acoustic enclosures, that one must be cautious in constraining nodal derivative quantities at boundary discontinuities. The constraint of nodal derivative quantities along continuous boundaries or at 90 degree corners to explicitly satisfy boundary conditions can lead to models with fewer degrees of freedom without sacrificing accuracy. However at acute or oblique angle corners and other discontinuities, for example, the end point of a turning vane, it was found best to leave the nodal quantities unconstrained and thus handled by the implicit boundary conditions.

The last subject treated in this thesis was the propagation of sound through duct junctions. The first junction considered was a simple junction with a 90 degree side branch having the same width as the main duct. With the finite element model extended one duct width into the connecting ducts it was found that only two elements could be used across the duct cross-section without exceeding the computer's memory capacity. In the absence of flow, a model with three elements across the duct cross-section, but with shortened regions in the connecting ducts, was used to confirm that the models with two elements across the duct width

gave sufficiently accurate results up to $ka = 6$ for plane wave and first cross mode propagation. Results for 10%, 50% and 90% of the flow out the side branch were obtained with an inlet Mach number of 0.1. It was found that the flow had only a small effect, changing the transmission loss values b[illegible] 1 decibel for the plane wave and first cross modes up to $ka = 6$ with the exception of near the cut-on for the first cross mode where differences of up to 3 dB were noted. Predictions were also made for a 90 degree side branch which has half the width of the main duct with equal flow velocities out the branch and continuing duct. The flow effects were similar to that obtained for the full width branch.

The last junction considered contained a 45 degree side branch and tapered section in the continuing duct just after the branch. The results for this junction showe[illegible] complex curves for the reflection loss and transmission loss as a function [illegible]ency than did the simple 90 degree side branches. There was also greater de[illegible]ation from the [illegible]ncy independent low frequency plane wave approximation. This problem also demonstrated one deficiency in the current procedure—it can only be used with the isoparametric Hermitian element for bends or junctions in which the connecting duct interfaces are parallel to the global coordinate axes, for cases where more than one element is used across the duct cross-section. This problem does not occur if conventional isoparametric elements are used.

5.2 Areas of Further Research

There were several areas encountered in this work concerning the development and testing of the ISOHERM32 element which could be investigated further.

In Section 2.2.2, it was noted that this new element has C^1 continuity when undistorted but generally has only C^0 continuity when distorted. It was observed that if the elements formed segments of a polar grid then C^1 continuity was also achieved. It would be interesting to consider in more detail types of distortions which maintain the C^1 continuity of this element.

In Section 2.3.2.3, it was observed that the twisting of the common plane between two ISOHERM32 elements forming a rectangular enclosure caused large increases in the prediction error of the eigenfrequency for the first axial mode perpendicular to this plane. This behavior did not occur in a similar model using the conventional isoparametric HEX32 element. It would be of interest to investigate this further to determine the reason for this difference in behavior between these elements. The problem of the curved bend with a turning vane discussed in Section 4.3 showed some discrepancies between the predicted FEM results and experiment and FDM results of another researcher. Part of the problem appears to be the increased inaccuracies of the distorted elements, which means that a finer element mesh is needed to handle this problem—a model too large to run on the desk top computer used for the current work.

As indicated above, the last junction considered in this thesis was a 45 degree branch. This problem demonstrated that the present procedure can only model bends or junctions where the connecting straight duct interfaces are parallel to the global Cartesian coordinate axis for the case of more than one element across the duct cross-section. It should be possible to modify the global matrix equation for the finite element model given by Equation 3.84 so that nodal derivative quantities on the connecting duct interfaces are in terms of normal and tangential derivative quantities rather than derivatives with respect to the global axes. This would then

allow the modal matrix and modal recipe vectors for duct interfaces at any angle to be used in the finite element models. Also due to limitations of the computer system used for this work, all the bend and junction predictions have been made using a two-dimensional version of the element. Certainly much work could be done on a main frame computer, applying the element to three-dimensional bends and junctions for ducts of rectangular cross-section and also ducts with circular or oval cross-sections.

The duct network problem discussed in Section 1.3 was treated by Craggs and Stredulinsky [23] and Stredulinsky, Craggs and Faulkner [55] combining the transfer matrix and finite element methods, using exact plane wave solutions in straight ducts and FEM models in bends, junctions and other areas where two or three-dimensional effects are important. It should be possible to use the method developed in this thesis to consider higher order mode boundary conditions for the FEM models linked to straight ducts in which exact solutions including higher order modes are used, extending the predictions to higher frequencies including the convective effect of flow. The work in this thesis indicated that low Mach number flow had little effect on the bend and junction transmission losses, however, as indicated by the straight duct results of Section 3.3.2, the flow can have significant effect on phases of the acoustic waves. In the work for reference [55] it was observed that small changes in the duct network dimensions caused considerable change in the overall network transmission loss. Thus it is likely that the phase changes occurring in the bends and junctions and in the straight duct sections, even for flows at low Mach number, may have much greater influence on the overall duct network than observed for individual system components.

Other areas where further work is required, if the goal of obtaining more accurate methods for noise prediction in HVAC duct systems is to be achieved,

include implementing models with absorptive duct linings and flexible walled ducts and considering the problem of flow generated noise within the duct systems. Based on the work conducted in this thesis and references [23] and [55], the implementation of such a prediction scheme for a real HVAC system is probably still within the realm of a mainframe computer, but in view of the rapid development of computer technology, may soon be possible using a personal desk top computer and thus more accessible to design engineers.

BIBLIOGRAPHY

[1] American Society of Heating, Refrigeration and Air Conditioning Engineers, *Heating, Ventilation and Air Conditioning Systems and Applications*, Chapter 52, 1987.

[2] Astley, R.J., "A finite element, wave envelope formulation for acoustical radiation in moving flows", Journal of Sound and Vibration, Vol. 103, No. 4, 1985, pp. 471 - 485.

[3] Astley, R.J. and Eversman, W., "A finite element method for transmission in non-uniform ducts without flow: Comparison with the method of weighted residuals", Journal of Sound and Vibration, Vol. 57, No. 3, 1978, pp. 367 - 388.

[4] Astley, R.J. and Eversman, W., "A finite element formulation of the eigenvalue problem in lined ducts with flow", Journal of Sound and Vibration, Vol. 65, No. 1, 1979, pp. 61 - 74.

[5] Astley, R.J. and Eversman, W., "The finite element duct eigenvalue problem: An improved formulation with Hermitian Elements and no-flow condensation", Journal of Sound and Vibration, Vol. 69, No. 1, 1980, pp. 13 - 25.

[6] Astley, R.J. and Eversman, W., "Acoustic transmission in non-uniform ducts with mean flow, Part II: The finite element method", Journal of Sound and Vibration, Vol. 74, No. 1, 1981, pp. 103 - 121.

[7] Buma, C.J., *Multiple-source Excitation of Acoustic Resonances of Damped Small-Room Enclosures*, M.Sc.Thesis, University of Alberta, 1986.

[8] Burnett, D.S., *Finite Element Analysis from Concepts to Applications*, Addison-Wesley, Reading, Massachusetts, 1987.

[9] Cabelli, A., "The acoustic characteristics of duct bends", Journal of Sound and Vibration, Vol. 68, No. 3, 1980, pp. 369 - 388.

[10] Cabelli, A., "The influence of flow on the acoustic characteristics of a duct bend for higher order modes – a numerical study", Journal of Sound and Vibration, Vol. 82, No. 1, 1982, pp. 131 - 149.

[11] Cabelli, A., "Application of the time dependent finite difference theory to the study of sound and vibration interactions in ducts", Journal of Sound and Vibration, Vol. 103, No. 1, 1985, pp. 13 - 23.

BIBLIOGRAPHY (continued)

[12] Cabelli, A., "The propagation of sound in a square duct with a non-rigid side wall", Journal of Sound and Vibration, Vol. 103, No. 3, 1985, pp. 379 - 394.

[13] Cabelli, A. and Shepherd, I.C., "The influence of geometry on the acoustic characteristics of duct bends for higher order modes", Journal of Sound and Vibration, Vol. 78, No. 1, 1981, pp. 119 - 129.

[14] Cabelli, A. and Shepherd, I.C., "Duct acoustics – a numerical technique for the higher order mode solution of three-dimensional problems with rigid walls and no flow", Journal of Sound and Vibration, Vol. 92, No. 3, 1984, pp. 419 - 426.

[15] Chung, J.Y. and Blaser, D.A., "Transfer function method of measuring in-duct acoustic properties. I. Theory", Journal of the Acoustical Society of America, Vol. 68, No. 3, 1980, pp. 907 - 913.

[16] Chung, J.Y. and Blaser, D.A., "Transfer function method of measuring in-duct acoustic properties. II. Experiment", Journal of the Acoustical Society of America, Vol. 68, No. 3, 1980, pp. 914 - 921.

[17] Craggs, A., "The transient response of a coupled plate-acoustic system using plate and acoustic finite elements", Journal of Sound and Vibration, Vol. 15, No. 4, 1971, pp. 509 - 528.

[18] Craggs, A., "The use of simple three dimensional acoustic finite elements for determining the natural modes and frequencies of complex shaped enclosures", Journal of Sound and Vibration, Vol. 23, No. 3, 1972, pp. 331 - 339.

[19] Craggs, A., "An acoustic finite element approach for studying boundary flexibility and sound transmission between irregular enclosures", Journal of Sound and Vibration, Vol. 30, No. 3, 1973, pp. 343 - 357.

[20] Craggs, A., "A finite element method for damped acoustic systems: An application to evaluate the performance of reactive mufflers", Journal of Sound and Vibration, Vol. 48, No. 3, 1976, pp. 377 - 392.

[21] Craggs, A., "A finite element method for modelling dissipative mufflers with a locally reactive lining", Journal of Sound and Vibration, Vol. 54, No. 2, 1977, pp. 285 - 296.

[22] Craggs, A. and Stead, G., "Sound transmission between enclosures – A study using plate and acoustic finite elements ", Acustica, Vol. 35, No. 2, 1976, pp. 89 - 98.

[23] Craggs, A. and Stredulinsky, D.C., "Analysis of acoustic wave transmission in a piping network", Journal of the Acoustical Society of America, Submitted for publication, 1989.

BIBLIOGRAPHY (continued)

[24] Cummings, A., "Sound transmission in curved duct bends", Journal of Sound and Vibration, Vol. 35, No. 4, 1974, pp. 451 - 477.

[25] Cummings, A., "Sound transmission in 180° duct bends of rectangular section", Journal of Sound and Vibration, Vol. 41, No. 3, 1975, pp. 321 - 334.

[26] Doak, P.E., "Excitation, transmission and radiation of sound from source distributions in hard-walled ducts of finite length (I): The effects of duct cross-section geometry and source distribution space-time pattern ", Journal of Sound and Vibration, Vol. 31, No. 1, 1973, pp. 1 - 72.

[27] Doak, P.E., "Excitation, transmission and radiation of sound from source distributions in hard-walled ducts of finite length (II): The effects of duct length", Journal of Sound and Vibration, Vol. 31, No. 2, 1973, pp. 137 - 174.

[28] Eversman, W., "Computation of axial and transverse wave numbers for uniform two-dimensional ducts with flow using a numerical integration scheme", Journal of Sound and Vibration, Vol. 41, No. 2, 1975, pp. 252 - 255.

[29] Eversman, W., "A reciprocity relationship for transmission in non-uniform hard walled ducts without flow", Journal of Sound and Vibration, Vol. 47, No. 4, 1976, pp. 515 - 521.

[30] Eversman, W., "Acoustic energy in ducts: Further observations", Journal of Sound and Vibration, Vol. 62, No. 4, 1979, pp. 517 - 532.

[31] Eversman, W. and Astley R.J., "Acoustic transmission in non-uniform ducts with mean flow, Part I: The method of weighted residuals", Journal of Sound and Vibration, Vol. 74, No. 1, 1981, pp. 89 - 101.

[32] Eversman, W., Cook, E.L. and Beckemeyer, R.J., "A method of weighted residuals for the investigation of sound transmission in non-uniform ducts without flow", Journal of Sound and Vibration, Vol. 38, No. 1, 1975, pp. 105 - 123.

[33] Fuller, C.R. and Bies, D.A., "Propagation of sound in a curved bend containing a curved axial partition", Journal of the Acoustical Society of America, Vol. 63, No. 3, 1978, pp. 681 - 686.

[34] Gladwell, G.M.L., "A finite element method for acoustics", 5^{e} Congres International D'Acoustique, Paper No. L33, 1965.

BIBLIOGRAPHY (continued)

[35] Kaizer, A.J.M., and Leeuwestein, A., "Calculation of the sound radiation of a nonrigid loudspeaker diaphragm using the finite-element method", Journal of the Audio Engineering Society, Vol. 36, No. 7/8, 1988, pp. 539 - 551.

[36] Ling S.F., Hamilton J.F., Allen J.J., "A Two-dimensional isoparametric Galerkin Finite Element for Acoustic-Flow problems", Transactions of the ASME, Journal of Mechanical Design, Paper No. 82-DET-97, 1982.

[37] Lippert, W.K.R., "The measurement of sound reflection and transmission at right-angled bends in rectangular tubes", Acustica, Vol. 4, 1954, pp. 313 - 319.

[38] Lippert, W.K.R., "Wave transmission around bends of different angles in rectangular ducts", Acustica, Vol. 5, 1955, pp. 274 - 278.

[39] Miles, J.W., "The diffraction of sound due to right-angled joints in rectangular tubes", Journal of the Acoustical Society of America, Vol. 19, No. 4, 1947, pp. 572 - 579.

[40] Morfey, C.L., "Sound transmission and generation in ducts with flow", Journal of Sound and Vibration, Vol. 14, No. 1, 1971, pp. 37 - 55.

[41] Morse,M., *Vibration and Sound*, American Institute of Physics, 1986.

[42] Munjal, M.L., *Acoustics of Ducts and Mufflers with Application to Exhaust and Ventilation System Design*, John Wiley & Sons, New York, 1987.

[43] Osborne, W.C., "Calculation of the angular propagation constant for a bend", Journal of Sound and Vibration, Vol. 37, No. 1, 1974, pp. 65 - 77.

[44] Panton, L., *Incompressible flow*, John Wiley & Sons, New York, 1984.

[45] Peat, K.S. "Evaluation of four-pole parameters for ducts with flow by the finite element method", Journal of Sound and Vibration, Vol. 84, No. 3, 1982, pp. 389 - 395.

[46] Redmore, T.L., and Mulholland, K.A., "The application of mode coupling theory to the transmission of sound in the sidebranch of a rectangular duct system", Journal of Sound and Vibration, Vol. 85, No. 3, 1982, pp. 323 - 331.

BIBLIOGRAPHY (continued)

[47] Rostafinsky, W., "On propagation of long waves in curved ducts", Journal of the Acoustical Society of America, Vol. 52, No. 5, 1972, pp. 1411 - 1420.

[48] Rostafinsky, W., "Analysis of propagation of waves of acoustic frequencies in curved ducts", Journal of the Acoustical Society of America, Vol. 56, No. 1, 1974, pp. 11 - 15.

[49] Rostafinsky, W., "Acoustic systems containing curved duct sections", Journal of the Acoustical Society of America, Vol. 60, No. 1, 1976, pp. 23 - 28.

[50] Seybert A.F., and Cheng C.Y.R., "Application of the boundary element method to acoustic cavity response and muffler analysis", Transactions of the ASME, Journal of Vibration, Acoustics, Stress and Reliability, Vol. 109, 1987, pp. 15 - 21.

[51] Shepherd, I.C. and Cabelli, A., "Transmission and reflection of higher order acoustic modes in a mitred duct bend", Journal of Sound and Vibration, Vol. 77, No. 4, 1981, pp. 495 - 511.

[52] Shuku, T. and Ishihara, K., "The analysis of the acoustic field in irregularly shaped rooms by the finite element method", Journal of Sound and Vibration, Vol. 29, No. 1, 1973, pp. 67 - 76.

[53] Sigman, R.K., Majjigi, R.K. and Zinn, B.T., "Determination of turbofan inlet acoustics using finite elements", American Institute of Aeronautics and Astronautics Journal, Vol. 16, No. 11, 1978, pp. 1139 - 1145.

[54] Stead, G., *Finite element approach to sound transmission*, M. Sc. thesis, University of Alberta, 1973.

[55] Stredulinsky, D.C., Craggs, A., Faulkner, M.G., "Acoustics of piping and ducts", Canadian Acoustics, Vol. 15, No. 4, 1987, pp. 3 - 14.

[56] Vo, P.T. and Eversman, W., "A method of weighted residuals with trigonometric basis functions for sound transmission in circular ducts", Journal of Sound and Vibration, Vol. 56, No. 2, 1978, pp. 243 - 250.

[57] von Said, A., "Theorie der schallausbreitung in kanälen mit rechtwinkligen ecken und verzweigungen", Acustica, Vol. 33, 1975, pp. 203 - 210.

[58] Young, C.J. and Crocker, M.J., "Prediction of transmission loss in mufflers by the finite-element method', Journal of the Acoustical Society of America, Vol. 57, No. 1, 1975, pp. 144 - 148.